Assessment of Cartilage Contact and Early Degeneration Following ACL Reconstruction

By

Jarred Kaiser

A dissertation submitted in partial fulfillment of

the requirements for the degree of

Doctor of Philosophy

(Mechanical Engineering)

at the

UNIVERSITY OF WISCONSIN-MADISON

2015

Date of final oral examination: 12/9/15

The dissertation is approved by the following members of the Final Oral Committee:

Darryl G. Thelen, Professor, Mechanical Engineering
Krishnan Suresh, Associate Professor, Mechanical Engineering
Oliver Wieben, Associate Professor, Biomedical Engineering
Richard Kijowski, Professor, Radiology
Bryan Heiderscheit, Professor, Orthopedics and Rehabilitation
Geoffrey Baer, Assistant Professor, Orthopedics and Rehabilitation

ProQuest Number: 3741508

All rights reserved

INFORMATION TO ALL USERS
The quality of this reproduction is dependent upon the quality of the copy submitted.

In the unlikely event that the author did not send a complete manuscript
and there are missing pages, these will be noted. Also, if material had to be removed,
a note will indicate the deletion.

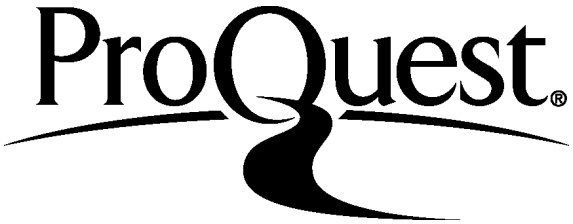

ProQuest 3741508

Published by ProQuest LLC (2015). Copyright of the Dissertation is held by the Author.

All rights reserved.
This work is protected against unauthorized copying under Title 17, United States Code
Microform Edition © ProQuest LLC.

ProQuest LLC.
789 East Eisenhower Parkway
P.O. Box 1346
Ann Arbor, MI 48106 - 1346

Acknowledgements

This thesis could not have been completed without the help of many others. Many thanks to the past and present members of the UW Neuromuscular Biomechanics Lab, including Christopher Westphal, Robert Bradford, Rachel Lenhart, Mike Vignos, Colin Smith, Arezu Monawer, Brett Paredo, and James Hermus.

Thanks to the support of the UW MRI and Radiology groups, specifically Oliver Wieben, Richard Kijowski, Kevin Johnson, Fang Liu, and Rajeev Chaudhary, in developing the dynamic and quantitative MR scans, as well as aiding in validation scans. Thanks to the MRI techs (Kelli Hellibrand, Sara John, and Jenelle Fuller) for their help with scans and for several lunches.

Thanks to my thesis committee (Krishnan Suresh, Oliver Wieben, Richard Kijowski, Bryan Heiderscheit, and Geoffrey Baer) for their guidance and support throughout the project.

Thanks for my parents and wife for their personal support and sacrifice over the past five years.

Finally, thanks to my advisor, Darryl Thelen, for putting me in a position to succeed with the project, and for his continue support and guidance.

Abstract

While ACL-reconstruction following injury restores knee stability and allows patients to return to activity, rates of early osteoarthritis post-surgery are high, with some reports as high as 80% of patients showing degeneration within 20 years. Many believe that early OA is due to residual abnormalities in joint mechanics after ACL-reconstruction. Proving a direct link between altered mechanics and cartilage degeneration, however, requires an imaging modality which can both measure *in vivo* joint motion with high accuracy and detect early degeneration. This thesis uses a new dynamic imaging sequence to measure in vivo joint motion and advanced quantitative MR sequences to assess cartilage composition to investigate potential links between cartilage loading and degeneration following ACL-reconstruction. We first validated the novel dynamic MR sequence, termed SPGR-VIPR, showing it is able to track tibiofemoral rotations and translations with precisions less than 0.8° and 0.5 mm, respectively. We then confirmed that healthy subjects exhibit bilateral symmetry in tibiofemoral kinematics during active knee flexion, which supports the use of the contralateral knee as a control in ACL-reconstructed knees. We then performed the dynamic imaging protocol on patients who previously had unilateral, primary ACL-reconstruction 1-3 years prior. We found that an inertial loading paradigm elicited significant asymmetries in knee kinematics, with the ACL-reconstructed knees exhibiting greater external tibial (~2°) and patellar (~1.3°) rotation during active flexion. These kinematic abnormalities lead to a shift in contact in both the medial and lateral tibial plateaus. The quantitative MR sequence, termed MC-DESPOT, also identified a significant decrease in proteoglycan-bound water metrics in both the medial and lateral tibial plateau, which may be indicative of early cartilage degeneration. We conclude that early biomarkers of osteoarthritis coincide with the time at which abnormal knee mechanics can be observed in ACL-reconstructed knees.

Table of Contents

List of Figures

Chapter 5

Appendices

List of Tables

Introduction to Thesis

There are approximately 250,000 tears of the anterior cruciate ligament (ACL) every year in the United States [5]. The ACL is the primary restraint to anterior tibial translation and internal tibial rotation at the knee and secondary restraint to medial translation and abduction [6]. When torn, the knee typically exhibits excessive laxity, making an individual feel their knee is not sufficiently stable to return to full activity. In the US, more than 50% of ACL tears are surgically repaired [7, 8], with a donor graft taken from either the patient's patellar or hamstring tendon. Reconstruction of the ACL has a high success rate (>85%) restoring normal anterior-posterior laxity to the knee [5], which often is sufficient for the patient to return to full activity after approximately 6 months of rehabilitation [9-11].

Long term outcomes following ACL-reconstructive surgery are less favorable however. Approximately 50-80% of patients who have undergone ACL-reconstruction (ACLR) have signs of osteoarthritis (OA) within 10-20 years [12-14]. This is especially problematic as these patients are typically young and, with no current treatment to stop or reverse OA, patients may have to live up to 20 years with limited knee function until total knee replacement becomes viable [15].

The reason for early OA in this population is not well-understand. One prevalent hypothesis is that small kinematic abnormalities persist following ACLR, loading the cartilage in a destructive manner [5, 16, 17]. Cartilage is a well-adapted tissue with thicker cartilage in areas of highest loading [18, 19]. The arrangement of collagen fibers in the superficial layer of cartilage also systematically varies across the surface, with randomly aligned fibers in areas of greatest compression and more regular transverse fiber alignment in adjacent regions that undergo tensile loading [20, 21]. While normal loading can increase cartilage proteoglycan content and mechanical

strength [22-25], the low adaptation potential of mature cartilage may make it unable to withstand altered loading patterns, initiating a catabolic response which ends in OA [17].

Morphological changes associated with OA occur over long time periods, making it difficult to systematically study links between the treatment of ACL tears and the prevalence of OA. Magnetic resonance (MR) imaging can reduce the time periods for detection of OA through the use of MR biomarkers. MR relaxation metrics, T1rho and T2, are physically related to how water interacts with its surrounding local environment. T1rho has been shown to correlate with proteoglycan content [26], while T2 has been correlated with collagen integrity [27]. Thus, a change in either parameter could be sensitive to early cartilage degeneration in OA. Indeed, abnormal T1rho and T2 relaxation rates have been detected in tibiofemoral cartilage within 1-2 years of ACL reconstructive surgery (Fig. 1, [1, 28]). A more recent T2 decomposition sequence,

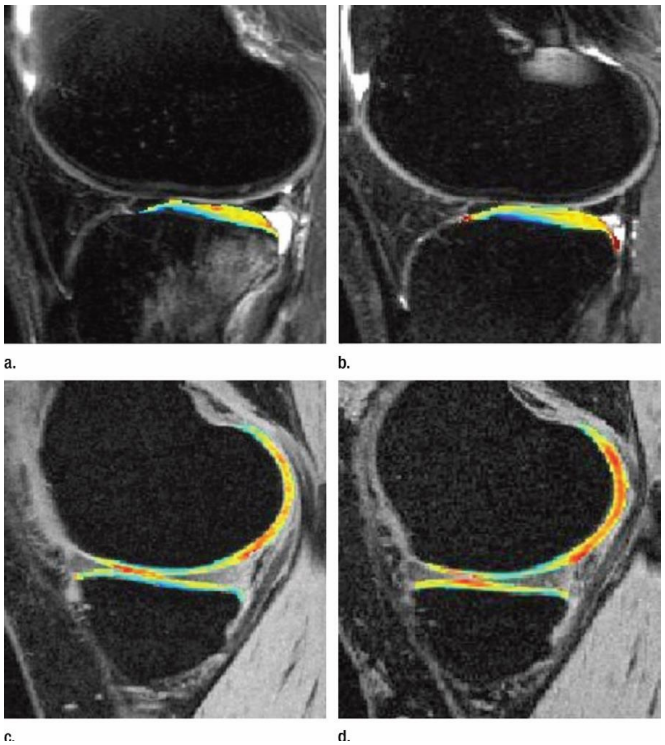

Figure 1. T1rho maps of (a,b) lateral and (c,d) medial side of an ACL-injured knee at (a,c) baseline and (b,d) one-year follow-up. Elevated T1rho values, indicating cartilage degeneration, can be seen in the posterior lateral tibia and in the medial weight-bearing femur and tibia *(Image taken from [1])*

mcDESPOT [29-31], can provide relative measures of free bulk water and water bound by proteoglycan [32]. However, it remains unclear whether biomechanical factors may contribute to the changes in cartilage composition.

An early attempt at linking abnormal knee mechanics following ACLR and early OA correlated anterior tibial shifts in ACLR knees under static loads to signs of cartilage degradation [33]. However, static loads do not capture the dynamic loading situation at the knee during functional use. Observations of gait via motion capture have revealed bilateral kinematic and kinetic changes at the knee following ACLR, including a more extended knee and decreased knee flexion and adduction moments [34, 35]. Some studies report small secondary kinematic changes at the knee, including external tibial rotation of ~2° [36, 37], however these results may be less precise due to errors associated with optical tracking of skin mounted markers. Marker placement and skin motion artifacts can create errors on the order of 2-17 mm, obscuring potentially small kinematic changes [38]. Thus, advanced imaging technologies, such as biplane fluoroscopy and magnetic resonance imaging, have been introduced to more accurately characterize *in vivo* skeletal and joint kinematics.

Biplane fluoroscopy uses two orthogonal high-powered video x-rays to capture joint motion at speeds up to 250 fps with high accuracy (translation and angular precisions of <0.75 mm and 1.0°, respectively [39]). This technology has enabled studies of knee kinematics during quasi-static single leg lunges [40, 41] and downhill running [42]. In studies of ACL-reconstructed knees, consistent shifts toward external tibia rotation of ~3° and medial tibial translation of ~1.5 mm have been measured during downhill running [43, 44]. A longitudinal study of subjects who have undergone unilateral ACLR has also revealed small, but significant, changes in the healthy contralateral limb during running shortly after surgery [44], calling the use of a patient's healthy

contralateral limb as a kinematic control into question. A drawback of biplane fluoroscopy, however, is that it requires highly specialized equipment and exposes the subject to ionizing radiation. As a result, the number of tasks and trials performed by individual subjects is often limited by radiation dosage limits. Further, fluoroscopy is unable to image soft tissue, such that additional imaging modalities (e.g. MRI) must also be used to assess cartilage morphology and composition.

MRI is an attractive imaging modality due to its wide availability, the use of non-ionizing radiation, and its ability to image soft tissue. However, MR image acquisition is much slower than fluoroscopy which requires some modifications to facilitate imaging of dynamic tasks. Real time imaging of joint motion is typically limited to a single planar view of a relatively slow moving task [45-47]. An alternative is to acquire 3D information by imaging bone tissue velocities of multiple slices [2, 48, 49] or volumetric data over a whole volume [50] over repeat motion cycles. Such approaches, often termed 'cine' imaging, requires highly repeatable cyclic motion and a triggering signal to delineate motion cycles. Cine imaging sequences have been developed and widely used to image cardiac motion with electrocariographic signals used to delineate motion cycles [51, 52]. More recent studies have adapted these cine sequences to image musculoskeletal motion [50, 53], which then requires some measure of the joint motion to delineate movement cycles.

Knee kinematics are load-dependent [54, 55], meaning that interpretation of abnormal knee kinematics post-ACLR must take load into account. It has previously been argued that abnormal kinematics may only be present during strenuous activities, such as high speed cutting or downhill running [56]. Indeed, this may explain the lack of significant kinematic differences in some cadaveric experiments [57, 58], which omit complex muscle activation patterns and high inertial

loads present with movement. Using MRI to collect dynamic images of knee motion is challenging due to the size limitations of a MR bore (standard closed bore diameters are 60 cm) and the requirement that the loading device be non-ferrous.

Upright MR bores have been used to measure knee kinematics under static weight-bearing conditions at multiple knee angles [59]. Others have tried to repeat this loading paradigm within a traditional clinical MR bore, which are both more available and have higher field strength, by applying a load directly to the foot via platforms [33]. This loading paradigm however ignores inertial effects and dynamic muscle coordination during motion. Cine PC has been used to capture tibiofemoral and patellofemoral kinematics during voluntary knee flexion-extension against gravity [2, 49]. However, gravity loads are relatively small and may be too low to elicit significant kinematic differences in ACL reconstructed knees. These limitations have led to the development of MR-compatible loading devices, which can deliver higher rotational resistances to mimic the extensive moments experienced at the knee during gait [54]. It has yet to be shown if significant kinematic differences can be elicited in ACLR knees using this loading paradigm. If kinematic differences consistent with previous locomotor studies are able to be observed with dynamic MRI, then the ability to image soft tissue morphology and biomarkers in MRI can be leveraged to measure knee contact, by combining kinematic information with volumetric models of cartilage, and cartilage health.

The goal of this dissertation was to use quantitative and dynamic MR imaging techniques to investigate tibiofemoral kinematics, cartilage contact patterns and biomarkers of cartilage composition in ACL-reconstructed knees. We sought to test the overall hypothesis that altered knee mechanics persist following ACL-reconstruction and contribute to the pathogenesis of early cartilage degeneration. The first chapter introduces the dynamic imaging technology and shows its

potential of measuring *in vivo* knee kinematics in asymptomatic subjects. The following chapter then validates the dynamic imaging technique using a motor-actuated motion phantom which mimics knee motion. Chapter 3 explores using an individual's contralateral knee as a control when assessing joint kinematics. The effect of loading on tibiofemoral and patellofemoral kinematics of ACL-reconstructed knees are then presented in Chapter 4. Chapter 5 expands upon this work by examining how tibial cartilage morphology, biomarkers and contact change in the reconstructed knee. The thesis concludes with a brief summary of the dissertation and provides suggestions for future projects.

References

[1] Stergiou, N., Ristanis, S., Moraiti, C., and Georgoulis, A. D., 2007, "Tibial rotation in anterior cruciate ligament (ACL)-deficient and ACL-reconstructed knees: A theoretical proposition for the development of osteoarthritis," J Sports Med, 37(7), p. 13.

[2] Li, X., Kuo, D., Theologis, A., Carballido-Gamio, J., Stehling, C., Link, T. M., Ma, C. B., and Majumdar, S., 2011, "Cartilage in anterior cruciate ligament-reconstructed knees: MR T1rho and T2-initial experience with 1-year follow-up," Radiology, 258(2), p. 10.

[3] Takeda, Y., Xerogeanes, J. W., Livesay, G. A., Fu, F. H., and Woo, S. L., 1994, "Biomechanical function of the human anterior cruciate ligament," Arthroscopy: The Journal of Arthroscopic & Related Surgery, 10(2), pp. 140-147.

[4] Frank, C. B., and Jackson, D. W., 1997, "Current Concepts Review - The Science of Reconstruction of the Anterior Cruciate Ligament*," The Journal of Bone & Joint Surgery, 79(10), pp. 1556-1576.

[5] Evans, S., Shaginaw, J., and Bartolozzi, A., 2014, "ACL RECONSTRUCTION-IT'S ALL ABOUT TIMING," International journal of sports physical therapy, 9(2), p. 268.

[6] Otto, D., Pinczewski, L. A., Clingeleffer, A., and Odell, R., 1998, "Five-year results of single-incision arthroscopic anterior cruciate ligament reconstruction with patellar tendon autograft," Am J Sports Med, 26(2), pp. 181-188.

[7] Spindler, K. P., Warren, T. A., Callison, J. C., Jr., Secic, M., Fleisch, S. B., and Wright, R. W., 2005, "Clinical outcome at a minimum of five years after reconstruction of the anterior cruciate ligament," J Bone Joint Surg Am, 87(8), pp. 1673-1679.

[8] Bach, B. R., Jr., Tradonsky, S., Bojchuk, J., Levy, M. E., Bush-Joseph, C. A., and Khan, N. H., 1998, "Arthroscopically assisted anterior cruciate ligament reconstruction using patellar tendon autograft. Five- to nine-year follow-up evaluation," Am J Sports Med, 26(1), pp. 20-29.

[9] Hanypsiak, B. T., Spindler, K. P., Rothrock, C. R., Calabrese, G. J., Richmond, B., Herrenbruck, T. M., and Parker, R. D., 2008, "Twelve-year follow-up on anterior cruciate ligament reconstruction: long-term outcomes of prospectively studied osseous and articular injuries," Am J Sports Med, 36(4), pp. 671-677.

[10] van der Hart, C. P., van den Bekerom, M. P., and Patt, T. W., 2008, "The occurrence of osteoarthritis at a minimum of ten years after reconstruction of the anterior cruciate ligament," J Orthop Surg, 3, p. 24.

[11] Liden, M., Sernert, N., Rostgard-Christensen, L., Kartus, C., and Ejerhed, L., 2008, "Osteoarthritic changes after anterior cruciate ligament reconstruction using bone-patellar tendon-bone or hamstring tendon autografts: a retrospective, 7-year radiographic and clinical follow-up study," Arthroscopy, 24(8), pp. 899-908.

[12] Roos, H., Adalberth, T., Dahlberg, L., and Lohmander, L. S., 1995, "Osteoarthritis of the knee after injury to the anterior cruciate ligament or meniscus: the influence of time and age," Osteoarthritis Cartilage, 3(4), pp. 261-267.

[13] Andriacchi, T. P., Mundermann, A., Smith, R. L., Alexander, E. J., Dyrby, C. O., and Koo, S., 2004, "A framework for the in vivo pathomechanics of osteoarthritis at the knee," Ann Biomed Eng, 32(3), p. 11.

[14] Chaudhari, A. M. W., Briant, P. L., Bevill, S. L., Koo, S., and Andriacchi, T. P., 2008, "Knee Kinematics, Cartilage Morphology, and Osteoarthritis after ACL Injury," Med Sci Sports Exerc, 40(2), p. 8.

[15] Koo, S., and Andriacchi, T. P., 2007, "A comparison of the influence of global functional loads vs. local contact anatomy on articular cartilage thickness at the knee," J Biomech, 40(13), pp. 2961-2966.

[16] Li, G., Park, S. E., DeFrate, L. E., Schutzer, M. E., Ji, L., Gill, T. J., and Rubash, H. E., 2005, "The cartilage thickness distribution in the tibiofemoral joint and its correlation with cartilage-to-cartilage contact," Clin Biomech (Bristol, Avon), 20(7), pp. 736-744.

[17] Bullough, P. G., Yawitz, P. S., Tafra, L., and Boskey, A. L., 1985, "Topographical variations in the morphology and biochemistry of adult canine tibial plateau articular cartilage," J Orthop Res, 3(1), pp. 1-16.

[18] Clark, J. M., 1991, "Variation of collagen fiber alignment in a joint surface: a scanning electron microscope study of the tibial plateau in dog, rabbit, and man," J Orthop Res, 9(2), pp. 246-257.

[19] Wong, M., and Carter, D. R., 2003, "Articular cartilage functional histomorphology and mechanobiology: a research perspective," Bone, 33(1), pp. 1-13.

[20] Jurvelin, J., Kiviranta, I., Tammi, M., and Helminen, H. J., 1986, "Effect of physical exercise on indentation stiffness of articular cartilage in the canine knee," Int J Sports Med, 7(2), pp. 106-110.

[21] Saamanen, A. M., Tammi, M., Kiviranta, I., and Helminen, H. J., 1988, "Running exercise as a modulatory of proteoglycan matrix in the articular cartilage of young rabbits," Int J Sports Med, 9(2), pp. 127-133.

[22] Kiviranta, I., Tammi, M., Jurvelin, J., Saamanen, A. M., and Helminen, H. J., 1988, "Moderate running exercise augments glycosaminoglycans and thickness of articular cartilage in the knee joint of young beagle dogs," J Orthop Res, 6(2), pp. 188-195.

[23] Duvvuri, U., Kudchodkar, S., Reddy, R., and Leigh, J. S., 2002, "T1ρ relaxation can assess longitudinal proteoglycan loss from articular cartilage in vitro," Osteoarthritis and Cartilage, 10(11), pp. 838-844.

[24] Mosher, T. J., Dardzinski, B. J., and Smith, M. B., 2000, "Human Articular Cartilage: Influence of Aging and Early Symptomatic Degeneration on the Spatial Variation of T2—Preliminary Findings at 3 T 1," Radiology, 214(1), pp. 259-266.

[25] Su, F., Hilton, J. F., Nardo, L., Wu, S., Liang, F., Link, T. M., Ma, C. B., and Li, X., 2013, "Cartilage morphology and T 1ρ and T 2 quantification in ACL-reconstructed knees: a 2-year follow-up," Osteoarthritis and Cartilage, 21(8), pp. 1058-1067.

[26] Liu, F., Chaudhary, R., Hurley, S. A., Rio, A., Alexander, A. L., Samsonov, A., Block, W. F., and Kijowski, R., 2014, "Rapid multicomponent T2 analysis of the articular cartilage of the human knee joint at 3.0 T," Journal of Magnetic Resonance Imaging, 39(5), pp. 1191-1197.

[27] Liu, F., Choi, K. W., Samsonov, A., Spencer, R. G., Wilson, J. J., Block, W. F., and Kijowski, R., 2015, "Articular Cartilage of the Human Knee Joint: In Vivo Multicomponent T2 Analysis at 3.0 T," Radiology, p. 142201.

[28] Deoni, S. C., Rutt, B. K., Arun, T., Pierpaoli, C., and Jones, D. K., 2008, "Gleaning multicomponent T1 and T2 information from steady-state imaging data," Magnetic Resonance in Medicine, 60(6), pp. 1372-1387.

[29] Reiter, D. A., Lin, P. C., Fishbein, K. W., and Spencer, R. G., 2009, "Multicomponent T2 relaxation analysis in cartilage," Magnetic Resonance in Medicine, 61(4), pp. 803-809.

[30] Haughom, B., Schairer, W., Souza, R. B., Carpenter, D., Ma, C. B., and Li, X., 2012, "Abnormal tibiofemoral kinematics following ACL reconstruction are associated with early cartilage matrix degeneration measured by MRI T1rho," Knee, 19(4), pp. 482-487.

[31] Zabala, M. E., Favre, J., Scanlan, S. F., Donahue, J., and Andriacchi, T. P., 2013, "Three-dimensional knee moments of ACL reconstructed and control subjects during gait, stair ascent, and stair descent," J Biomech, 46, p. 6.

[32] Bush-Joseph, C. A., Hurwitz, D. E., Patel, R. R., Bahrani, Y., Garretson, R., Bach, B. R., and Andriacchi, T. P., 2001, "Dynamic function after anterior cruciate ligament reconstruction with autologous patellar tendon," Am J Sports Med, 29(1), pp. 36-41.

[33] Scanlan, S. F., Chaudhari, A. M., Dyrby, C. O., and Andriacchi, T. P., 2010, "Differences in tibial rotation during walking in ACL reconstructed and healthy contralateral knees," J Biomech, 43(9), pp. 1817-1822.

[34] Georgoulis, A. D., Ristanis, S., Chouliaras, V., Moraiti, C., and Stergiou, N., 2007, "Tibial rotation is not restored after ACL reconstruction with a hamstring graft," Clin Orthop Relat Res, 454, pp. 89-94.

[35] Sati, M., De Guise, J., Larouche, S., and Drouin, G., 1996, "Quantitative assessment of skin-bone movement at the knee," Knee, 3(3), pp. 121-138.

[36] Anderst, W., Zauel, R., Bishop, J., Demps, E., and Tashman, S., 2009, "Validation of three-dimensional model-based tibio-femoral tracking during running," Med Eng Phys, 31(1), pp. 10-16.

[37] Li, G., Van de Velde, S. K., and Bingham, J. T., 2008, "Validation of a non-invasive fluoroscopic imaging technique for the measurement of dynamic knee joint motion," J Biomech, 41(7), pp. 1616-1622.

[38] DeFrate, L. E., Sun, H., Gill, T. J., Rubash, H. E., and Li, G., 2004, "In vivo tibiofemoral contact analysis using 3D MRI-based knee models," J Biomech, 37(10), pp. 1499-1504.

[39] Tashman, S., and Anderst, W., 2003, "In-Vivo Measurement of Dynamic Joint Motion Using High Speed Biplane Radiography and CT: Application to Canine ACL Deficiency," J Biomech Eng, 125(2), p. 238.

[40] Tashman, S., 2004, "Abnormal Rotational Knee Motion During Running After Anterior Cruciate Ligament Reconstruction," American Journal of Sports Medicine, 32(4), pp. 975-983.

[41] Hofbauer, M., Thorhauer, E. D., Abebe, E., Bey, M., and Tashman, S., 2014, "Altered Tibiofemoral Kinematics in the Affected Knee and Compensatory Changes in the Contralateral Knee After Anterior Cruciate Ligament Reconstruction," Am J Sports Med, p. 0363546514549444.

[42] Draper, C. E., Santos, J. M., Kourtis, L. C., Besier, T. F., Fredericson, M., Beaupre, G. S., Gold, G. E., and Delp, S. L., 2008, "Feasibility of using real-time MRI to measure joint kinematics in 1.5T and open-bore 0.5T systems," J Magn Reson Imaging, 28(1), pp. 158-166.

[43] Draper, C. E., Besier, T. F., Santos, J. M., Jennings, F., Fredericson, M., Gold, G. E., Beaupre, G. S., and Delp, S. L., 2009, "Using real-time MRI to quantify altered joint kinematics

in subjects with patellofemoral pain and to evaluate the effects of a patellar brace or sleeve on joint motion," J Orthop Res, 27(5), pp. 571-577.

[44] Lin, C.-C., Zhang, S., Frahm, J., Lu, T.-W., Hsu, C.-Y., and Shih, T.-F., 2013, "A slice-to-volume registration method based on real-time magnetic resonance imaging for measuring three-dimensional kinematics of the knee," Medical Physics, 40, p. 102302.

[45] Borotikar, B. S., Sipprell III, W. H., Wible, E. E., and Sheehan, F. T., 2012, "A methodology to accurately quantify patellofemoral cartilage contact kinematics by combining 3D image shape registration and cine-PC MRI velocity data," J Biomech, 45(6), pp. 1117-1122.

[46] Seisler, A. R., and Sheehan, F. T., 2007, "Normative three-dimensional patellofemoral and tibiofemoral kinematics: A dynamic, in vivo study," IEEE Trans Biomed Eng, 54(7), p. 9.

[47] Barrance, P. J., Williams, G. N., Snyder-Mackler, L., and Buchanan, T. S., 2006, "Altered knee kinematics in ACL-deficient non-copers: a comparison using dynamic MRI," J Orthop Res, 24(2), pp. 132-140.

[48] Kaiser, J., Bradford, R., Johnson, K., Wieben, O., and Thelen, D. G., 2013, "Measurement of tibiofemoral kinematics using highly accelerated 3D radial sampling," Magnetic Resonance in Medicine, 69(5), pp. 1310-1316.

[49] Wentland, A. L., Wieben, O., François, C. J., Boncyk, C., Munoz Del Rio, A., Johnson, K. M., Grist, T. M., and Frydrychowicz, A., 2013, "Aortic pulse wave velocity measurements with undersampled 4D flow-sensitive MRI: comparison with 2D and algorithm determination," Journal of Magnetic Resonance Imaging, 37(4), pp. 853-859.

[50] Kecskemeti, S., Johnson, K., Wu, Y., Mistretta, C., Turski, P., and Wieben, O., 2012, "High resolution three-dimensional cine phase contrast MRI of small intracranial aneurysms using a stack of stars k-space trajectory," Journal of Magnetic Resonance Imaging, 35(3), pp. 518-527.

[51] Sheehan, F. T., Zajac, F. E., and Drace, J. E., 1998, "Using cine phase contrast magnetic resonance imaging to non-invasively study in vivo knee dynamics," J Biomech, 31(1), p. 6.

[52] Westphal, C. J., Schmitz, A., Reeder, S. B., and Thelen, D. G., 2013, "Load-dependent variations in knee kinematics measured with dynamic MRI," J Biomech.

[53] Victor, J., Labey, L., Wong, P., Innocenti, B., and Bellemans, J., 2010, "The influence of muscle load on tibiofemoral knee kinematics," J Orthop Res, 28(4), pp. 419-428.

[54] Tashman, S., Kopf, S., and Fu, F. H., 2008, "The Kinematic Basis of ACL Reconstruction," Oper Tech Sports Med, 16(3), pp. 116-118.

[55] Kondo, E., Merican, A. M., Yasuda, K., and Amis, A. A., 2011, "Biomechanical comparison of anatomic double-bundle, anatomic single-bundle, and nonanatomic single-bundle anterior cruciate ligament reconstructions," Am J Sports Med, 39(2), pp. 279-288.

[56] Bedi, A., Musahl, V., Steuber, V., Kendoff, D., Choi, D., Allen, A. A., Pearle, A. D., and Altchek, D. W., 2011, "Transtibial Versus Anteromedial Portal Reaming in Anterior Cruciate Ligament Reconstruction: An Anatomic and Biomechanical Evaluation of Surgical Technique," Arthroscopy: The Journal of Arthroscopic & Related Surgery, 27(3), pp. 380-390.

[57] Draper, C. E., Besier, T. F., Fredericson, M., Santos, J. M., Beaupre, G. S., Delp, S. L., and Gold, G. E., 2011, "Differences in patellofemoral kinematics between weight-bearing and non-weight-bearing conditions in patients with patellofemoral pain," J Ortho Research.

[58] Borotikar, B. S., and Sheehan, F. T., 2013, "In vivo patellofemoral contact mechanics during active extension using a novel dynamic MRI-based methodology," Osteoarthritis and Cartilage, p. 9.

Chapter 1

Measurement of 3D Tibiofemoral Kinematics using Volumetric SPGR-VIPR Imaging

Jarred Kaiser, Robert Bradford, Kevin Johnson, Oliver Wieben, Darryl G. Thelen

(Note that this chapter is published in Magnetic Resonance in Medicine)

Abstract

This study investigated the use of dynamic, volumetric MRI to measure 3D skeletal motion. Ten healthy subjects were positioned on a MR-compatible knee loading device and instructed to harmonically flex and extend their knee at 0.5 Hz. The device induced active quadriceps loading with knee flexion, similar to the load acceptance phase of gait. Volumetric images were continuously acquired for five minutes using a 3D cine SPGR sequence in conjunction with vastly under-sampled isotropic projections (SPGR-VIPR). Knee angle was simultaneously monitored and used retrospectively to sort images into 60 frames over the motion cycle. High resolution static knee images were acquired and segmented to create subject-specific models of the femur and tibia. At each time frame, bone positions and orientations were determined by automatically registering the skeletal models to the dynamic images. Three-dimensional tibiofemoral translations and rotations were consistent across healthy subjects. Internal tibia rotations of $7.8 \pm 3.5°$ were present with $35.8 \pm 3.8°$ of knee flexion, a pattern consistent with knee kinematic measures during walking. We conclude that VIPR volumetric imaging is a promising approach for non-invasively measuring 3D joint kinematics, which may be useful for assessing cartilage contact and investigating the causes and treatment of joint abnormalities. Keywords: dynamic imaging; knee mechanics; joint motion.

Introduction

Magnetic resonance (MR) imaging is routinely used to identify structural damage (e.g. ligament tears and cartilage defects) and inflammation in musculoskeletal joints (1). However, imaging is normally performed in unloaded static postures, preventing insight into the function of joint tissues during normal movement (2). This is important to consider since the causes and symptoms of musculoskeletal pathology are often linked to function. For example, anterior knee pain can result from patellar maltracking that is only evident with active quadriceps loading (3,4). Further, abnormal knee kinematics in reconstructed knees may alter cartilage loading in a way that contributes to osteoarthritis risk (5).

Dynamic MR imaging is a powerful approach to measure functional *in vivo* joint motion (2), which can in turn be coupled with high resolution musculoskeletal models to characterize joint rotation axes (6), lever arms of muscles (7) and cartilage contact (8). Prior MR studies have used real-time (3), cine phase contrast (PC) (9) and fast multi-planar (10) sequences to measure skeletal kinematics. Real-time imaging represents an ideal approach, but current temporal and spatial constraints only allow for a single planar image of relatively slow motion to be captured (3,11). Cine PC imaging has been used to measure three-dimensional tissue velocities, which are then integrated to estimate 3D skeletal motion (9,12,13). However, only a single cine PC image plane can be acquired in reasonable scan times, making it challenging to register absolute skeletal position and orientation in 3D space. In addition, numerical integration drift may contribute to errors at the position level. Dynamic anatomical scans of multiple, parallel planes provide 3D data to which high resolution skeletal models can be registered (10). Again however, only a few imaging planes can be captured in reasonable scan times, which likely limits the accuracy with which 3D orientation and position can be ascertained.

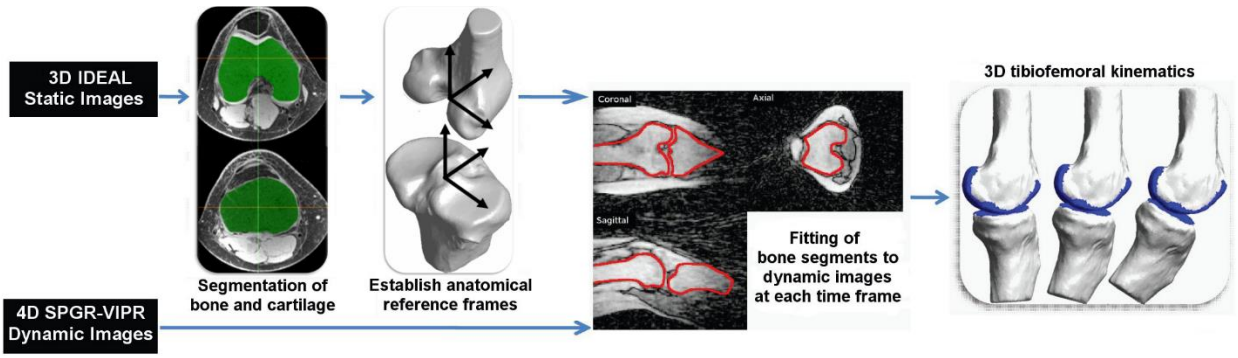

Figure 1: Flow chart of dynamic imaging approach to track tibiofemoral kinematics. Volumetric models of the femur and tibia are segmented from static images, and then registered with dynamic SPGR-VIPR images at each frame of the motion. The final result is a 3D reconstruction of tibiofemoral kinematics.

The purpose of this study was to investigate the feasibility of using a novel dynamic, volumetric MR imaging sequence to measure 3D skeletal motion at the knee. Volumetric imaging is achieved using radially undersampled trajectories, termed vastly under-sampled isotropic projection (VIPR), which reduces scan time to a reasonable level while maintaining excellent resolution (14). In this study, we show that high resolution skeletal models derived from static images can be registered to the volumetric VIPR images, thereby providing quantitative measures of skeletal position and orientation throughout a cyclic motion (Fig. 1). The relevance of such information for investigating *in vivo* joint mechanics and pathologies is discussed.

Methods

Subjects

We collected images bilaterally on ten healthy subjects (five females, five males, age: 24.6 ± 3.2 y; mass: 65.1 ± 5.0 kg) who had no history of past knee injuries, pathologies, surgeries or chronic knee pain. Informed consent was obtained prior to testing according to a protocol approved by the University of Wisconsin's Health Sciences Institutional Review Board.

Knee Flexion-Extension Task

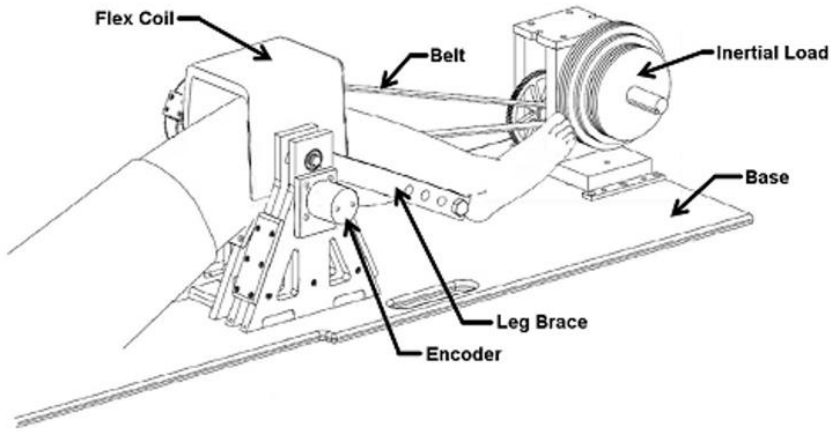

Figure 2: Subjects performed cyclic knee flexion/extension in an MR-compatible loading device. A set of rotating inertial discs induces active quadriceps loading with knee flexion. A MR-compatible encoder is used to continuously measure knee angle throughout the dynamic imaging scan.

Subjects were asked to perform a cyclic knee flexion-extension task. Subjects were positioned supine in a MR-compatible dynamic knee loading device (15), with the knee aligned to a leg brace rotation axis (Fig. 2). An inertial load was generated by a set of rotating disks that were geared to the knee rotation axis. The device induces quadriceps loading with knee flexion, as seen in the stance phase of gait (16,17).

The subjects first practiced the task in a laboratory, while external loading and knee motion were monitored to assess the repeatability and biomechanics of the task. Subjects were asked to flex and extend their knees at 0.5 Hz for five minutes. A semi-circular structure was placed around the leg to mimic the bore size of the MR scanner used in this study. Applied load was measured at 1000 Hz using load cells embedded in the top and bottom belts (500lb LCM-300, Futek, Irvine, California). An MR-compatible rotary encoder (Micronor, Newbury Park, California) placed on the knee axis shaft was used to monitor knee flexion angle at 50 Hz. Load and angle data were used together with an inverse dynamics analysis of the lower leg to ascertain the net internal knee extensor moment throughout the task.

MR Image Acquisition

The imaging session involved the acquisition of two volumetric data sets: a) high resolution static images which were segmented to obtain volumetric models of the femur and tibia, and b) lower resolution dynamic images which were continuously acquired while the subject performed the cyclic movement within the bore of a scanner.

High resolution static imaging of the subject's knee was performed using a 3D IDEAL SPGR sequence (512 x 512 x 304 cubic voxels with 0.37 mm spacing, 9 minute scan) in a clinical 3.0T MR scanner (MR750, General Electric Healthcare, Waukesha, Wisconsin). For these scans, an 8-channel phased-array extremity coil (Precision Eight TX/TR High Resolution Knee Array; Invivo, Orlando, Fla.) was positioned about the knee. The tibia and femur were manually segmented (MIMICS, Materialise Group, Leuven, Belgium) from the static images to create subject specific bone models. The resulting models were smoothed (Geomagic, Research Triangle Park, North Carolina) and decimated to approximately 15,000 vertices per bone. Local anatomical coordinate systems were separately established for the femur and tibia using a localization algorithm that establishes orthogonal anatomical axes for each bone based on geometric and inertial properties of the 3D segments (18). The repeatability and accuracy of this approach has previously been established for the knee (18).

Dynamic MR images of the knee were acquired while the subjects performed the cyclic, repeatable knee flexion-extension task within the bore of a scanner. A single channel General Purpose Flex Coil (General Electric Healthcare, Waukesha, Wisconsin) was attached to the loading device and held in a fixed position over the knee, with the coil parallel to the primary magnetic field. The subject was instructed to flex and extend their knee at 0.5 Hz for five minutes. Cadence was maintained via a metronome played over headphones. Volumetric images were continuously acquired using a spoiled gradient-echo sequence in conjunction with vastly under-

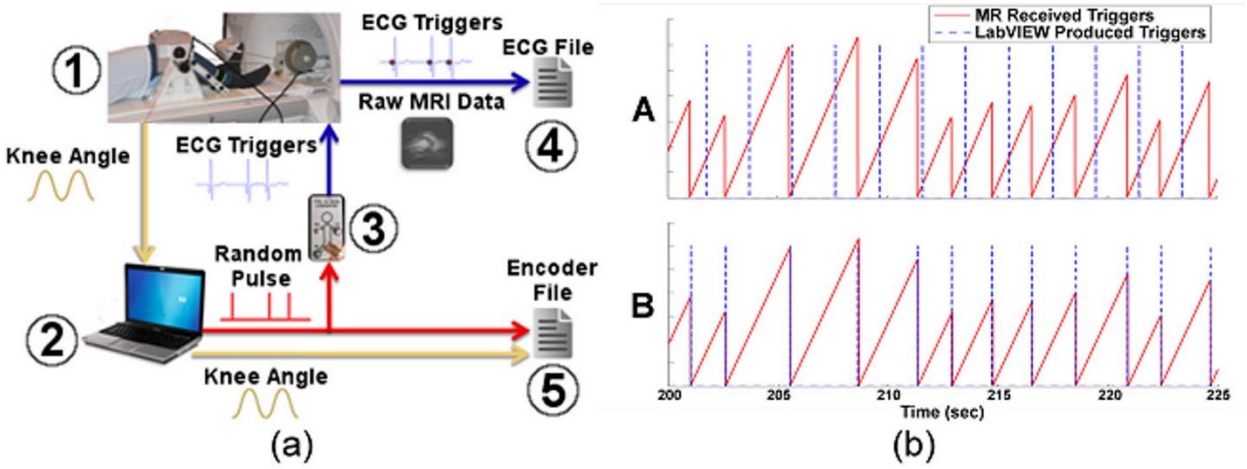

Figure 3: a. Data acquisition during dynamic knee motion. Knee angle (1) is monitored in real-time (2). Simultaneously, a random pulse is generated and converted into an artificial ECG signal (3) that is monitored via the scanner (4). Generated pulse and knee angle are saved separate from MRI data (5). ECG triggers are subsequently used for retrospective alignment of the knee angle and image data.
b. Unaligned (A) and aligned (B) triggers as recorded by the MR scanner and LabVIEW. The randomly spaced triggers were easily aligned in post-hoc analysis, allowing for synchronization of the encoder and image information.

sampled isotropic projection reconstruction (SPGR-VIPR). The order of the projection angles was determined with a pseudo-random 2D-bit reverse algorithm, which allows retrospective selection of projection numbers per time frame with an almost even distribution of angles. Relevant imaging parameters include: 1.5 mm isotropic acquired resolution, TR/TE = 4 ms/1.4 ms, flip angle= 8°, receiver bandwidth = 62.5 kHz, 75,000 unique radial lines, 48 cm field of view, scan time = 5 minutes.

Knee flexion angle was measured in the scanner via the MR-compatible rotary encoder mounted at the leg brace shaft. The encoder data was used to synchronize the image and motion data to allow for image reconstruction based on knee position. To do this, a LabVIEW (National Instruments, Austin, Texas) program was used to monitor encoder counts at 50 Hz while generating randomly timed pulse triggers that were read into the scanner's cardiac gating system

(Fig. 3). A custom MATLAB routine was used to retrospectively align the randomly generated triggers in LabVIEW with those measured by the MR gating module, allowing for both scaling corrections and a bulk time offset between the scanner-based and encoder-based times. Once aligned, the encoder data were interpolated to match the scanner-based time values, enabling the separation of all scanner-based data into position-based cycles. The beginning and end of each cycle was defined as the point at which the subject, during extension, reached the overall mean knee flexion angle. Then, a percent value was assigned to each projection based on when the projection was acquired in the flexion-extension cycle. Scanner matrix data was sorted by percent cycle and a vector of the reordered projection reference numbers was output to a separate file.

Image reconstruction software reorganized the raw image data based on the reordered projections and binned the data into 60 equally sized 3D image frames. Each frame represented an average of image data acquired during 1.67%, or 33 ms, of the 2 s flexion-extension cycle. Each 3D image was reconstructed utilizing a conjugate gradient least squares minimization (19). Unlike standard gridding reconstructions, this iterative technique did not require sampling density compensation, which is difficult to obtain for the irregularly spaced sampling present with retrospectively motion gating.

Registering Subject Specific Bone Models

To establish a rough registration in the first 3D dynamic image frame, we first manually aligned anatomical landmarks that were visible in both the models and the image. We then used Powell's numerical optimization method (20) to align each bone segment to the dynamic image data at each time frame. This was done by finding the bone segment position and orientation that minimized the sum-squared intensities of the dynamic image at the locations of the model vertices. This routine drives the vertices of the bone segment models to the dark, low intensity outlines of

the bones in the dynamic images. The search region was bounded with a penalty function to prevent a solution in the low-intensity regions outside of the limb. The optimization solution for one frame was then used recursively as the initial guess for bone positions and orientations in the subsequent frame. This process was repeated for all 60 frames for each bone segment. The final result was a set of 3D translational and angle trajectories for the femur and tibia over the motion cycle. Kinematic trajectories were subsequently low-pass filtered with a 5 Hz cutoff frequency, which is ten times higher than the nominal cycle rate. Knee angles were characterized by three successive body-fixed rotations that describe the orientation of the tibia relative to the femur (21).

Influence of Dynamic Image Reconstruction Parameters

We separately performed a sensitivity analysis to assess the effects of scan time and number of reconstructed frames on the measured knee kinematics. Shorter scan times were simulated by undersampling the full acquired data by factors of 2, 3, and 4 to nominally represent information that would be obtained with scan times of 2.5, 1.67, and 1.25 minutes. Each cyclic image set was initially binned into 60 frames. We then assessed the effect of binning the full data of three subjects into 30, 45, and 75 frames. The root mean squared difference of kinematic measures from the nominal condition (five minute scan time, 60 frames) was used to quantify the effect of shorter scan times and different number of frames.

Results

Repeatability

All subjects maintained a desired average cyclic motion period of 2.0 s, with standard deviations of less than 40 ms over 150 consecutive cycles. The range of knee flexion achieved in the scanner by the subjects was 35.8 ± 3.8°. For individual subjects, the peak knee flexion and

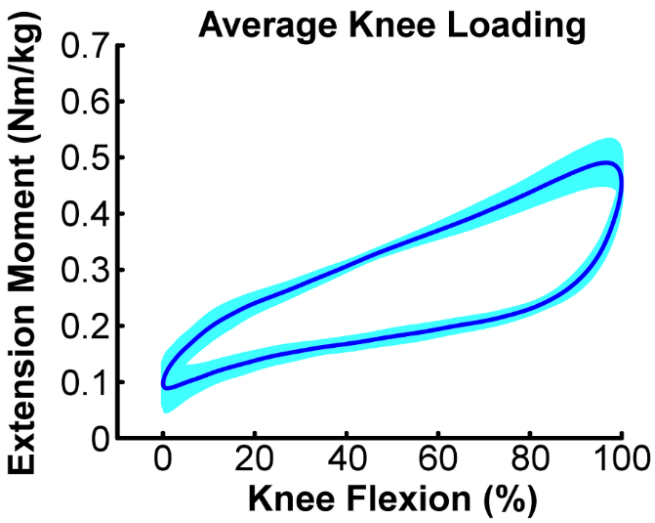

Figure 4: Average (± 1 sd) knee extension moment induced over 150 consecutive knee flexion-extension motion cycles.

extension angles exhibited standard deviations of <0.7° over repeat cycles. The loading device induced maximum knee extension moments of ~0.5 Nm/kg, with peak loading coinciding with the knee flexion phase of the motion (Fig. 4).

Tibiofemoral Kinematics

The optimization routine produced bone positions and orientations that visually agree well with the dynamic image volumes (Fig. 5). The tibiofemoral kinematic trajectories were generally similar across knees, with all subjects exhibiting little frontal plane motion and internal tibia

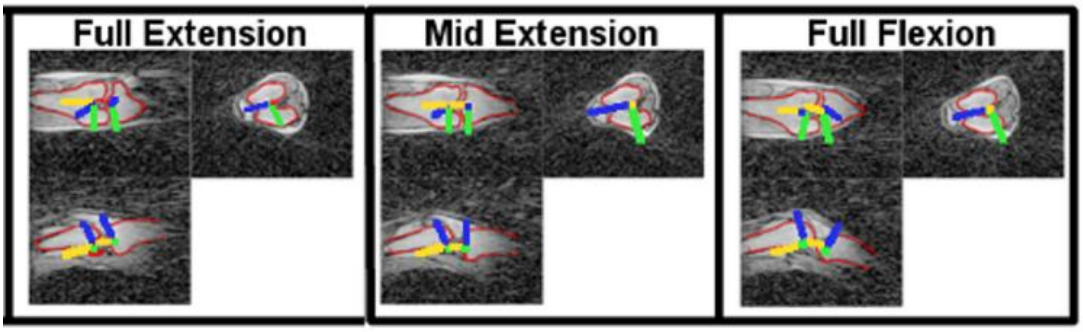

Figure 5: Projections of the registered femur and tibia bone models (red lines) in the coronal (top left), axial (top right) and sagittal (bottom left) image planes. Local reference frames for both the femur and tibia are shown.

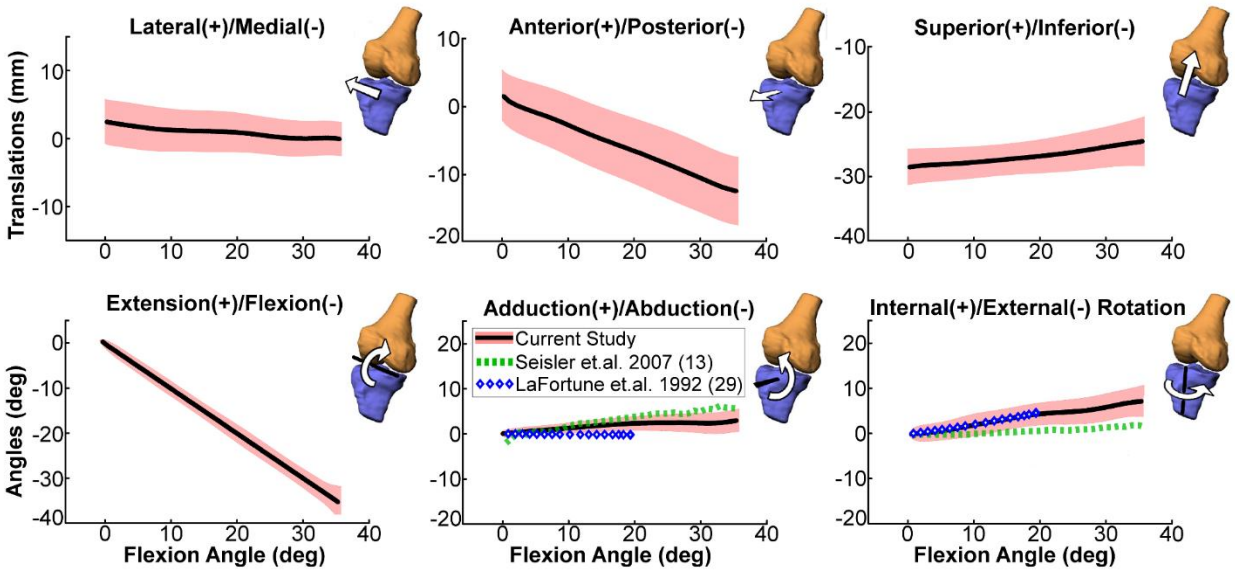

Figure 6: Ensemble average tibiofemoral kinematics (shaded curves represent mean ±1 s.d.) for the dominant knee of ten asymptomatic subjects over a flexion-extension motion cycle as measured using SPGR-VIPR. For comparison, the average adduction and rotation angle data measured by cine-PC MRI during unloaded knee flexion-extension (13) and via intra-cortial traction pins during normal gait (29) are shown. Our data shows greater internal tibia rotation with knee flexion compared to cine PC, which may be related to greater quadriceps activation induced by our loading device (35).

rotation with knee flexion (Fig. 6). The magnitude of internal tibia rotation averaged 7.8 ± 3.5° across subjects. The primary tibiofemoral translations were in the sagittal plane, with the tibia reference frame translating posterior and superior with knee flexion.

Dynamic Image Reconstruction

Varying the number of reconstruction frames between 30 and 75 had a relatively small effect on the knee kinematics obtained, with a maximum root-mean-squared difference of <1° in tibia angles over the motion cycle (Fig. 7). Reducing scan times had a greater effect on tibia rotation measures than adduction or flexion angles (Fig. 7). On average, changes in adduction and

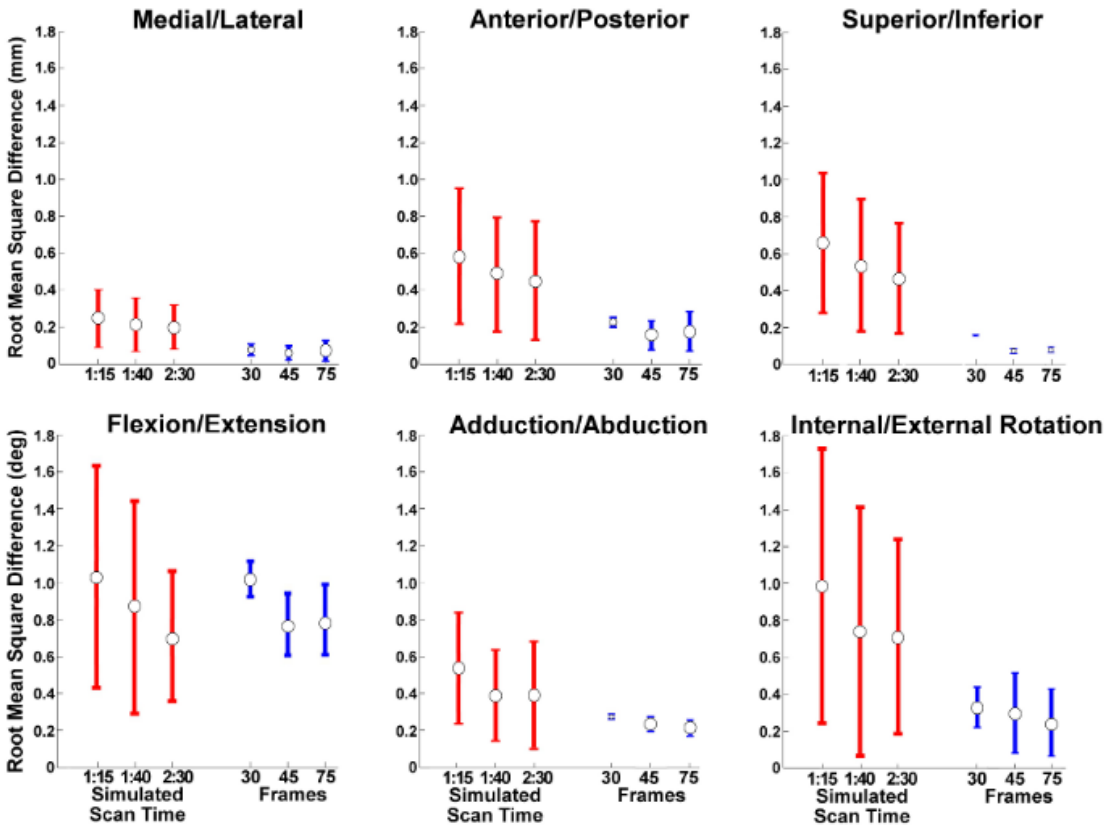

Figure 7: Effects of scan time (for all subjects) and the number of reconstructed frames (three subjects) on tibiofemoral kinematics. The values shown are the average (±1 s.d.) root mean square difference in joint angles and translations, with respect to a 5:00 minute scan reconstructed to 60 frames. Acceleration factors of 2, 3, and 4 correspond to simulated scan times of 2:30, 1:40, and 1:15 respectively.

rotation angles varied 0.4°and 0.7° from the nominal case. Tibia translations remained within 0.75 mm root mean squared difference with the nominal case.

Discussion

In this study, we have demonstrated the potential for using volumetric SPGR-VIPR imaging to track *in vivo* skeletal kinematics. A key to our approach is the use of radially under-sampled (VIPR) acquisitions, which allows one to obtain dynamic images with isotropic voxel resolution within a reasonable scan time. A second key was the simultaneous measurement of knee motion, which was used to retrospectively synchronize the dynamic images to the cyclic task. We

showed that high resolution bone models could be co-registered to the dynamic images, which allows for the quantitative assessment of skeletal position and orientation in three dimensions.

Previous studies have used cine phase-contrast (3) sequences to measure cyclic skeletal motion. However, Cartesian acquisition techniques used in these prior studies limited the number of imaging planes that could be acquired in reasonable scan times. For example, Seisler and Sheehan used a 2.75 minute sequence to image a single plane of tibiofemoral motion with 1.2 x 1.8 mm spatial resolution and 73.6 ms temporal resolution. We note that despite acquiring a single imaging plane, PC imaging does allow one to measure 3D velocities, which can be numerically integrated to estimate how 3D skeletal position and orientation evolve over time (9). A phantom study using cine PC reported average tracking errors of 0.33 mm for medial-lateral translation, 0.25 mm for anterior-posterior translation, and 0.9° for internal-external rotation (22). These errors may be attributable to numerical drift associated with integration. In addition, when cine-PC is used for *in vivo* imaging, there is potential for additional bias errors that arise from the inherent challenge of defining 3D anatomical reference frames by digitizing points in planar images (23).

The current standard for 3D dynamic imaging of *in vivo* skeletal motion is biplane fluoroscopy, which can be collected at high frame rates during functional tasks such as walking, running and stair climbing (24-26). When tantalum beads are embedded in the bones, fluoroscopy data can be used to track skeletal translations and orientation with a precision of 0.12 mm (24). Model-based tracking using biplane fluoroscopy is slightly less accurate with reported errors of less than 1° and 0.7 mm at the knee (24). While the real-time imaging and low errors are impressive, fluoroscopy requires highly specialized set-ups, exposes subjects to ionizing radiation and does not directly provide soft tissue information. In contrast, dynamic MRI is promising due to its wide availability, safety, and capacity to simultaneously image soft tissue and bone

morphology. These characteristics make dynamic MRI a potentially more viable option for clinical practice and longitudinal studies, in which one may wish to image skeletal motion at multiple time points to assess how joint mechanics adapt following musculoskeletal injuries, surgical treatment and/or rehabilitation. Additional soft tissue information could also provide insight into cartilage contact and tendon/ligament strain (27).

The VIPR acquisition in our technique offers some intrinsic advantages over standard Cartesian acquisitions. The radial undersampling allows for scan time reductions and for flexible retrospective gating while supporting relatively high spatial and temporal resolution. For comparison, a fully sampled Cartesian-based SPGR sequence with similar coverage and spatial and temporal resolution would require 102 (160 x 160 x 60 x 4 ms) minutes compared to our current scan time of five minutes using SPGR-VIPR. With radial sampling and pseudo-random view ordering, data sorting can be accomplished retrospectively with offline reconstruction. This is not possible with a Cartesian acquisition which would require real-time prospective gating with a position feedback loop or dramatic oversampling of the required phase encodings.

In this study, we imaged knee kinematics for five consecutive minutes over 150 cycles of knee flexion/extension performed at 0.5 Hz. We assessed inter-cycle repeatability via external kinematic and kinetic measures, which showed the subjects exhibited relatively low variations in cycle times, knee range of motion and net internal knee moments over the 150 repeat cycles (Fig. 4). The peak knee extension moment was ~0.5 Nm/kg, which is at the lower end of the magnitudes seen in the load acceptance phase of gait (17,28). Hence, the imaging task can be considered somewhat comparable to the quadriceps loads experienced during walking, and thus would not be considered overly fatiguing when performed for five minutes.

The measured non-sagittal knee angles agreed very well with knee motion measured using intra-cortical traction pins during gait (29) (Fig. 6). In particular, all knees exhibited internal tibia rotation with knee flexion (i.e. the screw-home mechanism) (30). We measured greater internal rotation than a prior cine PC study of the unloaded knee during flexion (Fig. 6). This difference could be attributed to the activation of quadriceps with knee flexion that was induced by our loading device (31), supporting the use of inertial loading to mimic functional knee loading seen in gait.

The sensitivity of the derived kinematics to scan time duration was sufficiently low, such that it may be feasible to reduce scan times to below two minutes without degrading the knee kinematic information obtained (Fig. 7). We note that the current results use a single channel flex coil that was available at the time of the study. We expect that the higher signal-to-noise ratio (SNR) achievable on multi-channel flex coils would further improve dynamic image quality, which could be used to either enhance image quality or further reduce scan time.

Our process uses a cine acquisition, which means that an average knee kinematic pattern is obtained, rather than a real-time assessment of each motion cycle. Hence, it would not be feasible to use the SPGR-VIPR approach to assess infrequent or non-repeatable motion abnormalities. However, an assessment of normative kinematic patterns may well be relevant for understanding the link between chronic loading and the progression of joint disease. For example, early-onset osteoarthritis (OA) is often seen within 10-15 years in patients who undergo surgical reconstruction of the anterior cruciate ligament (32). Recent literature suggests that abnormal joint kinematics can develop over time, and may contribute to OA development by inducing a chronic deviation from normative cartilage loading patterns (33). The dynamic MR imaging techniques illustrated here provide a potential mechanism by which to investigate this hypothesis by tracking

longitudinal changes in tibiofemoral kinematics. In addition, it may be feasible to couple high resolution bone and cartilage models together with the kinematic data to quantitatively assess cartilage contact patterns (Fig. 1). A prior sensitivity study found that cartilage contact estimates based on proximity functions are highly dependent on the accuracy of the measured knee kinematics (34). To get a quantitative assessment of the sensitivity, we investigated how a 0.2 mm deviation in any of the three translational degrees of freedom would affect the estimated center of cartilage contact using bone/cartilage models from a subject in this study. This analysis showed that a 0.2 mm deviation induced up to a 1.2 mm change in center of contact location, with an average shift of 0.5 mm. Given this level of accuracy exceeds current dynamic MRI techniques (22), an important next step is to use a 3D motion phantom to assess absolute accuracy of kinematic measures obtained with SPGR-VIPR to determine if resolution is sufficient to assess cartilage contact.

In summary, this paper describes a novel dynamic volumetric imaging (SPGR-VIPR) approach to measure *in vivo* knee kinematics. Initial results are very promising, with good agreement seen between our image-based measures and kinematics measured using more invasive techniques during gait (13,29). Hence, dynamic volumetric imaging provides a potentially powerful approach to quantitatively characterize changes in skeletal joint mechanics that can arise with injury, pathology and treatment.

Acknowledgements

The authors gratefully acknowledge the contributions of Rachel Lenhart, Kelli Hellenbrand, Sara Pladziewicz, Christopher Westphal, Richard Kijowski, MD, and Kwang Won Choi, and the financial support of NIH AR056201, NSF 0966535 and the Robert W. Bolz Distinguished Graduate Fellowship Program.

References

1. Carpenter RD, Majumdar S, Ma CB. Magnetic resonance imaging of 3-dimensional in vivo tibiofemoral kinematics in anterior cruciate ligament-reconstructed knees. Arthroscopy 2009;25(7):760-766.
2. Gold GE. Dynamic and functional imaging of the musculoskeletal system. Seminar in Musculoskeletal Radiology 2003;7(4):4.
3. Draper CE, Besier TF, Santos JM, Jennings F, Fredericson M, Gold GE, Beaupre GS, Delp SL. Using real-time MRI to quantify altered joint kinematics in subjects with patellofemoral pain and to evaluate the effects of a patellar brace or sleeve on joint motion. J Orthop Res 2009;27(5):571-577.
4. McNally EG, Ostlere SJ, Pal C, Phillips A, Reid H, Dodd C. Assessment of patellar maltracking using combined static and dynamic MRI. Eur Radiol 2000;10:5.
5. Tashman S, Kopf S, Fu FH. The Kinematic Basis of ACL Reconstruction. Oper Tech Sports Med 2008;16(3):116-118.
6. Sheehan FT. The finite helical axis of the knee joint (a non-invasive in vivo study using fast-PC MRI). J Biomech 2007;40(5):1038-1047.
7. Sheehan FT. The 3D patellar tendon moment arm: quantified in vivo during volitional activity. J Biomech 2007;40(9):1968-1974.
8. Patel VV, Hall K, Ries M, Lotz J, Ozhinsky E, Lindsey C, Lu Y, Majumdar S. A three-dimensional MRI analysis of knee kinematics. J Ortho Research 2004;22(2):283-292.
9. Sheehan FT, Zajac FE, Drace JE. Using cine phase contrast magnetic resonance imaging to non-invasively study in vivo knee dynamics. J Biomech 1998;31(1):6.

10. d'Entremont A, Nordmeyer-Massner J, Bos C, Wilson D, Pruessmann K. A dynamic measurement method for knee biomechanics. 2011; Montreal, Quebec, Canada.

11. Draper CE, Santos JM, Kourtis LC, Besier TF, Fredericson M, Beaupre GS, Gold GE, Delp SL. Feasibility of using real-time MRI to measure joint kinematics in 1.5T and open-bore 0.5T systems. J Magn Reson Imaging 2008;28(1):158-166.

12. Zhu Y, Drangova M, Pelc N. Fourier tracking of myocardial motion using cine PC data. Magnetic Resonance in Medicine 1996;35(4):10.

13. Seisler AR, Sheehan FT. Normative three-dimensional patellofemoral and tibiofemoral kinematics: A dynamic, in vivo study. IEEE Trans Biomed Eng 2007;54(7):9.

14. Johnson KM, Lum DP, Turski PA, Block WF, Mistretta CA, Wieben O. Improved 3D phase contrast MRI with off-resonance corrected dual echo VIPR. Magnetic Resonance in Medicine 2008;60(1):8.

15. Silder A, Westphal CJ, Thelen DG. A magnetic resonance-compatible loading device for dynamically imaging shortening and lengthening muscle contraction mechanics. J Med Devices 2009;3(3):53.

16. Winter D, Yack H. EMG profiles during normal human walking: stride-to-stride and inter-subject variability. Electroencephalography and clinical Neurophysiology 1987;67(5):402-411.

17. Besier TF, Fredericson M, Gold GE, Beaupre GS, Delp SL. Knee muscle forces during walking and running in patellofemoral pain patients and pain-free controls. J Biomech 2009;42(7):8.

18. Miranda DL, Rainbow MJ, Leventhal EL, Crisco JJ, Fleming BC. Automatic determination of anatomical coordinate systems for three-dimensional bone models of the isolated human knee. J Biomech 2010;43(8):4.

19. Pruessmann KP, Weiger M, Börnert P, Boesiger P. Advances in sensitivity encoding with arbitrary k-space trajectories. Magnetic Resonance in Medicine 2001;46(4):638-651.

20. Powell MJD. An efficient method for finding the minimum of a function of several variables without calculating derivatives. The Computer Journal 1964;7(2):155.

21. Grood E, Suntay W. A joint coordinate system for the clinical description of three-dimensional motions: application to the knee. J Biomech Eng 1983;105(2):9.

22. Behnam AJ, Herzka DA, Sheehan FT. Assessing the accuracy and precision of musculoskeletal motion tracking using cine-PC MRI on a 3.0T platform. J Biomech 2011;44(1):193-197.

23. Morton NA, Maletsky LP, Pal S, Laz PJ. Effect of variability in anatomical landmark location on knee kinematic description. J Ortho Research 2007;25(9):1221-1230.

24. Anderst W, Zauel R, Bishop J, Demps E, Tashman S. Validation of three-dimensional model-based tibio-femoral tracking during running. Med Eng Phys 2009;31(1):10-16.

25. Tashman S. Abnormal Rotational Knee Motion During Running After Anterior Cruciate Ligament Reconstruction. American Journal of Sports Medicine 2004;32(4):975-983.

26. Li G, Kozanek M, Hosseini A, Liu F, Van de Velde SK, Rubash HE. New fluoroscopic imaging technique for investigation of 6DOF knee kinematics during treadmill gait. J Orthop Surg Res 2009;4:6.

27. Sheehan FT, Drace JE. Human patellar tendon strain: a noninvasive, in vivo study. Clin Orthop Relat Res 2000;370:201.

28. Whittington B, Silder A, Heiderscheit B, Thelen DG. The contribution of passive-elastic mechanisms to lower extremity joint kinetics during human walking. Gait & Posture 2008;27:7.

29. Lafortune M, Cavanagh P, Sommer H, Kalenak A. Three-dimensional kinematics of the human knee during walking. J Biomech 1992;25(4):11.

30. Hallen L. The'screw-home'movement in the knee joint. Acta Orthop Scand 1966;37:97-106.

31. Victor J, Labey L, Wong P, Innocenti B, Bellemans J. The influence of muscle load on tibiofemoral knee kinematics. J Orthop Res 2010;28(4):419-428.

32. Lohmander LS, Englund PM, Dahl LL, Roos EM. The long-term consequence of anterior cruciate ligament and meniscus injuries: osteoarthritis. Am J Sports Med 2007;35(10):1756-1769.

33. Tashman S, Kolowich P, Collon D, Anderson K, Anderst W. Dynamic function of the ACL-reconstructed knee during running. Clin Orthop Relat Res 2007;454:66-73.

34. Yao J, Salo AD, Lee J, Lerner AL. Sensitivity of tibio-menisco-femoral joint contact behavior to variations in knee kinematics. J Biomech 2008;41(2):390-398.

35. Li G, Rudy T, Sakane M, Kanamori A, Ma C, Woo SLY. The importance of quadriceps and hamstring muscle loading on knee kinematics and in-situ forces in the ACL. J Biomech 1999;32(4):395-400.

Chapter 2

Accuracy of Model-based Tracking of Knee Kinematics and Cartilage Contact Measured by Dynamic Volumetric MRI

Jarred Kaiser, Arezu Monawer, Rajeev Chaudhary, Kevin Johnson, Oliver Wieben, Richard Kijowski, Darryl G. Thelen

(Note that this chapter has been submitted for publication in Medical Engineering Physics)

Abstract

The purpose of this study is to determine the accuracy of knee kinematics and cartilage contact measured by dynamic MR using 3D radial sampling. A motor-actuated phantom drove femur and tibia bone segments through cyclic, 3D motion patterns. Volumetric images were acquired using a 3D radially undersampled cine spoiled gradient echo sequence (SPGR-VIPR). Image data was binned based on position measured by rotary encoder. High-resolution static images were segmented to create bone models that were optimally registered to each frame in the SPGR-VIPR series. 3D tibiofemoral translations and orientations were reconstructed, and compared to kinematics obtained by tracking fiducial markers. Dynamic imaging was repeated on a healthy subject who performed cyclic knee flexion-extension. Cartilage contact was assessed by measuring the overlap between articular cartilage surfaces. Model-based tracking was able to track tibiofemoral angles and translations with precisions less than 0.8° and 0.5 mm. These precisions resulted in estimates of *in vivo* knee cartilage contact location with a precision less than 0.5 mm. Dynamic SPGR-VIPR imaging can accurately assess *in vivo* knee kinematics and cartilage contact during voluntary knee motion performed in a scanner. This technology could facilitate the quantitative investigation of links between joint mechanics and the development of osteoarthritis.

Key Words: dynamic MRI; knee kinematics; validation; biomechanics

Introduction

Magnetic resonance imaging (MRI) is an attractive imaging modality for investigating the development and progression of osteoarthritis (OA). High resolution MR images have classically been used to track changes in cartilage morphology associated with OA [1]. More recently, quantitative MRI techniques have emerged to track variations in cartilage composition that occur much earlier prior to the onset of cartilage volume loss [2]. Despite the widely held hypothesis that subtle abnormalities in knee cartilage contact may contribute to OA [3], knee mechanics remain challenging to assess using MRI.

Recent advances in dynamic imaging are providing new opportunities for directly measuring skeletal kinematics underlying movement [4-6]. Kinematics can be coupled with high resolution models of an individual's cartilage geometries to assess the location and magnitude of cartilage contact within a joint. Though dynamic imaging is a promising approach for investigating how injury- or treatment-induced changes in cartilage contact patterns may predispose an individual to OA, its relatively low temporal resolution makes it challenging to visualize skeletal motion. Previous studies have used sequential static images to visualize skeletal kinematics under load [7], real-time imaging to visualize slow joint motion in a single plane [8] or cine phase contrast techniques to measure skeletal velocities [5]. It is challenging however to characterize full 3D joint behavior with these techniques.

A previous study recently introduced a novel volumetric MR imaging technique, termed spoiled-gradient echo with Vastly under-sampled Isotropic PRojection imaging (SPGR-VIPR), to measure 3D tibiofemoral kinematics [6]. SPGR-VIPR uses radially undersampled trajectories to obtain volumetric images of dynamic motion within viable scan times. The purpose of the presented work was twofold. First, we used a motion phantom to determine the accuracy of SPGR-

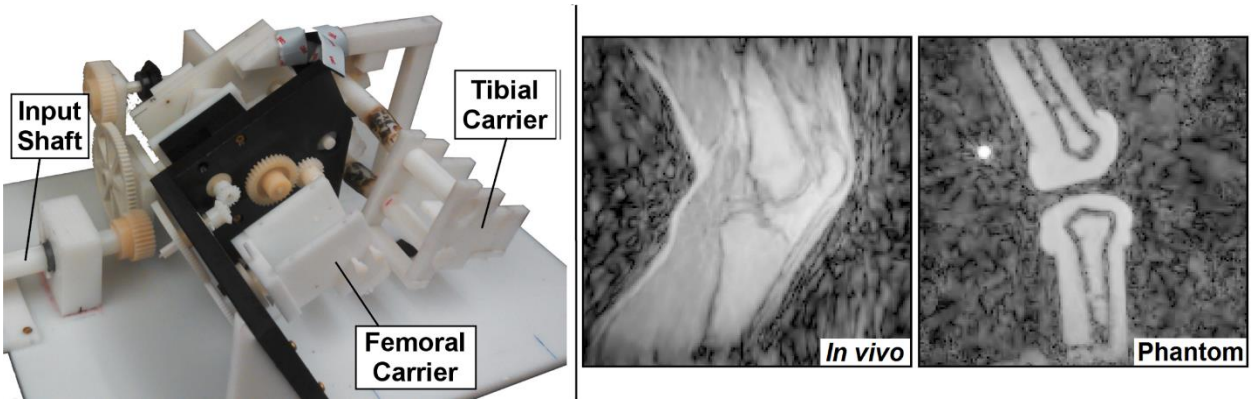

Figure 1. (*Left*) A stepper motor located outside the MRI bore drives the input shaft of the motion phantom, generating cyclic motion of bone segments mounted in the tibial and femoral carriers. *(Right)* Dynamic *SPGR-VIPR* images obtained during voluntary *in vivo* motion and motor actuated phantom motion. The bright spot posterior to the femur in the phantom image is a fiducial marker.

VIPR in tracking 3D joint motion. Second, we used SPGR-VIPR scans of voluntary knee movement to assess the sensitivity of cartilage contact to uncertainty in skeletal kinematics. Completion of these aims provides an estimate of the accuracy with which cartilage contact can be inferred from SPGR-VIPR images.

Materials and Methods

We constructed a MR-compatible motion phantom to cyclically move femoral and tibial bone segments over ranges of motion that mimic natural knee behavior (Fig. 1). Bone segments were 3D printed out of ABS plastic based of the geometry of a healthy young female (23 yrs, 1.65 m, 61 kg) and then embedded in an agar gel with MR relaxation parameters comparable to muscle tissue [9]. Embedded bone segments were rigidly secured to the motion phantom. Four ellipsoidal vitamin E pills (major/minor diameters: 15/10 mm), acting as fiduciary markers, were secured to each bone segment to allow for an independent assessment of skeletal kinematics.

The motion phantom was placed into the bore of a clinical 3.0 T MR scanner (MR750, General Electric Healthcare, Waukesha, WI) and a 16-channel flex coil (GEM Flex, NeoCoil,

Pewaukee, WI) was placed over the motion volume. A continuously rotating stepper motor actuated the phantom. The bone segments were driven at a rate of 0.5 Hz with the tibia rotating through 31.7±0.7° of flexion and the femur rotating 12.0±0.4° about its long axis. A MR-compatible rotary encoder (MR310, Micronor, Newbury Park, CA) mounted on the phantom was used to delineate motion cycles in the scanner (Fig. 1).

A high resolution static SPGR sequence was acquired first. We then collected continuous dynamic SPGR-VIPR (1.5x1.5x1.5 mm^3 acquired spatial resolution, TR/TE= 4 ms/ 1.4 ms, flip angle = 8°, BW= 62.5 kHz, FOV= 24x24x24 cm^3, 75,000 unique radial lines) images of the actuated phantom over five minutes. Dynamic images were reconstructed by using the rotary encoder to retrospectively sort the acquired projections into 60 frames over a motion cycle with no view sharing between temporal frames [6]. Three unique trials were sequentially collected during the same imaging session.

The position and orientation of the bone segments were measured from each frame of the dynamic MR series with two independent techniques. We first used a model-based tracking technique, the details of which can be found in [6]. Briefly, bone models were registered to each dynamic image frame using numerical optimization to find the 3D bone pose that minimized the sum-squared intensities of the dynamic image at the locations of the model vertices, driving the bone models to the low-intensity outlines in the dynamic images (Fig. 1). We separately used the fiducial markers to measure kinematics by applying a threshold to the dynamic images such that the bright fiducials remained visible without surrounding signal. A spherical search region (radius =2 cm) was initialized at the center of each fiducial. The centers of each fiducial were then automatically determined at each frame by calculating the average location of pixels within the search region weighted by their intensities. The static images were used to establish the location

of each fiducial in the anatomical bone reference frames. We then used a singular value decomposition approach to determine the bone pose that optimally fit the bones to the fiducial marker positions [10].

Tibiofemoral kinematics were computed as the translation and orientation of the tibia segment relative to the femoral segment and were low-pass filtered with a 5 Hz cutoff frequency. Error for the fiducial-based tracking was calculated as the standard deviation of the inter-fiducial distance averaged over the three trials. Accuracy of the model-based tracking was characterized by bias (average difference between tracked kinematics), precision (standard deviation of differences) and root mean squared (RMS) error metrics. Error metrics were averaged over the three repeat trials.

Static IDEAL SPGR and dynamic SPGR-VIPR imaging were also acquired on a healthy female subject (18 yrs, 66 kg, 165 cm), who gave informed written consent for the IRB-approved protocol. IDEAL SPGR images were first collected with the subject's knee extended and an eight-channel phased-array extremity coil (Invivo, Orlando, FL) positioned about the knee. A FSE Cube sequence (TR/TE= 2066.7/19.7 ms, voxel size= 0.31x0.31x1 mm^3) was used to facilitate segmention of femur and tibia articular cartilage geometries. In the dynamic imaging task, the subject laid supine on an MR-compatible knee loading device [6] with a 16-channel wrap coil centered around the knee. The subject was asked to cyclically flex and extend her knee through ~35° of motion against an inertial load at 0.5 Hz for 5 minutes. SPGR-VIPR images were reconstructed into 60 frames over a motion cycle and model-based tracking was used to determine knee kinematics. We repeated the optimal fitting 10 times with random initial translations of +/- 2 mm and initial segment rotation angles of +/- 2° to evaluate the repeatability.

To assess contact, we registered cartilage geometries to the bone models at each frame of the motion cycle. We calculated the proximity between the femur and tibia cartilage surfaces at each face in the tibia cartilage surface mesh. Center of contact was defined as the average position of contact on the tibia weighted by proximity. Kinematics were then varied by 0.1 mm / degree at every 5° of knee flexion to determine the sensitivity of measured tibial cartilage contact location and contact area to joint translations and orientation angles. Sensitivities were computed at each frame and then averaged over all 60 frames of the motion cycle. To determine the uncertainty in cartilage contact metrics from tracked kinematics, we multiplied the average sensitivities by the precision of the model-based tracking as measured by the motion phantom.

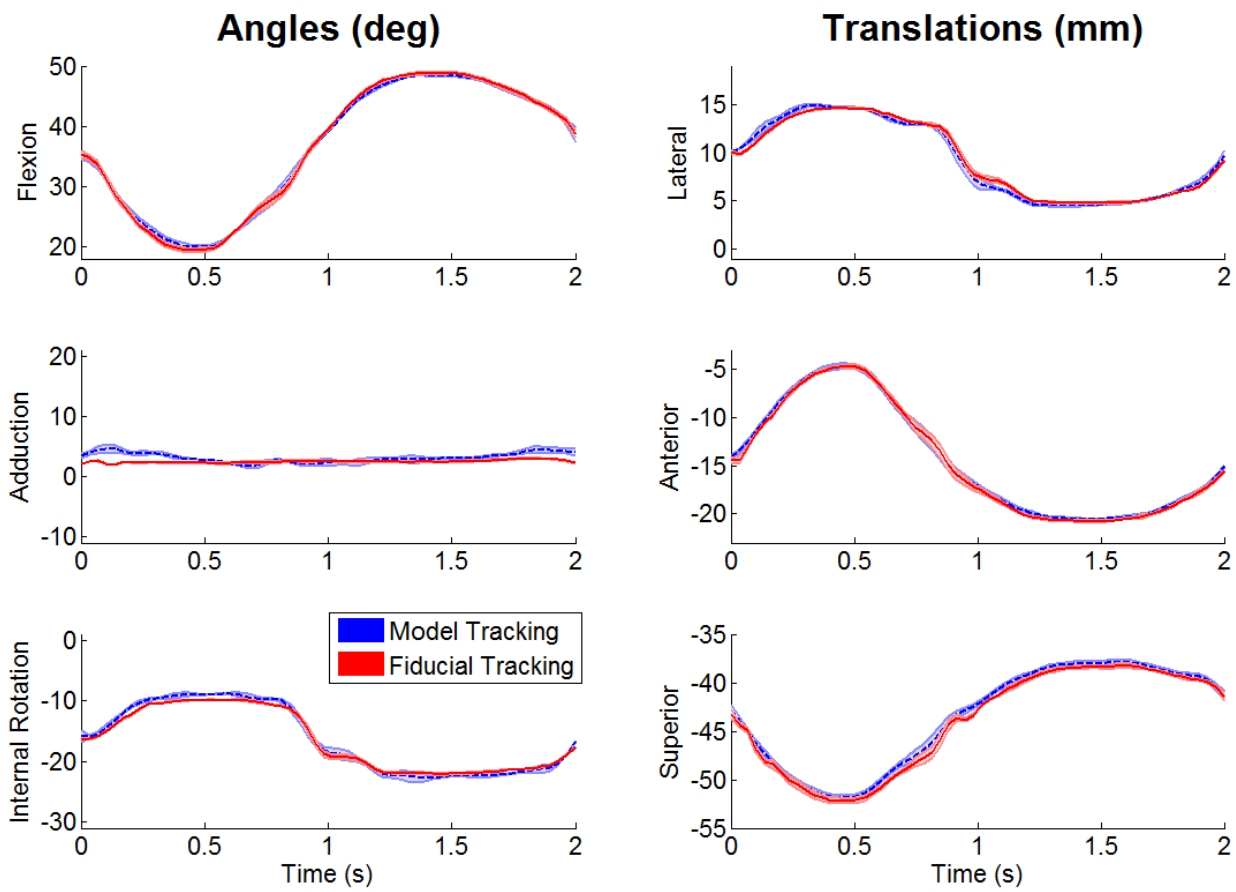

Figure 2. Angular and translational kinematics of the tibia relative to the femur in the motion phantom. Good temporal agreement is seen between kinematic trajectories obtained using model-based and fiducial tracking algorithms.

RESULTS

Fiducial-based tracking of the phantom motion had errors of 0.16 mm in medial, anterior, and superior directions for the femur and 0.20 mm, 0.19 mm, and 0.18 mm in the medial, anterior, and superior directions for the tibia. Relative to fiducial marker tracking, model-based tracking was able to measure tibiofemoral flexion with an average bias of 0.03°, precision of 0.47° and RMS error of 0.47° (Fig. 2). Tibiofemoral internal rotation was measured with an average bias of 0.21°, a precision of 0.69° and RMS error of 0.72° deg (Table 1). All three tibiofemoral translations were tracked with precisions less than 0.5 mm.

Model-based tracking of the *in vivo* case was highly repeatable with standard deviations less than 0.02° and 0.01 mm over ten repeat optimization solutions. The anterior-posterior center of contact was most sensitive to sagittal plane angles and translations, whereas the medio-lateral center of contact was sensitive to lateral tibia translation and tibiofemoral adduction (Table 2). Contact area exhibited the greatest sensitivity to superior tibia translation and tibiofemoral adduction.

When combined with kinematic precision metrics, an uncertainty of <0.50 mm in medial-lateral center of contact could arise from errors in tibiofemoral adduction and lateral translation (Table 3). Uncertainty in anterior-posterior center of contact was slightly smaller with errors of 0.09 to 0.25 mm due to uncertainty in knee flexion angles and sagittal plane tibiofemoral translations. Imprecision in tibiofemoral adduction and superior translation resulted in an uncertainty in contact area of 56 mm^2 and 36 mm^2, respectively, on the medial plateau.

Table 1: Bias, precision, and root-mean squared error of model-based tracking of the tibiofemoral kinematics.

	Tibiofemoral Angles (deg)			**Tibiofemoral Translations (mm)**		
	Flexion	**Adduction**	**Int. Rot.**	**Lateral**	**Anterior**	**Superior**
Bias	0.03 ± 0.05	0.68 ± 0.09	0.21 ± 0.08	0.04 ± 0.03	0.19 ± 0.05	0.46 ± 0.06
Precision	0.47 ± 0.02	0.81 ± 0.12	0.69 ± 0.16	0.47 ± 0.08	0.23 ± 0.05	0.24 ± 0.03
RMS Error	0.47 ± 0.01	1.06 ± 0.13	0.72 ± 0.12	0.60 ± 0.08	0.30 ± 0.03	0.52 ± 0.06

Table 2: Sensitivity of contact measures to variations in tibiofemoral angles and translations.

		Angles (per deg)			Translations (per mm)		
		Flexion	**Adduction**	**Int. Rot**	**Lateral**	**Anterior**	**Superior**
Medial CoC (mm)	**Medial**	0.10± 0.07	0.60± 0.09	0.19± 0.15	1.06± 0.10	0.18 ± 0.16	0.17 ± 0.15
	Lateral	0.03± 0.02	0.52± 0.06	0.11± 0.08	0.99± 0.14	0.10± 0.04	0.28± 0.01
Anterior CoC (mm)	**Medial**	0.53 ± 0.09	0.05± 0.05	0.32 ± 0.10	0.12 ± 0.06	0.58± 0.20	0.59 ± 0.27
	Lateral	0.29 ± 0.05	0.05± 0.04	0.19± 0.03	0.09± 0.04	0.43± 0.03	0.36 ± 0.11
Contact Area (mm^2)	**Medial**	21.2± 13.8	68.6 ± 43.3	22.2 ± 18.1	36.7 ± 20.4	42.0 ± 31.0	149.8 ± 80.3
	Lateral	15.5 ± 9.4	24.3 ± 14.6	10.8 ± 6.7	40.4± 12.6	29.8 ± 22.5	106.7 ± 25.6

Table 3. Estimated uncertainty in cartilage contact metrics due to precision errors in tracking tibiofemoral angles and translations.

		Tibiofemoral Angles			Tibiofemoral Translations		
		Flexion	**Adduction**	**Int. Rot**	**Lateral**	**Anterior**	**Superior**
ML CoC (mm)	**Medial**	0.05	0.49	0.13	0.49	0.04	0.04
	Lateral	0.01	0.43	0.08	0.46	0.02	0.07
AP CoC (mm)	**Medial**	0.25	0.04	0.22	0.06	0.13	0.14
	Lateral	0.14	0.04	0.13	0.04	0.10	0.09
Contact Area (mm^2)	**Medial**	9.97	55.88	15.25	17.07	9.50	35.75
	Lateral	7.32	19.82	7.45	18.82	6.74	25.48

Discussion

Due to its excellent soft tissue contrast, MRI provides an attractive modality for investigating potential links between joint mechanics, cartilage morphology and osteoarthritis. A novel 3D dynamic imaging protocol using SPGR-VIPR was recently introduced for tracking *in vivo* joint motion, which addresses some of the registration challenges that arise with planar dynamic MRI techniques [11, 12]. This study showed that SPGR-VIPR images can reconstruct

joint kinematics with reasonably high precision, averaging less than 0.5 mm and 0.9°. The kinematic precisions achieved are smaller than asymmetric variations in kinematics seen in ACL-deficient [13] and reconstructed knees [14], such that SPGR-VIPR may be viable to detect clinically relevant abnormalities in knee mechanics.

Our kinematic tracking accuracy metrics are comparable to those reported via biplane fluoroscopy and other dynamic MR techniques. Biplane fluoroscopy is currently the most widely used approach for tracking skeletal motion underlying movement via model-based tracking. A prior study found model-based tracking of biplane fluoroscopy achieved sub-voxel precision of tracking individual bones but tibiofemoral kinematic precisions (0.9°/0.7 mm) and RMS errors (1.75°/1.54 mm) that are larger than ours, though these were achieved during a more demanding physical task of running [4]. The most common dynamic MRI approach for tracking 3D skeletal motion uses phase contrast (PC) imaging. PC imaging provides 3D bone velocity information, which can be numerically integrated to obtain bone pose throughout a cyclic motion task [5]. Validation studies have reported cine PC MRI has an accuracy of 0.97°/0.33 mm for tracking skeletal motion [11], though these error metrics do not include potential registration errors that can arise in fitting 3D bone models to planar images.

Dynamic MR images can be co-registered with high resolution static images to assess cartilage contact in joint movement. This coupling is needed because the dynamic images lack the resolution (1.5x1.5x1.5 mm^3) to delineate thin cartilage structures (2-5 mm, [15]) seen in the knee. Similar to prior studies [16, 17], we assessed contact by segmenting the unloaded cartilage tissue in high resolution images, registering them to bone models tracked in dynamic images and then quantifying proximity maps between cartilage surfaces within the joint. Based on the results of this study, we estimate that the center of cartilage contact computed this way could be estimated

to within 0.5 mm, with the greatest dependence on frontal plane joint angles and translations. Cartilage contact area uncertainties ranged up to 56 mm^2, which would represent ~15% of the medial tibiofemoral contact area measured in intact cadaveric knees [18]. These results suggest that while the current errors associated with model-based tracking would allow an accurate assessment of center of contact location, further advancements in tracking precision may be necessary to accurately determine subtle changes in contact area.

There are limitations in the current study that are important to understand in interpreting results. Similar to other studies [4, 11], we relied on fiducial markers to assess the validity of our model-based tracking technique. The precision of tracking the fiducial markers was 0.2 mm, which is nearly twice the precision of our model-based tracking. Ideally, the kinematic standard would provide greater precision (~10x) than the technique being evaluated, which is difficult to achieve in dynamic imaging situations. Second, our cine imaging technique requires repeatable cyclic movement. In separate motion analysis experiments done on the phantom, the device generated 31.7±0.7° of tibia flexion and 12.0±0.4° of femoral rotation over 450 motion cycles. These excursions are comparable to average knee ranges of motion (flexion=37.1°, tibia rotation =10.6°) and inter-cycle standard deviations (0.8°) we observed when using SPGR-VIPR to track knees kinematics in 10 healthy young adults [6]. Thus, the phantom variability reasonably represented that seen in humans. Finally, the thickness (5-7 mm) of the walls of the fabricated bone geometries exceeds thickness we see in human bone segments (Fig. 1). This discrepancy may slightly degrade the accuracy of our optimal bone fitting algorithm, where thick walled segments have greater leeway when registered to low signal bone edges visible in the images.

In conclusion, model-based tracking of dynamic, 3D SPGR-VIPR is capable of measuring tibiofemoral kinematics with precision of less than a degree in rotations and less than 0.5 mm in

translations. This precision facilitates reasonably accurate estimates in the location of tibiofemoral cartilage contact *in vivo*. Hence, 3D SPGR-VIPR provides a powerful new approach for empirically examining potential links between abnormal cartilage contact patterns and the development of osteoarthritis.

Conflict of Interest Statement

The authors have no conflict of interest to disclose.

Acknowledgements

The authors gratefully acknowledge the funding provided by the NIH (EB015410, AR062733) and the contributions of Rob Bradford, Jonathon Mantes, David Bunger, and Kelli Hellenbrand.

References

[1] Burgkart R, Glaser C, Hyhlik-Dürr A, Englmeier KH, Reiser M, Eckstein F. Magnetic resonance imaging–based assessment of cartilage loss in severe osteoarthritis: Accuracy, precision, and diagnostic value. Arthritis & Rheumatism. 2001;44:2072-7.

[2] Liu F, Chaudhary R, Hurley SA, Rio A, Alexander AL, Samsonov A, et al. Rapid multicomponent T2 analysis of the articular cartilage of the human knee joint at 3.0 T. Journal of Magnetic Resonance Imaging. 2014;39:1191-7.

[3] Andriacchi TP, Koo S, Scanlan SF. Gait mechanics influence healthy cartilage morphology and osteoarthritis of the knee. J Bone Joint Surg Am. 2009;91 Suppl 1:95-101.

[4] Anderst W, Zauel R, Bishop J, Demps E, Tashman S. Validation of three-dimensional model-based tibio-femoral tracking during running. Med Eng Phys. 2009;31:10-6.

[5] Sheehan FT, Zajac FE, Drace JE. Using cine phase contrast magnetic resonance imaging to non-invasively study in vivo knee dynamics. J Biomech. 1998;31:6.

[6] Kaiser J, Bradford R, Johnson K, Wieben O, Thelen D. Measurement of Tibiofemoral Kinematics Using Highly Accelerated 3D Radial Sampling. Magnetic Resonance in Medicine. 2013;Wiley Subscription Services, Inc., A Wiley Company:7.

[7] Shin CS, Carpenter RD, Majumdar S, Ma CB. Three-dimensional in vivo patellofemoral kinematics and contact area of anterior cruciate ligament-deficient and -reconstructed subjects using magnetic resonance imaging. Arthroscopy. 2009;25:1214-23.

[8] Draper CE, Besier TF, Fredericson M, Santos JM, Beaupre GS, Delp SL, et al. Differences in patellofemoral kinematics between weight-bearing and non-weight-bearing conditions in patients with patellofemoral pain. J Ortho Research. 2011.

[9] Kato H, Kuroda M, Yoshimura K, Yoshida A, Hanamoto K, Kawasaki S, et al. Composition of MRI phantom equivalent to human tissues. Medical Physics. 2005;32:3199-208.

[10] Söderkvist I, Wedin P-Å. Determining the movements of the skeleton using well-configured markers. J Biomech. 1993;26:1473-7.

[11] Behnam AJ, Herzka DA, Sheehan FT. Assessing the accuracy and precision of musculoskeletal motion tracking using cine-PC MRI on a 3.0T platform. J Biomech. 2011;44:193-7.

[12] Draper CE, Santos JM, Kourtis LC, Besier TF, Fredericson M, Beaupre GS, et al. Feasibility of using real-time MRI to measure joint kinematics in 1.5T and open-bore 0.5T systems. J Magn Reson Imaging. 2008;28:158-66.

[13] Van de Velde SK, Gill TJ, Li G. Evaluation of kinematics of anterior cruciate ligament-deficient knees with use of advanced imaging techniques, three-dimensional modeling techniques, and robotics. J Bone Joint Surg Am. 2009;91 Suppl 1:108-14.

[14] Scanlan SF, Chaudhari AM, Dyrby CO, Andriacchi TP. Differences in tibial rotation during walking in ACL reconstructed and healthy contralateral knees. J Biomech. 2010;43:1817-22.

[15] Coleman JL, Widmyer MR, Leddy HA, Utturkar GM, Spritzer CE, Moorman III CT, et al. Diurnal variations in articular cartilage thickness and strain in the human knee. J Biomech. 2013;46:541-7.

[16] Bingham JT, Papannagari R, Van de Velde SK, Gross C, Gill TJ, Felson DT, et al. In vivo cartilage contact deformation in the healthy human tibiofemoral joint. Rheumatology (Oxford). 2008;47:1622-7.

[17] Borotikar BS, Sipprell III WH, Wible EE, Sheehan FT. A methodology to accurately quantify patellofemoral cartilage contact kinematics by combining 3D image shape registration and cine-PC MRI velocity data. J Biomech. 2012;45:1117-22.

[18] Fukubayashi T, Kurosawa H. The contact area and pressure distribution pattern of the knee: a study of normal and osteoarthrotic knee joints. Acta Orthopaedica. 1980;51:871-9.

Chapter 3

Functional Symmetry of Tibiofemoral Kinematics Assessed via Dynamic MRI

Jarred Kaiser, Robert Bradford, Michael F. Vignos, Kevin M. Johnson, Oliver Wieben, Darryl G. Thelen

(Note that this chapter has been submitted for publication in Journal of Biomechanics)

Abstract

When studying knee kinematics after injury or surgery, the uninjured, contralateral knee is commonly used as a reference to monitor recovery and determine success of surgery. However, few studies have researched the bilateral kinematic symmetry of healthy knees. The purpose of this study was to test the hypothesis that functional bilateral kinematic symmetry exists between dominant and non-dominant knees of healthy subjects and that intra-subject (dominant to non-dominant) variability is less than inter-subject (dominant to dominant between subjects) variability. Twenty healthy subjects performed a cyclic knee flexion/extension task against a physiological load imposed by a magnetic resonance (MR) compatible loading device. Knee kinematics were obtained using a novel 3D dynamic MR imaging sequence combined with a bone tracking algorithm. Intra-subject variability and inter-subject variability were both calculated. Only bilateral measures of adduction at peak knee flexion and range of medial translation were significantly different. However, inter-subject variability was greater than intra-subject variability for all metrics and all degrees of freedom were positively correlated bilaterally. This study supports the use of the uninjured, contralateral knee as a functional kinematic reference after injury or surgery.

1. Introduction

The contralateral knee has often been used as a reference when evaluating the effects of unilateral pathologies and treatment on joint behavior. Knee stability, for example, has been evaluated by comparing bilateral measures of laxity (Anderson et al., 1992; Dargel et al., 2009; Eckstein, 2002; Gokeler et al., 2003; Jonsson et al., 1993; Tashman, 2004), while movement disorders have been assessed by comparing joint angles between the affected and contralateral knee (Andriacchi et al., 2009; Kozanek et al., 2008; Papannagari et al., 2006; Tashman, 2004). Contralateral comparisons are based partly on the premise that symmetry in joint structure will contribute to symmetric joint behavior. There is ample evidence of bilateral symmetry in knee morphology, with prior studies showing that cartilage thickness and volume (Eckstein, 2002), ACL geometry (Dargel et al., 2009; Jamison et al., 2010), and skeletal morphology (Dargel et al., 2009) are significantly more consistent between limbs of the same individual than within a group of healthy subjects. Joint motion, however, also depends on neuromuscular coordination and soft tissue mechanical properties.

The emergence of dynamic imaging technologies such as biplane fluoroscopy (Li et al., 2009; Tashman et al., 2007) and dynamic MRI (Draper et al., 2009; Gold, 2003; Kaiser et al., 2013; Sheehan et al., 1998) allows for accurate characterization of six degree of freedom joint kinematics. Such techniques have identified subtle bilateral differences in secondary knee kinematics in both single joint and multi-joint movements following injury and treatment. For example, anterior cruciate ligament (ACL)-deficient and reconstructed knees tend to exhibit small, but consistent, asymmetries in anterior translation and internal-external rotation during gait (Andriacchi and Dyrby, 2005; Papannagari et al., 2006; Tashman, 2004; Van de Velde et al., 2009). It is suggested that small changes in knee kinematics could substantially alter cartilage loading in

a way that pre-disposes the tissue to long-term degeneration (Andriacchi et al., 2009; Chaudhari et al., 2008; Tashman, 2004). Hence, while subtle bilateral differences in knee movement may be important to consider in terms of assessing joint health, one needs to consider normal bilateral variations when using the contralateral knee as the reference control.

The purpose of this study was to assess bilateral symmetry in tibiofemoral kinematics of healthy adults as a basis for determining the suitability of bilateral comparisons to detect pathological knee behavior. To do this, we used a new 3D dynamic MR imaging technique to quantitatively track tibiofemoral kinematics during a knee flexion/extension task performed against an inertial load (Kaiser et al., 2013). We hypothesized that intra-subject variability in tibiofemoral kinematics would be less than inter-subject variability, supporting the use of the contralateral knee as a reference for identifying kinematic abnormalities after injury and/or clinical treatment.

2. Materials and Methods

2.1. Subjects

The dominant and non-dominant knees of 20 healthy subjects were tested (8 females, 12 males, age, 23.6 ± 3.0y; height, 1.79 ± 0.12m; mass, 70.8 ± 10.3kg). Exclusion criteria included history of knee injury, pathology, surgery or chronic knee pain. Each subject gave informed consent according to a protocol approved by the University of Wisconsin's Institutional Review Board. Leg dominance was self-determined as the limb that the subject would use to kick a ball.

2.2. Pre-scan laboratory testing

Subjects first practiced the flexion-extension task in a laboratory setting in order to ensure reproducibility during MRI testing. Subjects were positioned supine on a customized MRI-compatible dynamic knee loading device (Silder et al., 2009), with the knee aligned with the leg

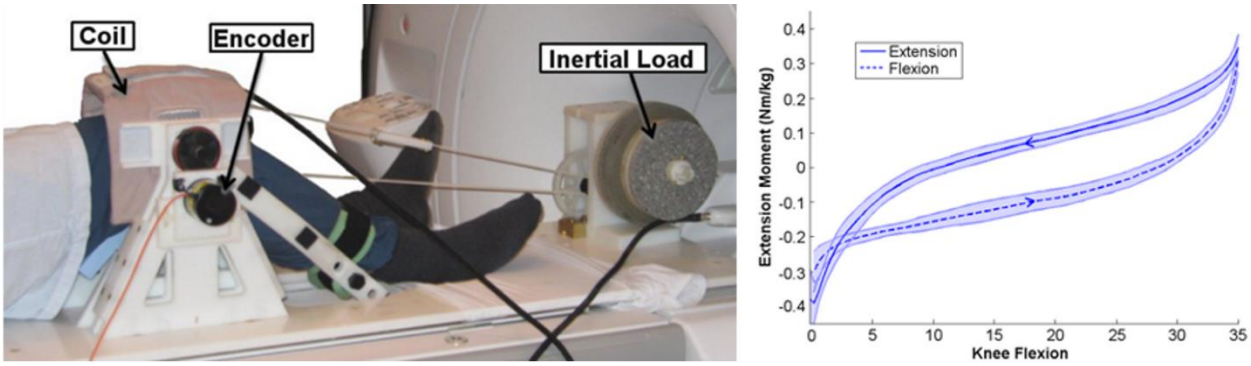

Figure 1. Subjects were placed supine on an MR-compatible loading device and instructed to flex and extend their leg at 0.5 Hz (*Left)*. An inertial load created eccentric loading of the quadriceps with a peak extension moment at peak knee flexion and a peak flexion moment at peak knee extension (*Right)*.

brace rotation axis. A semi-circular structure was placed about the lower limb to mimic the 60 cm bore of the MR scanner used in this study. Subjects were instructed to cycle between knee flexion and extension against an inertial load at a rate of 0.5 Hz indicated by an audible metronome. The inertial load was generated by a set of rotating disks that were geared to the knee rotation axis with the equivalent rotational moment of inertia about the knee of 4.66 kg-m^2. The device induced lengthening quadriceps loading with knee flexion, similar to stance phase of gait (Westphal, 2009). Subjects reached peak flexion and extension moments of ~0.4 Nm^2/kg at extension and flexion, respectively (Fig. 1). Each subject performed a five minute trial for each limb, with the order of limbs randomized.

2.3. MRI testing

On a separate day, subjects repeated the flexion-extension task in a clinical 3.0T MR scanner (Discovery MR750, GE Healthcare, Waukesha, WI). The device was placed in the scanner and the subject was positioned supine on the device with the knee surrounded by a 16-channel flex coil (GEM Flex, NeoCoil, Pewaukee, WI) (Fig. 1). Subjects were again instructed to flex and extend their knee at 0.5 Hz with cadence maintained via metronome. A spoiled gradient recalled vastly under-sampled isotropic projection (SPGR-VIPR, 160x160x160 cubic voxels with 1.5 mm

spacing, 75,000 unique projection angles, 5 min scan time) sequence, recently developed at the University of Wisconsin-Madison (Johnson et al., 2008), continuously recorded three-dimensional volumetric image data. An MRI-compatible rotary encoder (Micronor, Newbury Park, California) recorded knee angle throughout the trial at 50 Hz. Knee angle data was then used post-hoc to bin and reconstruct image data into 60 equally spaced image frames, each representing a time window of 33 ms, over the motion cycle. Images were reconstructed without view sharing utilizing iterative non-Cartesian SENSE(Pruessmann et al., 2001) with an L1-wavelet penalty (Lustig et al., 2008).

High resolution static imaging of each knee was performed separately using a 3D SPGR sequence with fat suppression (512x512x304 cubic voxels with 0.37x0.37x0.9 mm^3 resolution, TR/TE= 10.48 ms/ 2.24 ms, (Gerdes et al., 2007)). For these scans, the knee was positioned in an eight channel phased-array extremity coil (Precision Eight TX/TR High Resolution Knee Array; Invivo, Orlando, Fla.). Static images were manually segmented (MIMICS, Materialise Group, Leuven, Belgium) to create subject-specific representations of the femur and tibia bone geometry.

2.4. Kinematic Measures

Anatomical coordinate systems were first automatically defined for the bone segments using the geometric and inertial properties of the individual bones (Miranda et al., 2010). The flexion axis of the femur was defined as the centerline of the cylinder which best fits the condyles, with the origin of the coordinate system placed at the cylinder's centroid. The superior axis of the femur was defined as the first inertial axis of the isolated diaphysis. The tibial coordinate system was defined using the isolated plateau, with the first, second and third inertial axes as the axes of the coordinate system and the center of mass as the origin. This algorithm defines the anatomical coordinate systems with low variability (<1.5 mm, <2.5°) (Miranda et al., 2010). However, to further reduce the effect of the axes definition variability on measured

kinematic variability, we manually registered the axes of the non-dominant leg to align with the dominant leg.

Bone segment position and orientation were then manually placed in the first image frame. Kinematics were automatically determined at each frame of the motion trial by performing a point-cloud co-registration between the high-resolution 3D bone models and the dynamic image bone outlines (Powell, 1964). The result was a set of 3D segment translational and angle trajectories of the femur and tibia over the motion cycle. Tibiofemoral angles were defined as a series of three sequential Cardan rotation angles (flexion-adduction-internal rotation) that defined the orientation of the tibia reference frame relative to the femur reference (Wu and Cavanagh, 1995). A 5 Hz low-pass filter smoothed the tibiofemoral translational and angular trajectories.

2.5. Statistics

Inter-subject and intra-subject differences in kinematic ranges of motion and values at peak flexion and extension were assessed. Inter-subject differences between dominant and non-dominant knees were determined using paired t-tests and significance was set at $p < 0.05$. The absolute percentage side difference for ranges of motion were compared to the overall coefficient of variation to evaluate intra-subject versus inter-subject variability. For the peak flexion and extension metrics, the ratio of the standard deviation of side differences to the overall standard deviation of the dominant knees was calculated. A ratio greater than 1 indicates that inter-subject variability was greater than intra-subject variability for a given kinematic metric (Eckstein, 2002).

Univariate linear regression analysis was applied to determine whether kinematics of the dominant knee can predict kinematics of the non-dominant knee (Statistica, StatSoft, Tulsa, OK). A two-way repeated measures ANOVA then assessed the effect of knee dominance and knee

flexion angle on secondary kinematics during flexion and extension. If a significant difference was found ($p<0.05$), a post-hoc Tukey test was performed to identify the temporal location of leg differences.

3. Results

The task was highly repeatable with subjects displaying little variability in cycle period (s.d.= 0.01 s) and range of motion (s.d.= 0.15°) over 150 consecutive motion cycles. On average, the subjects exhibited characteristic internal tibia rotation and posterior tibia translation with knee flexion (Fig. 2). The subjects exhibited no significant bilateral kinematic differences, with the exception of a slightly greater range of medial translation on the dominant limb and a larger adduction angle at peak flexion in the non-dominant limb. Secondary kinematic ranges of motion

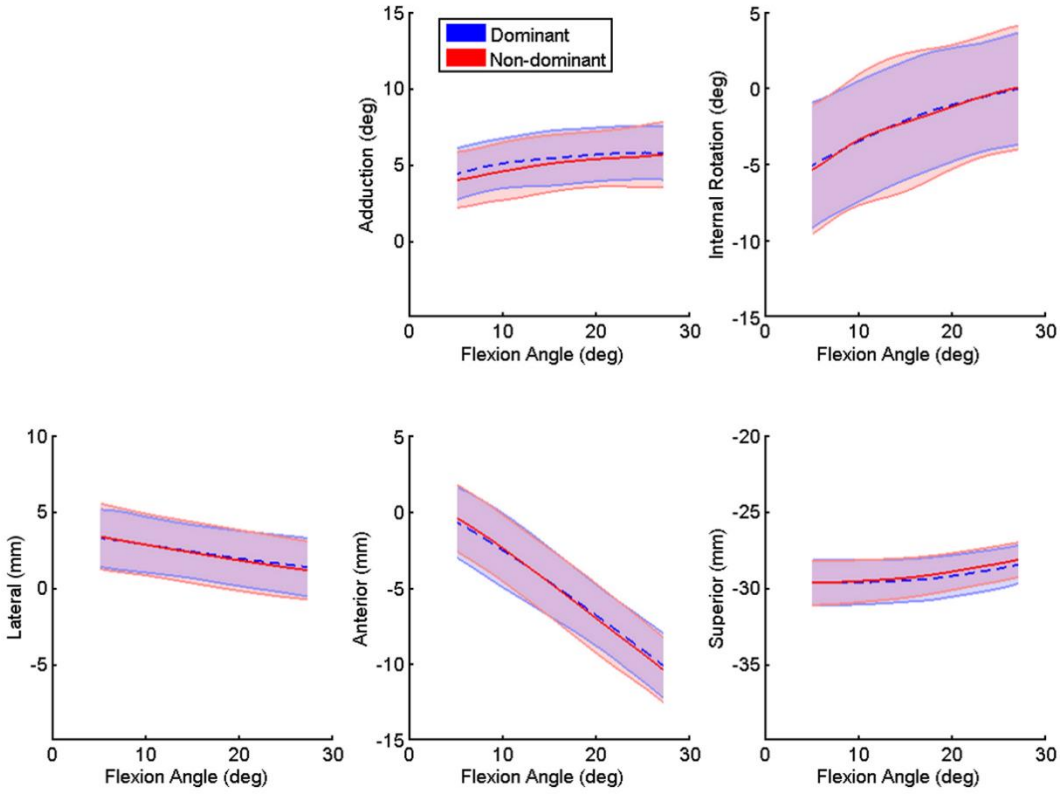

Figure 2. Profiles of secondary kinematics (mean ± standard deviation) during flexion for the dominant and non-dominant legs. No significant differences were detected between legs. Further, inter-subject variability was higher than intra-subject variability for every degree of freedom.

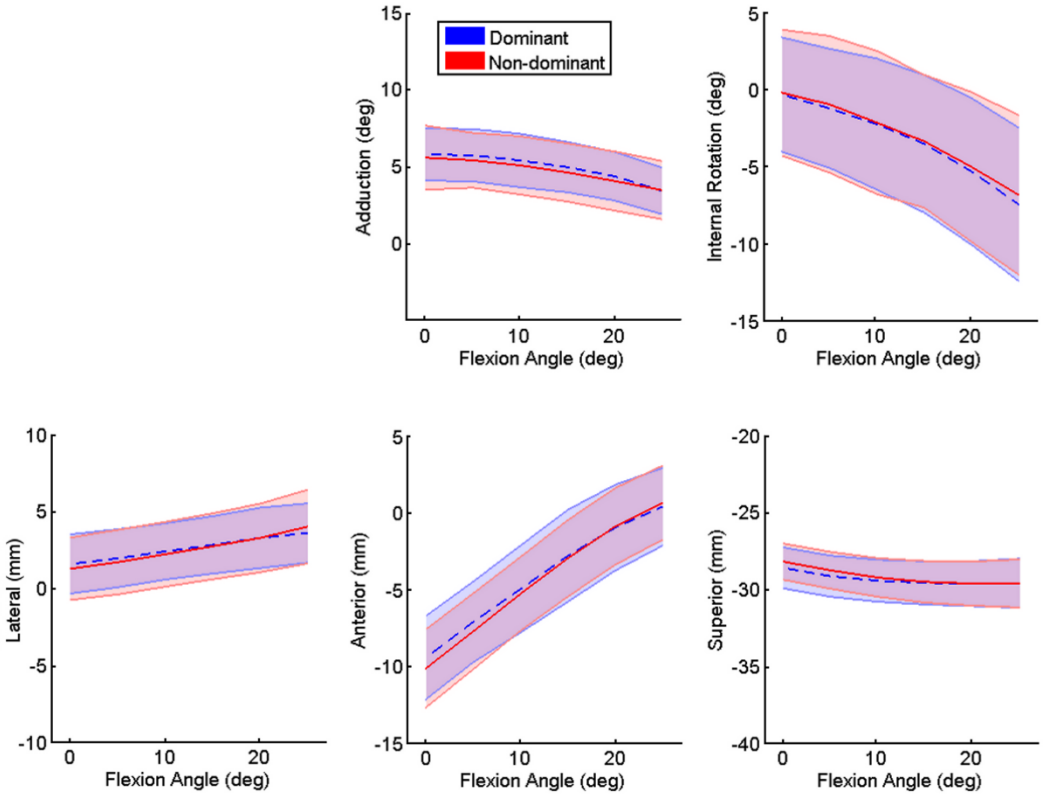

Figure 3. Profiles of secondary kinematics (mean ± standard deviation) during extension for the dominant and non-dominant legs. No significant differences were detected between legs and inter-subject variability was higher than intra-subject variability for every degree of freedom.

(Table 1) and values at peak extension (Table 2) and peak flexion (Table 3) were all more consistent between limbs than between subjects. Sagittal plane range of motion metrics exhibited slightly greater bilateral symmetry (CV ratios>2.0) than non-sagittal rotations and medio-lateral translation (Table 1). At peak extension and peak flexion, tibiofemoral translations and internal rotation exhibited higher bilateral symmetry than frontal plane angles.

Table 1. Range of knee kinematics. Values and intra-subject side differences are reported as mean ± standard deviation (SD). Inter-subject variation is given as the standard deviation of the population (bold denotes p<0.05).

		Dominant	Non-Dominant	T test (p)	% Bilateral Difference	Variation		Correlation	
		Mean ± SD	Mean ± SD			%CV	Ratio	r	p
Rotations (deg)	**Flexion**	36.78 ± 4.32	37.12 ± 4.38	0.57	5.78	11.80	2.04	0.82	<0.01
	Adduction	3.56 ± 1.55	3.35 ± 1.27	0.43	20.17	37.88	1.88	0.70	<0.01
	Internal Rotation	8.77 ± 3.16	9.24 ± 3.70	0.26	26.66	40.05	1.50	0.48	0.03
Translations (mm)	**Lateral**	3.67 ± 1.07	3.13 ± 0.89	0.02	22.42	28.26	1.26	0.58	<0.01
	Anterior	16.40 ± 2.76	16.18 ± 2.92	0.59	7.93	18.05	2.28	0.81	<0.01
	Superior	3.74 ± 2.02	3.51 ± 1.61	0.27	18.63	45.85	2.46	0.90	<0.01

Table 2. Knee kinematics at peak extension. Values and intra-subject side differences are reported as mean ± standard deviation (SD). Inter-subject variation is given as the standard deviation of the population (bold denotes p<0.05).

		Dominant	Non-Dominant	T test (p)	SD Bilateral Difference	Variation		Correlation	
		Mean ± SD	Mean ± SD			SD	Ratio	r	p
Rotations (deg)	**Flexion**	0.74 ± 2.29	0.03 ± 1.99	0.11	1.23	1.99	1.62	0.53	0.02
	Adduction	3.46 ± 1.88	3.42 ± 1.51	0.85	0.66	1.54	2.27	0.83	<0.01
	Internal Rotation	-6.86 ± 5.17	-7.48 ± 4.97	0.24	1.49	4.97	3.35	0.90	<0.01
Translations (mm)	**Lateral**	4.01 ± 2.38	3.59 ± 1.92	0.09	1.92	1.92	2.94	0.90	<0.01
	Anterior	0.63 ± 2.38	0.37 ± 2.52	0.41	2.52	2.52	2.88	0.84	<0.01
	Superior	-29.61 ± 1.56	-29.59 ± 1.59	0.92	1.59	1.59	5.43	0.95	<0.01

Table 3. Knee kinematics at peak flexion. Values and intra-subject side differences are reported as mean ± standard deviation (SD). Inter-subject variation is given as the standard deviation of the population (bold denotes $p<0.05$).

		Dominant	Non-Dominant	T test (p)	SD Bilateral Difference	Variation		Correlation	
		Mean ± SD	Mean ± SD			SD	Ratio	r	p
Rotations (deg)	**Flexion**	37.52 ± 3.87	37.09 ± 4.97	0.43	1.47	4.97	3.38	0.88	<0.01
	Adduction	6.11 ± 2.18	5.29 ± 2.24	0.02	1.18	2.26	1.92	0.80	<0.01
	Internal Rotation	0.46 ± 4.10	0.34 ± 4.14	0.78	1.30	4.13	3.18	0.89	<0.01
Translations (mm)	**Lateral**	0.76 ± 1.92	0.97 ± 1.63	0.24	0.55	1.63	2.99	0.92	<0.01
	Anterior	-15.39 ± 2.27	-15.51 ± 2.00	0.65	0.66	2.00	3.02	0.86	<0.01
	Superior	-26.31 ± 1.59	-26.56 ± 1.47	0.13	0.47	1.47	3.13	0.90	<0.01

Bilateral kinematic values were highly correlated at both peak flexion (Fig. 4) and extension (Fig. 5), with coefficient of correlation values greater than 0.80 for all degrees of freedom but peak extension angle. Bilateral ranges of motion were also all significantly correlated, though the strengths of these correlations were generally weaker with coefficient values ranging from 0.48 for internal rotation to 0.90 for superior translation.

The two-way repeated measures ANOVA found no significant differences in secondary kinematics between limbs during flexion (Fig. 2) or extension (Fig. 3). Correlations at every

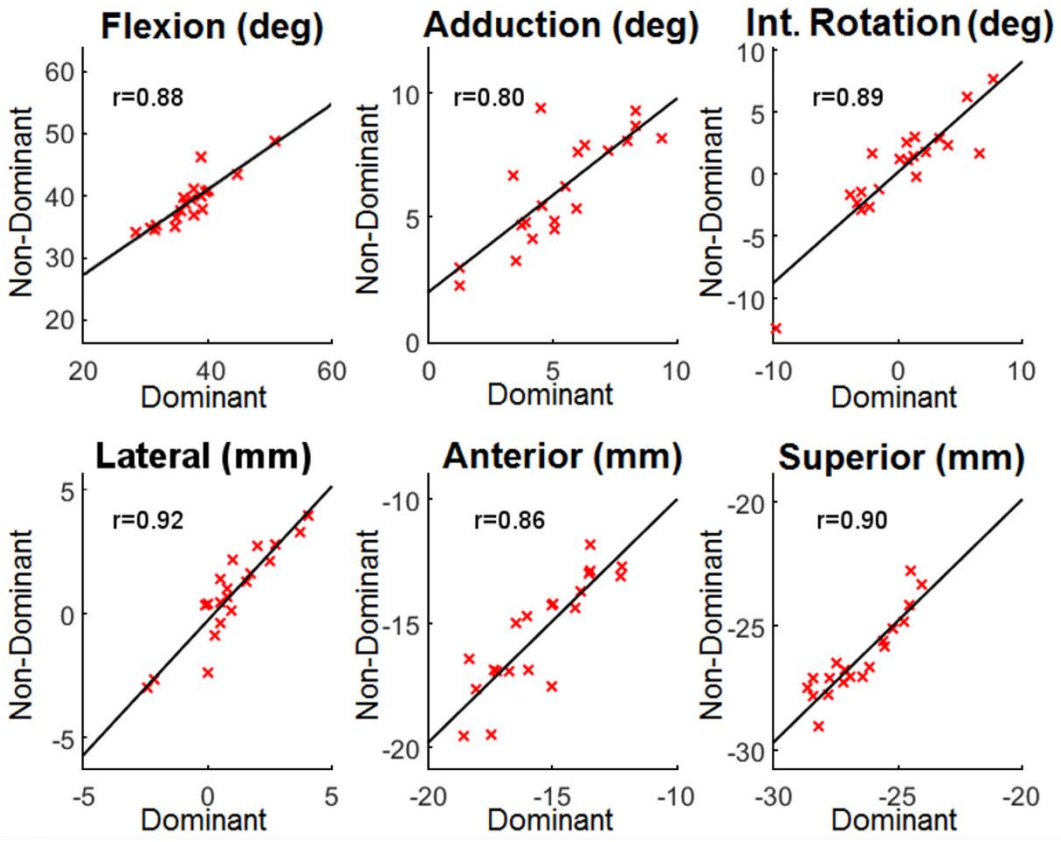

Figure 4. Correlations of kinematic values of the dominant and non-dominant legs at peak flexion. All correlations were significant.

flexion angle were significant with average correlation coefficients ranging from 0.73 for adduction angle during extension to 0.95 for internal rotation during extension.

4. Discussion

We found that healthy knees generally exhibit bilateral symmetry in secondary kinematics during isolated flexion-extension tasks. Specifically, tibiofemoral translations and non-sagittal rotations were substantially more consistent between limbs than between individuals. We did find significant bilateral differences in the range of medial tibial translation and the adduction angle at peak flexion, though the differences were generally small (~0.5 mm, <1°) and the variability ratios were greater than 1 for both metrics. Hence, our data suggests that bilateral comparisons of

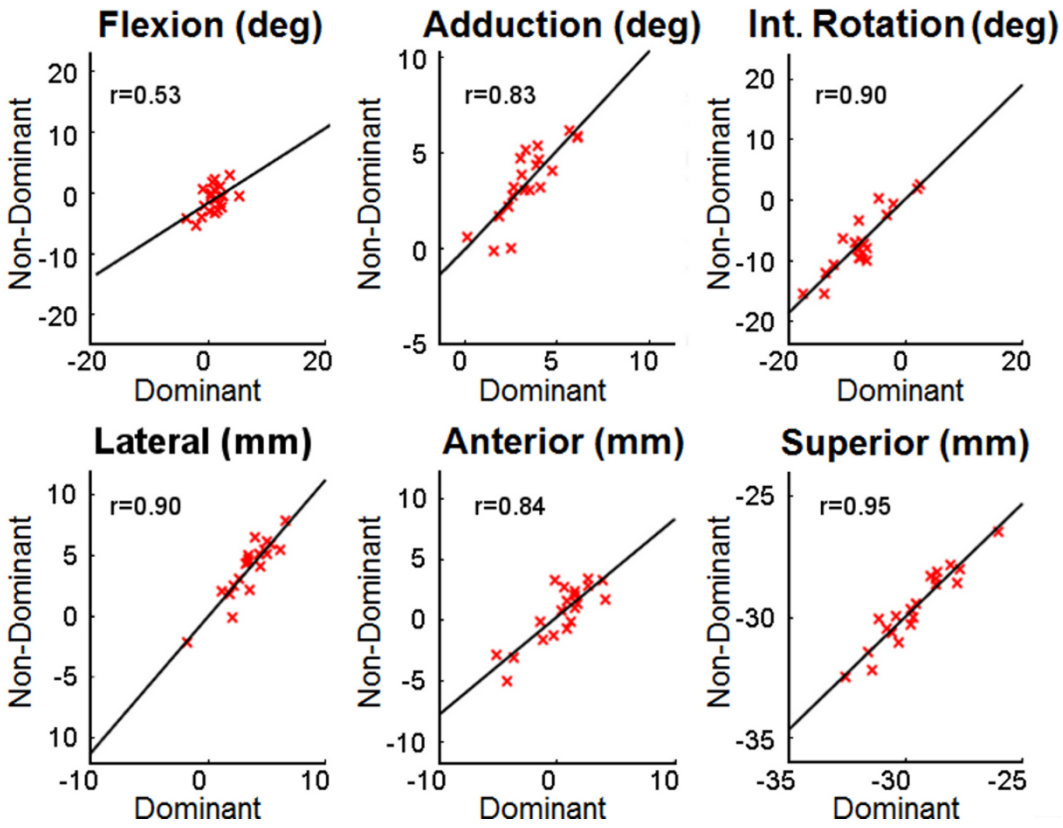

Figure 5. Correlations of kinematic values of the dominant and non-dominant legs at peak extension. All correlations were significant.

kinematics are likely a better alternative than group-based comparisons when investigating residual changes that can arise following injury, surgical treatment and/or rehabilitation.

In vivo knee joint motion depends on morphology, tissue material properties and neuromuscular coordination (Besier et al., 2005). For the knee flexion-extension task we studied, morphology and tissue properties were likely the prominent factors since the isolated task limits the variability in coordination observed during whole limb movements (Heiderscheit, 2000; Holt et al., 1995). Further, there is abundant evidence that joint morphology is quite symmetric. For example, substantial bilateral symmetry has been observed in morphological measures of cadaveric bone geometry and ligament insertion points (Dargel et al., 2009). The variability ratios from this study were of similar magnitude (ratios of 1 to 3) as the kinematic metrics seen in our study.

Interestingly, we observed the high variability ratios for tibial rotation at peak flexion and extension. This result could arise from the strong dependence of tibial rotation on femoral condyle depth (Iwaki et al., 2000) and cruciate ligament properties (Gollehon et al., 1987; Wilson et al., 1998) both of which were shown to have greater intersubject variability than side differences, with variability ratios ranging from 3.2 to 6.9 for these metrics (Dargel et al., 2009). Further evidence of the strong ligament dependence is found in prior studies of ACL-deficient and ACL-reconstructed knees (Stergiou et al., 2007; Tashman, 2004), which have often found internal tibia rotation to be the degree-of-freedom that exhibits the greatest difference relative to both controls and the contralateral knee.

Prior studies have analyzed whether the contralateral knee behaves normally in individuals with prior unilateral pathology. For example, Kozanek et al. used biplane fluoroscopy to compare kinematics of aged-matched healthy individuals with the kinematics of contralateral uninjured knees in ACL-deficient and PCL-deficient individuals during a quasi-static lunge (Kozanek et al., 2008). They determined that no significant differences existed between the healthy knees of these groups, indicating that kinematics of the contralateral limb were unaffected by the injured knee. Conversely, during gait, Hofbauer et al. discovered longitudinal changes in the uninjured contralateral knee of subjects who previously underwent unilateral ACL-reconstructive surgery and contributed these changes due to compensatory adaptations, such as muscle strength, in the intact limb (Hofbauer et al., 2014). Indeed, the intact limb has been shown to display altered knee and hip extensor moments during gait over two years following ACL-reconstruction with a trend towards greater bilateral symmetry (Roewer et al., 2011). These prior studies suggest that compensatory factors are important to consider when performing bilateral comparisons in multi-joint motions such as gait. The use of the single joint task performed in this study likely mitigates

some of these compensatory factors, and hence may better isolate underlying changes in knee mechanics.

There are some study limitations to consider in interpreting our results. First, the absolute joint angles we compute are directly dependent on our ability to place anatomical reference frames in a consistent manner. To reduce the effects of variability in coordinate system definition, we first used an automatic method to establish reference frames in the dominant limb. We then reflected the contralateral bone geometries and registered them to the dominant limb bones to further reduce bilateral variability in the coordinate system definition. Our analysis also depends on the accuracy with which we can track six degree of freedom kinematics. We previously performed a phantom study of our dynamic imaging technique and found bias errors less 0.5 mm and 0.7°, and precision better than 0.5 mm and 0.8°. These kinematic errors are considerably smaller than the differences we saw between limbs. Finally, our study population consisted of healthy young adults. Further study with other age-groups and pathological populations is warranted.

We conclude that healthy young adults exhibit substantial bilateral symmetry in three-dimensional knee kinematics, such that the contralateral knee may be an appropriate reference for assessing subtle changes in secondary knee motion due to injury or surgical treatment.

Conflict of interest

No conflicts of interest exist for the authors.

Acknowledgements

The authors gratefully acknowledge the contributions of Kelli Hellenbrand, Sara John, and Christopher Westphal, and the financial support of NIH AR056201 and the Robert W. Bolz Distinguished Graduate Fellowship Program.

References

Anderson, A.F., Snyder, R.B., Federspiel, C.F., Lipscomb, A.B., 1992. Instrumented evaluation of knee laxity: a comparison of five arthrometers. Am J Sports Med 20, 135.

Andriacchi, T.P., Dyrby, C.O., 2005. Interactions between kinematics and loading during walking for the normal and ACL deficient knee. J Biomech 38, 293-298.

Andriacchi, T.P., Koo, S., Scanlan, S.F., 2009. Gait mechanics influence healthy cartilage morphology and osteoarthritis of the knee. J Bone Joint Surg Am 91 Suppl 1, 95-101.

Besier, T.F., Gold, G.E., Beaupré, G.S., Delp, S.L., 2005. A modeling framework to estimate patellofemoral joint cartilage stress in vivo. Medicine & Science in Sports & Exercise 37, 1924.

Chaudhari, A.M.W., Briant, P.L., Bevill, S.L., Koo, S., Andriacchi, T.P., 2008. Knee Kinematics, Cartilage Morphology, and Osteoarthritis after ACL Injury. Med Sci Sports Exerc 40, 8.

Dargel, J., Feiser, J., Gotter, M., Pennig, D., Koebke, J., 2009. Side differences in the anatomy of human knee joints. Knee Surg Sports Traumatol Arthrosc 17, 1368-1376.

Draper, C.E., Besier, T.F., Santos, J.M., Jennings, F., Fredericson, M., Gold, G.E., Beaupre, G.S., Delp, S.L., 2009. Using real-time MRI to quantify altered joint kinematics in subjects with patellofemoral pain and to evaluate the effects of a patellar brace or sleeve on joint motion. J Orthop Res 27, 571-577.

Eckstein, F., 2002. Side differences of knee joint cartilage volume, thickness, and surface area, and correlation with lower limb dominance—an MRI-based study. Osteoarthritis and Cartilage 10, 914-921.

Gerdes, C.M., Kijowski, R., Reeder, S.B., 2007. IDEAL imaging of the musculoskeletal system: robust water fat separation for uniform fat suppression, marrow evaluation, and cartilage imaging. AJR Am J Roentgenol 189, W284-291.

Gokeler, A., Schmalz, T., Knopf, E., Freiwald, J., Blumentritt, S., 2003. The relationship between isokinetic quadriceps strength and laxity on gait analysis parameters in anterior cruciate ligament reconstructed knees. Knee Surgery, Sports Traumatology, Arthroscopy 11, 372-378.

Gold, G.E., 2003. Dynamic and functional imaging of the musculoskeletal system. Seminar in Musculoskeletal Radiology 7, 4.

Gollehon, D.L., Torzilli, P., Warren, R., 1987. The role of the posterolateral and cruciate ligaments in the stability of the human knee. A biomechanical study. The Journal of Bone & Joint Surgery 69, 233-242.

Heiderscheit, B.C., 2000. Movement variability as a clinical measure for locomotion. Journal of Applied Biomechanics 16, 419-427.

Hofbauer, M., Thorhauer, E.D., Abebe, E., Bey, M., Tashman, S., 2014. Altered Tibiofemoral Kinematics in the Affected Knee and Compensatory Changes in the Contralateral Knee After Anterior Cruciate Ligament Reconstruction. Am J Sports Med, 0363546514549444.

Holt, K.G., Jeng, S.F., Ratcliffe, R., Hamill, J., 1995. Energetic cost and stability during human walking at the preferred stride frequency. Journal of motor behavior 27, 164-178.

Iwaki, H., Pinskerova, V., Freeman, M.A.R., 2000. Tibiofemoral movement1: the shapes and relative movements of the femur and tibia in the unloaded cadaver knee. J Bone Joint Surg [Br] 82-B, 7.

Jamison, S., Flanigan, D., Nagaraja, H., Chaudhari, A., 2010. Side-to-side differences in anterior cruciate ligament volume in healthy control subjects. J Biomech 43, 576-578.

Johnson, K.M., Lum, D.P., Turski, P.A., Block, W.F., Mistretta, C.A., Wieben, O., 2008. Improved 3D phase contrast MRI with off-resonance corrected dual echo VIPR. Magnetic Resonance in Medicine 60, 8.

Jonsson, H., Kärrholm, J., Elmqvist, L.G., 1993. Laxity after cruciate ligament injury in 94 knees: the KT-1000 arthrometer versus roentgen stereophotogrammetry. Acta Orthopaedica 64, 567-570.

Kaiser, J., Bradford, R., Johnson, K., Wieben, O., Thelen, D.G., 2013. Measurement of tibiofemoral kinematics using highly accelerated 3D radial sampling. Magnetic Resonance in Medicine 69, 1310-1316.

Kozanek, M., Van de Velde, S.K., Gill, T.J., Li, G., 2008. The contralateral knee joint in cruciate ligament deficiency. Am J Sports Med 36, 2151-2157.

Li, G., Kozanek, M., Hosseini, A., Liu, F., Van de Velde, S.K., Rubash, H.E., 2009. New fluoroscopic imaging technique for investigation of 6DOF knee kinematics during treadmill gait. J Orthop Surg Res 4, 6.

Lustig, M., Donoho, D.L., Santos, J.M., Pauly, J.M., 2008. Compressed sensing MRI. Ieee Signal Proc Mag 25, 72-82.

Miranda, D.L., Rainbow, M.J., Leventhal, E.L., Crisco, J.J., Fleming, B.C., 2010. Automatic determination of anatomical coordinate systems for three-dimensional bone models of the isolated human knee. J Biomech 43, 4.

Papannagari, R., Gill, T.J., DeFrate, L.E., Moses, J.M., Petruska, A.J., Li, G., 2006. In vivo kinematics of the knee after anterior cruciate ligament reconstruction. Am J Sports Med 34.

Powell, M.J.D., 1964. An efficient method for finding the minimum of a function of several variables without calculating derivatives. The Computer Journal 7, 155.

Pruessmann, K.P., Weiger, M., Bornert, P., Boesiger, P., 2001. Advances in sensitivity encoding with arbitrary k-space trajectories. Magn Reson Med 46, 638-651.

Roewer, B.D., Di Stasi, S.L., Snyder-Mackler, L., 2011. Quadriceps strength and weight acceptance strategies continue to improve two years after anterior cruciate ligament reconstruction. J Biomech 44, 1948-1953.

Sheehan, F.T., Zajac, F.E., Drace, J.E., 1998. Using cine phase contrast magnetic resonance imaging to non-invasively study in vivo knee dynamics. J Biomech 31, 6.

Silder, A., Westphal, C.J., Thelen, D.G., 2009. A magnetic resonance-compatible loading device for dynamically imaging shortening and lengthening muscle contraction mechanics. J Med Devices 3, 53.

Stergiou, N., Ristanis, S., Moraiti, C., Georgoulis, A.D., 2007. Tibial rotation in anterior cruciate ligament (ACL)-deficient and ACL-reconstructed knees: A theoretical proposition for the development of osteoarthritis. J Sports Med 37, 13.

Tashman, S., 2004. Abnormal Rotational Knee Motion During Running After Anterior Cruciate Ligament Reconstruction. American Journal of Sports Medicine 32, 975-983.

Tashman, S., Kolowich, P., Collon, D., Anderson, K., Anderst, W., 2007. Dynamic function of the ACL-reconstructed knee during running. Clin Orthop Relat Res 454, 66-73.

Van de Velde, S.K., Gill, T.J., Li, G., 2009. Evaluation of kinematics of anterior cruciate ligament-deficient knees with use of advanced imaging techniques, three-dimensional modeling techniques, and robotics. J Bone Joint Surg Am 91 Suppl 1, 108-114.

Westphal, C.J., 2009. Load dependent variations in knee kinematics measured by dynamic magnetic resonance imaging. University of Wisconsin, Madison, WI.

Wilson, D., Feikes, J., O'connor, J., 1998. Ligaments and articular contact guide passive knee flexion. J Biomech 31, 1127-1136.

Wu, G., Cavanagh, P.R., 1995. ISB recommendations for standardization in the reporting of kinematic data. J Biomech 28, 1257-1262.

Chapter 4

Effect of Loading on In Vivo Kinematics of Healthy and ACL-Reconstructed Knees

Jarred Kaiser, Michael F. Vignos, Richard Kijowski, Geoffrey Baer, Darryl G. Thelen

(Note that this chapter has been prepared for submission to Journal of Biomechanics)

Abstract

Abnormal tibiofemoral kinematics have been reported after ACL-reconstruction during locomotor tasks and have been hypothesized to contribute to the high rates of early osteoarthritis within twenty years of surgery. MRI is an attractive imaging modality to test this hypothesis due to its ability to image cartilage morphology and biomarkers of osteoarthritis. While recent advances in MRI allow for accurate measure of knee motion, clinically significant kinematic measures may not be possible within a MR bore due to limitations in motion and loading. The purpose of this study was to test the effect of loading on healthy and ACL-reconstructed knee kinematics during knee flexion and extension with a clinical MR bore. The bilateral knees of twelve subjects who had recently underwent unilateral ACL-reconstruction were imaged for this study. Subjects were placed within an MR-compatible loading device and were instructed to flex and extend their knee at 0.5 Hz under passive and active loading conditions. A 3D dynamic volumetric MRI sequence captured six degree-of-freedom tibiofemoral and patellofemoral kinematics. A two-way ANOVA was then used to test the effect of surgery and tibiofemoral flexion angle on secondary tibiofemoral and patellofemoral kinematics. We found that loading induced internal tibial rotation and translation differences, as well as differences in all six degrees of freedom in the patellofemoral joint, in all knees when compared with passive loading. While no kinematic differences were found in the ACL-reconstructed knee during passive loading, we found a more externally rotated tibia and patella in the reconstructed knees during active flexion-

extension, consistent with previous studies of upright, dynamic movement. This study supports the use of a loaded dynamic task within an MR bore for testing abnormal knee mechanics following ACL-reconstruction.

Keywords: knee kinematics; ACL-reconstruction; biomechanics; MRI

1. Introduction

Tibiofemoral kinematic abnormalities have been observed in anterior cruciate ligament-reconstructed (ACLR) knees during high loading functional tasks such as gait (1, 2), downhill running (3) and quasi-static lunges (4). It is hypothesized that these small kinematic changes may shift tibiofemoral contact onto thinner regions of cartilage, initiating osteoarthritis (OA) (5), thus potentially explaining the high rates of tibiofemoral osteoarthritis post-ACLR surgery.

Precise tibiofemoral kinematics are difficult to measure using traditional motion capture technology however, leading to the development and use of advanced imaging techniques. Recent advances in magnetic resonance (MR) imaging allows for reconstruction of six degree of freedom tibiofemoral and patellofemoral kinematics during dynamic tasks with high accuracy (<0.8°, 0.5 mm). MRI also has the ability to image soft tissue, enabling easy coupling of knee kinematics with models of cartilage geometry to measure cartilage contact. Thus, MRI is an attractive modality to explore potential links between altered cartilage mechanics and early OA.

Imaging knee kinematics within an MR bore, however, limits tasks to static weight bearing (6), and unloaded (7) and loaded (8) knee flexion tasks with a limited range of motion. Previous work has shown that knee kinematics are load-dependent (9-11) and abnormal knee kinematics post-ACLR may only be detected during a highly loaded task, such as pivoting, jumping, or downhill running (12). Thus, it is unclear if abnormal knee kinematics can be measured post-ACLR with dynamic MRI.

The goal of this paper was to use a novel dynamic, volumetric 3D MRI sequence in conjuncture with a loading device to determine if abnormal tibiofemoral and patellofemoral kinematics can be elicited and detected during a simple knee flexion task. We hypothesize that abnormal tibiofemoral and patellofemoral kinematics following ACLR surgery can be detected during active flexion against load but not during passive motion.

2. Materials and Methods

2.1. Subjects

The bilateral knees of 12 subjects (6 M/6 F, age, 25.1 ± 4.6 y; height, 1.76 ± 0.09 m; mass, 83.2 ± 17.0 kg; 2.2 ± 0.7 years post-surgery; 7 bone-patellar-tendon-bone grafts; 2 subjects with partial lateral meniscetomies) were tested after obtaining informed consent according to an IRB-approved protocol. Subjects underwent a unilateral, primary ACLR within 1-4 years of being tested, had no concurrent ligament damage and had no post-operative complications. The contralateral knee of the subjects had no history of pain, injury, or surgery and no history of inflammatory or crystalline induced arthritis.

2.2. MRI testing

The ACLR and healthy contralateral knees of the patient subjects were imaged in this study. Subjects were first placed supine within a clinical 3.0T MR scanner (MR750, General Electric Healthcare, Waukesha, WI) with an eight-channel phased array extemity coil (Precision Eight TX/pulse repetition time (TR) High Resolution Knee Array; InVivo, Orlando, FL) centered over their knee. A 3D IDEAL SPGR sequence (TR/TE = 10.48/2.24 ms, in-plane resolution = 0.37x0.37 mm, slice thickness = 0.90 mm resolution, image matrix size = 512x512x304 pixels) was then collected.

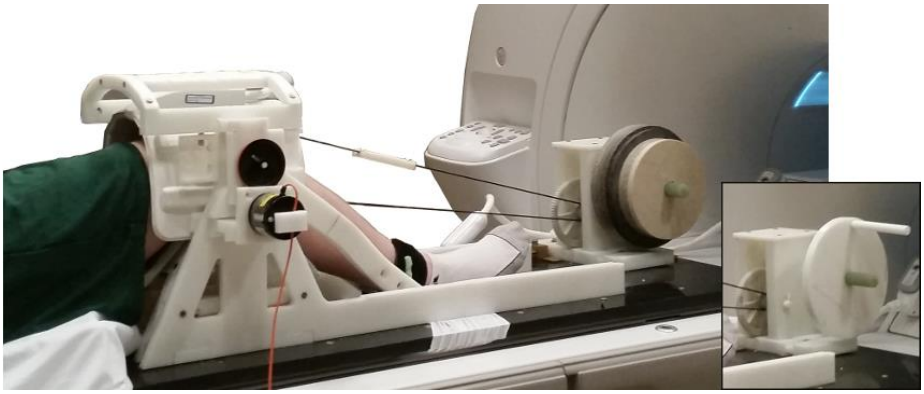

Figure 1. MRI-compatible loading device with inertial disks used for active loading scenario and (insert) handle to facilitate passive loading scenario.

Subjects were then placed supine on an MR-compatible loading device with their lower leg secured to a rotating lever arm (Fig. 1). Subjects performed two separate tasks at 0.5 Hz within this device, with the order of task randomized. The first task was active knee flexion and extension against an inertial load. The inertial load induces eccentric contraction of the quadriceps during flexion. The inertial loads were removed for the second task. A researcher then moved the subject's leg through flexion and extension while the subject laid passive. Subjects were instructed to relax and neither aid nor impede movement.

SPGR-VIPR images were continuously collected for five minutes during both flexion tasks. SPGR-VIPR uses undersampled radial projections to produce 3D volumetric cine images. An MR-compatible rotary encoder (Micronor, Newbury Park, CA), placed at the rotation axis of the loading device, measured knee flexion angle during the tasks. The knee flexion angle was used post-hoc to sort SPGR-VIPR projections into 60 frames for image reconstruction with no temporal view sharing.

2.3. Kinematic Measures

Femoral, tibial and patellar bones were manually segmented (MIMCS, Materialise Group, Leuven, Belgium) from the IDEAL SPGR images to produce subject-specific bone models. Bone models were cleaned, smoothed, and meshed to 7000/7000/2000 triangles for the

femoral, tibial and patellar bones, respectively (Geomagic, Research Triangle Park, NC and MeshLab, Visual Computing Lab-ISTI-CNR). Anatomical coordinate systems were independently defined for each bone using an automatic algorithm which places the axes based on the bones' inertial and geometric properties (13, 14). The origins of the coordinate systems were placed at the centroid of a best-fit cylinder to the femoral condyles, at the center of mass of the tibial plateau, and at the centroid of the patella.

Bone models were then manually placed in the first frame of the dynamic images. Kinematic trajectories were automatically tracked using Powell's method for optimization (15), with an optimization function of the sum squared values of the dynamic images at the bone model vertices. The solution of a frame was used as the initial position and orientation for the following frame, until kinematic trajectories for each bone was determined for the full image set. We have previously shown that model-based tracking of SPGR-VIPR images has a precision of less than 0.8°/0.5 mm.

Tibiofemoral and patellofemoral kinematics were defined at each frame as the position and orientation of the tibia and patella relative to the femur, respectively (16). Kinematics were passed through a Butterworth low-pass filter with a cutoff frequency of 5 Hz. Secondary kinematics were then interpolated to every 2.5° of tibiofemoral flexion through both the flexion and extension phase of the kinematic cycle.

2.4. Statistics

A three-way repeated measures ANOVA tested the effect of limb status (reconstructed vs. healthy), load (active vs. passive) and flexion angle (every 2.5° flexion and extension) on differences in secondary tibiofemoral and patellofemoral kinematics. If an interaction effect was detected in either ANOVA ($p<0.10$, adjusted for reduced power for detection (17)), then a

Bonferroni test was used to determine group-based differences in limb status or loading. If no interaction effects were detected, the main effects were examined for differences. Significance was set to $p<0.05$ for all tests but the interaction effects.

3. Results

Knees displayed anterior tibial translation and external tibial rotation during active and passive knee extension. Active loading produced significant kinematic differences across all knees, including greater tibiofemoral internal rotation, and lateral translation near extension (Fig. 2). Loading also produced greater anterior and inferior during extension. Patellofemoral kinematic differences with loading included extension with knee extension, medial rotation, medial tilt, lateral translation at extension, anterior translation at flexion, and superior during extension translation (Fig. 3). Differences in patellofemoral kinematics were more pronounced during tibiofemoral extension.

ACLR knees displayed an externally rotated tibia and medially rotated patella when compared with the contralateral knee during only the active loading case. A superior tibia was detected during active flexion. A 0.6 to 1.0 mm shift in medial tibiofemoral kinematics was observed in the passive and active cases, though neither reached significance ($p=0.22$).

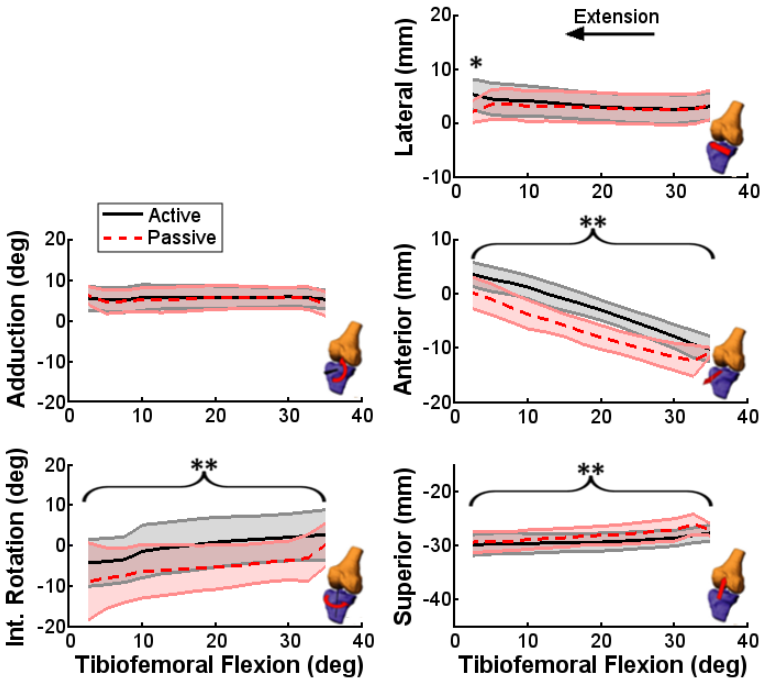

Figure 2. Load-dependent changes in secondary tibiofemoral kinematics of healthy contralateral knees. Active loading produced a significant increase in internal tibial rotation, anterior and superior translation, as well as lateral translation at extension (* denotes a load-by-angle difference, ** denotes a load difference).

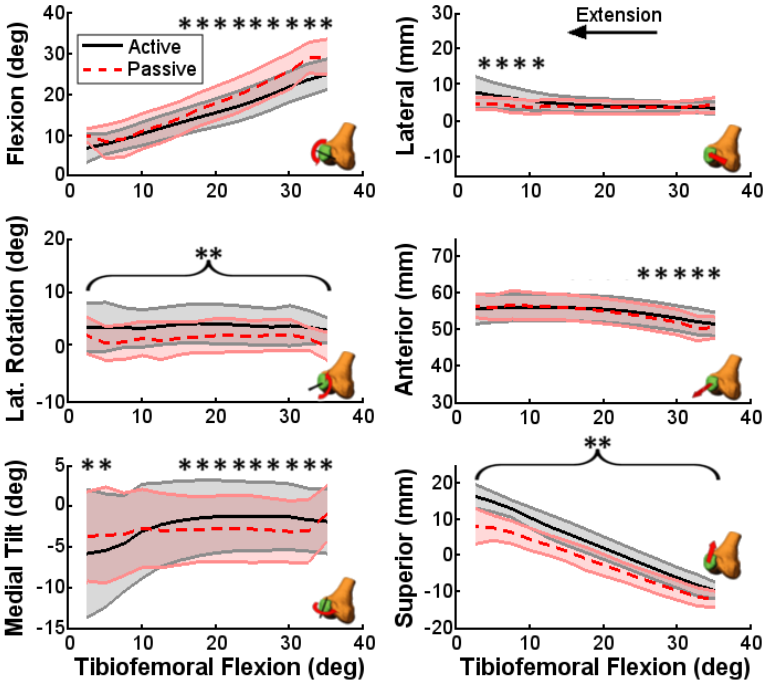

Figure 3. Load-dependent changes in patellofemoral kinematics of healthy contralateral knees. Active loading produced a significant increase in lateral rotation and superior translation, as well as extension, medial tilt, and anterior translation at flexion and medial tilt and lateral translation at extension (* denotes a load-by-angle difference, ** denotes a load difference).

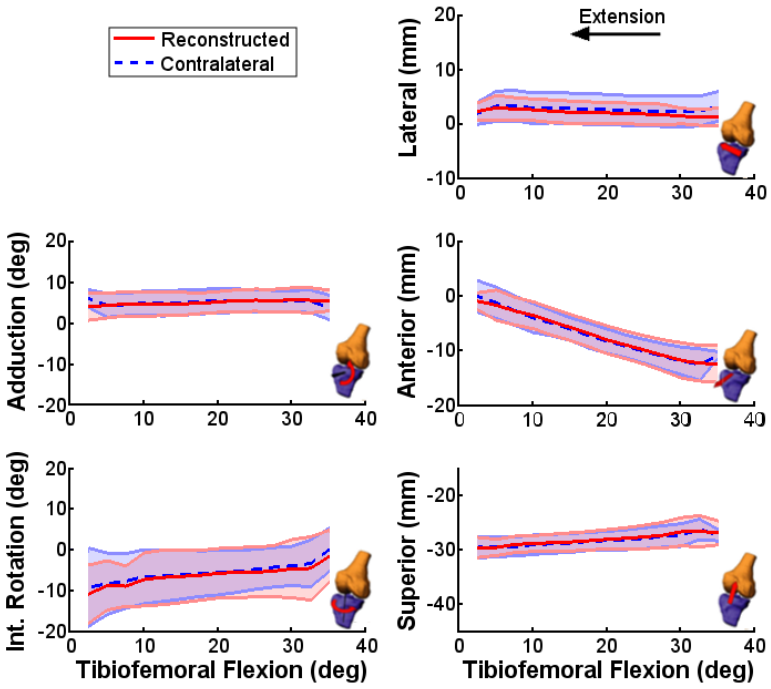

Figure 4. No significant leg differences in secondary tibiofemoral kinematics exist during passive extension.

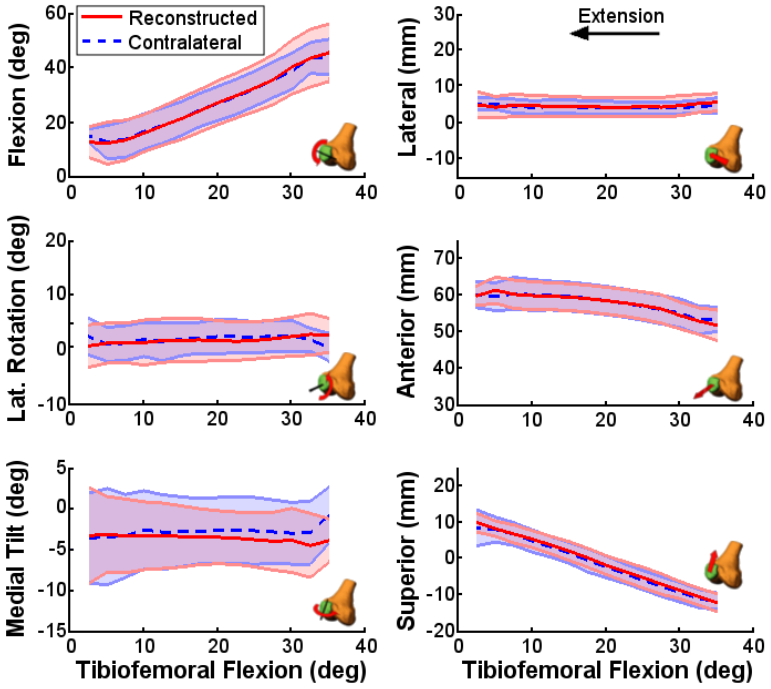

Figure 5. No significant leg differences in patellofemoral kinematics exist during passive extension.

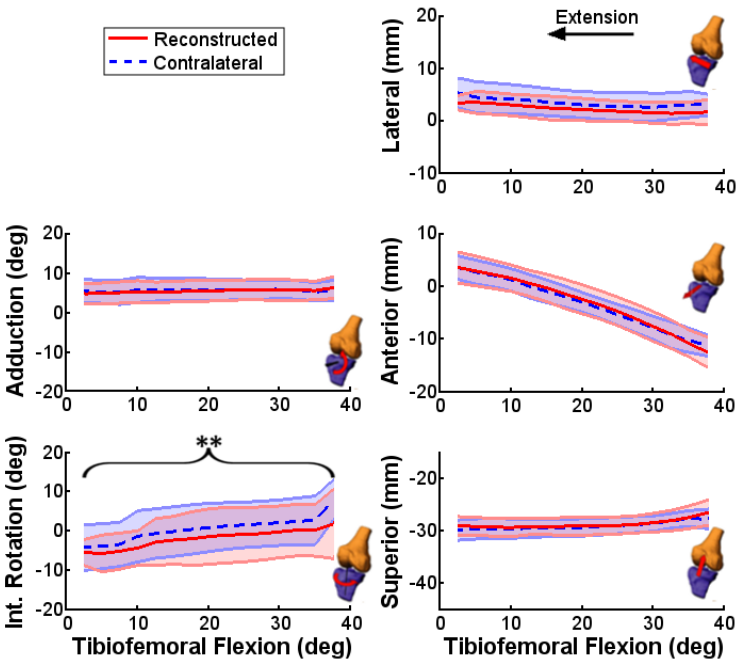

Figure 6. Secondary tibiofemoral kinematics during active extension. ACL-reconstructed knees exhibited greater external rotation throughout the entire flexion-extension cycle than contralateral knees (** denotes a leg difference).

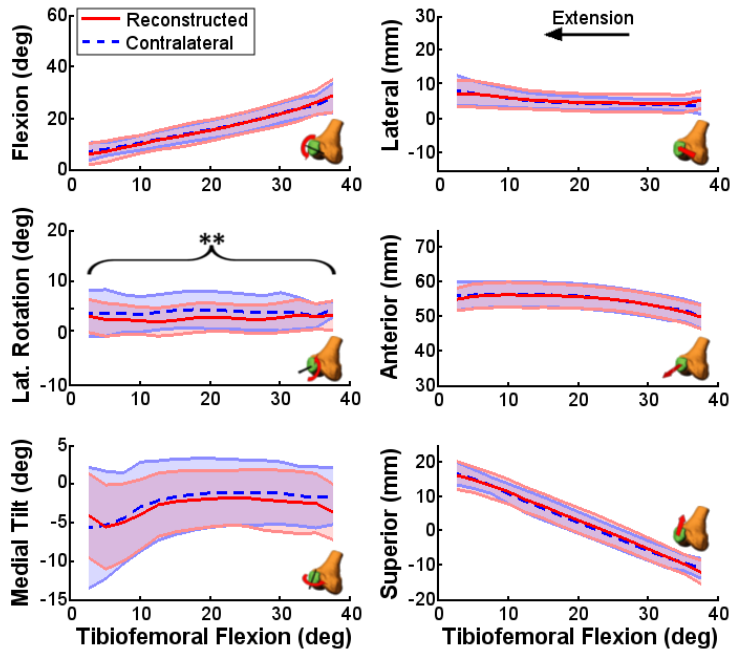

Figure 7. Patellofemoral kinematics during active extension. A significant leg difference and leg-by-angle difference was found in lateral rotation throughout the whole motion cycle and superior translation through extension, respectively (* denotes a leg-by-angle difference, ** denotes a leg difference).

4. Discussion

Using an MR-compatible loading device and a novel dynamic MRI sequence, we were able to (i) elicit significant differences tibiofemoral and patellofemoral kinematics with active loading and (ii) measure kinematic differences in ACLR knees. Specifically, loading induced internal tibial rotation and translational differences when compared to passive loading cases across all knees. In the active case, we observed a more externally rotated tibia and patella in ACLR knees when compared to healthy contralateral knees. While the direct consequence of these kinematic differences are unknown, they could have a potential link to anterior knee pain and early osteoarthritis in both the tibiofemoral and patellofemoral joints following ACLR.

Abnormal tibiofemoral kinematics have been well-studied following ACLR surgery. It has previously argued that a high loading task, such as downhill running, is necessary to elicit measureable differences in tibial rotation (12). Indeed, kinematic differences were not observed during passive flexion and extension, where motion is primarily guided by contact and soft tissue constraints.

In contrast to this observation, however, we were able to measure similar kinematic differences using a slower, low-load scenario when compared with other *in vivo* studies (1, 2, 4, 18). Specifically, we found excessive external tibial rotation with no differences in anterior tibial translation. A medial shift of the tibia post-ACLR has been under-reported in literature, but has recently been observed during running (19). While we did not observe a significant difference, we did observe a persistent medial shift of 0.6 and 1 mm, for the passive and active loading, respectively, which could imply a potential misalignment of the knee during surgery if continued to be observed across more subjects. One possible explanation of our observation of kinematic differences in a low load scenario is that our task is open-chained, which reduces hamstring co-contraction (20), and anterior knee stability (21). Tissue and geometric differences in the graft,

compared to the native ACL, then may be able to induce measureable kinematic differences under active loading conditions.

The ability to image kinematic differences in ACLR knees within an MRI bore is attractive due to the ability of MRI to image soft tissues morphology and biomarkers of composition. MR relaxation parameter T1rho has been shown to correlate with proteoglycan content (22) while T2 relaxation is sensitive to changes in collagen integrity (23). These relaxation parameters have been used to find signs of early OA within 1 year post-surgery, before any morphological changes to the cartilage (24). Additional information of ACL graft morphology (25) and health (26) can also provide insight into how surgical and rehabilitative choices affect short and long term outcomes post-ACLR. By combining kinematic or cartilage contact data under active loading with these morphological and compositional images, MRI provides the opportunity of directly linking altered cartilage mechanics after ACLR with signs of early OA.

While numerous studies have used dynamic imaging approaches to measure altered tibiofemoral kinematics, measures of patellofemoral kinematics have been limited to sequential static MR images under partial weight-bearing (27) or quasi-static fluoroscopy images of single-legged lunges (4). The lack of patellofemoral kinematic information post-ACLR is problematic. Clinical patellofemoral issues, such as quadriceps weakness, flexion contracture, or patellofemoral pain, are prevalent after ACLR (28). While lower than the rates of OA in the tibiofemoral joint, rates of patellofemoral OA reach approximately 50% within 15 of surgery (29-31).

Despite no evidence of patellofemoral kinematic changes following ACLR in cadaveric studies (32), imaging studies have found *in vivo* evidence of altered patellofemoral kinematics (4) and contact area (27) during quasi-static and static activities, respectively. Interestingly, there were no significant PF kinematic differences during the static activities, as is the case with our passive

loading. Increased patellar lateral rotation, lateral tilt and shift were observed during quasi-static single leg lunges in subjects who had underwent ACLR with a BPTB graft (4). We only observed abnormal lateral rotation during active extension, which could in part be explained by the excessive external tibial rotation in ACLR knees. The lack of findings in tilt and shift could be the result of a different loading scenario or from the mixed clinical presentation (e.g. meniscal health) and surgical techniques (e.g. graft selection) in our population, which could induce kinematic variability across our subjects and obscure smaller kinematic differences. Though controversial (33, 34), there is some evidence that knees reconstructed with different grafts can result in different functional outcomes (35, 36) due to the graft tissue properties, donor site weakness, and differences in graft geometry.

The contralateral knee was used as the kinematic control in our study, despite evidence of short-term kinematic changes in the healthy knee (19). While some tissue-level changes are possible in the contralateral knee, the observed changes are most likely due to compensation during a bilateral task such as gait. Further, we have previously shown that bilateral kinematic variability is lower than across-subjects variability, supporting the use of the contralateral knee as a control. However, a longitudinal study of both the reconstructed and contralateral knee is warranted to explore how both limbs adapt after ACLR.

In this study, we used a novel dynamic MRI protocol to explore *in* vivo tibiofemoral and patellofemoral changes in healthy and ACLR knees under different conditions. We found that active knee flexion/extension against an antagonist load induces significant kinematic changes consistent with previous studies of upright, dynamic movement. This study then supports the use of a loaded dynamic task in conjuncture with MRI to explore links between abnormal knee mechanics and early OA following ACLR.

Conflict of interest

No conflicts of interest exist for the authors.

Acknowledgements

The authors gratefully acknowledge the contributions of Rachel Lenhart, Colin Smith, Arezu Monawer, James Hermus, Kelli Hellenbrand, Sara John, and Christopher Westphal, and the financial support of NIH AR056201 and the Robert W. Bolz Distinguished Graduate Fellowship Program.

References

1. Butler RJ, Minick KI, Ferber R, Underwood F. Gait mechanics after ACL reconstruction: implications for the early onset of knee osteoarthritis. Br J Sports Med. 2009;43(5):366-70.

2. Scanlan SF, Chaudhari AM, Dyrby CO, Andriacchi TP. Differences in tibial rotation during walking in ACL reconstructed and healthy contralateral knees. J Biomech. 2010;43(9):1817-22. PMCID: 2882513.

3. Tashman S, Kolowich P, Collon D, Anderson K, Anderst W. Dynamic function of the ACL-reconstructed knee during running. Clin Orthop Relat Res. 2007;454:66-73.

4. Van de Velde SK, Gill TJ, DeFrate LE, Papannagari R, Li G. The effect of anterior cruciate ligament deficiency and reconstruction on the patellofemoral joint. Am J Sports Med. 2008;36(6):1150-9.

5. Stergiou N, Ristanis S, Moraiti C, Georgoulis AD. Tibial rotation in anterior cruciate ligament (ACL)-deficient and ACL-reconstructed knees: A theoretical proposition for the development of osteoarthritis. J Sports Med. 2007;37(7):13.

6. Carpenter RD, Majumdar S, Ma CB. Magnetic resonance imaging of 3-dimensional in vivo tibiofemoral kinematics in anterior cruciate ligament-reconstructed knees. Arthroscopy. 2009;25(7):760-6.

7. Seisler AR, Sheehan FT. Normative three-dimensional patellofemoral and tibiofemoral kinematics: A dynamic, in vivo study. IEEE Trans Biomed Eng. 2007;54(7):9.

8. Kaiser J, Bradford R, Johnson K, Wieben O, Thelen DG. Measurement of tibiofemoral kinematics using highly accelerated 3D radial sampling. Magnetic Resonance in Medicine. 2013;69(5):1310-6.

9. Westphal CJ, Schmitz A, Reeder SB, Thelen DG. Load-dependent variations in knee kinematics measured with dynamic MRI. J Biomech. 2013.

10. Moro-oka T-a, Hamai S, Miura H, Shimoto T, Higaki H, Fregly BJ, et al. Dynamic activity dependence of in vivo normal knee kinematics. J Ortho Research. 2008;26(4):428-34.

11. Victor J, Labey L, Wong P, Innocenti B, Bellemans J. The influence of muscle load on tibiofemoral knee kinematics. J Orthop Res. 2010;28(4):419-28.

12. Tashman S, Kopf S, Fu FH. The Kinematic Basis of ACL Reconstruction. Oper Tech Sports Med. 2008;16(3):116-8. PMCID: 2677828.

13. Rainbow MJ, Miranda DL, Cheung RT, Schwartz JB, Crisco JJ, Davis IS, et al. Automatic determination of an anatomical coordinate system for a three-dimensional model of the human patella. J Biomech. 2013.

14. Miranda DL, Rainbow MJ, Leventhal EL, Crisco JJ, Fleming BC. Automatic determination of anatomical coordinate systems for three-dimensional bone models of the isolated human knee. J Biomech. 2010;43(8):4.

15. Powell MJD. An efficient method for finding the minimum of a function of several variables without calculating derivatives. The Computer Journal. 1964;7(2):155.

16. Grood E, Suntay W. A joint coordinate system for the clinical description of three-dimensional motions: application to the knee. J Biomech Eng. 1983;105(2):9.

17. Maxwell SE, Delaney HD. Designing experiments and analyzing data: A model comparison perspective: Psychology Press; 2004.

18. Tashman S. Abnormal Rotational Knee Motion During Running After Anterior Cruciate Ligament Reconstruction. American Journal of Sports Medicine. 2004;32(4):975-83.

19. Hofbauer M, Thorhauer ED, Abebe E, Bey M, Tashman S. Altered Tibiofemoral Kinematics in the Affected Knee and Compensatory Changes in the Contralateral Knee After Anterior Cruciate Ligament Reconstruction. Am J Sports Med. 2014:0363546514549444.

20. Kvist J, Gillquist J. Sagittal Plane Knee Translation and Electromyographic Activity During Closed and Open Kinetic Chain Exercises in Anterior Cruciate Ligament-Deficient Patients and Control Subjects. Am J Sports Med. 2001;29(1):72-82.

21. Yack HJ, Collins CE, Whieldon TJ. Comparison of closed and open kinetic chain exercise in the anterior cruciate ligament-deficient knee. Am J Sports Med. 1993;21(1):49-54.

22. Duvvuri U, Kudchodkar S, Reddy R, Leigh JS. T1ρ relaxation can assess longitudinal proteoglycan loss from articular cartilage in vitro. Osteoarthritis and Cartilage. 2002;10(11):838-44.

23. Mosher TJ, Dardzinski BJ, Smith MB. Human Articular Cartilage: Influence of Aging and Early Symptomatic Degeneration on the Spatial Variation of T2—Preliminary Findings at 3 T 1. Radiology. 2000;214(1):259-66.

24. Li X, Kuo D, Theologis A, Carballido-Gamio J, Stehling C, Link TM, et al. Cartilage in anterior cruciate ligament-reconstructed knees: MR T1rho and T2-initial experience with 1-year follow-up. Radiology. 2011;258(2):10.

25. Scanlan SF, Donahue JP, Andriacchi TP. The in vivo relationship between anterior neutral tibial position and loss of knee extension after transtibial ACL reconstruction. Knee. 2014;21(1):74-9.

26. Biercevicz AM, Miranda DL, Machan JT, Murray MM, Fleming BC. In Situ, Noninvasive, T2*-Weighted MRI-Derived Parameters Predict Ex Vivo Structural Properties of an Anterior Cruciate Ligament Reconstruction or Bioenhanced Primary Repair in a Porcine Model. Am J Sports Med. 2013;41(3):560-6.

27. Shin CS, Carpenter RD, Majumdar S, Ma CB. Three-dimensional in vivo patellofemoral kinematics and contact area of anterior cruciate ligament-deficient and -reconstructed subjects using magnetic resonance imaging. Arthroscopy. 2009;25(11):1214-23.

28. Sachs RA, Daniel DM, Stone ML, Garfein RF. Patellofemoral problems after anterior cruciate ligament reconstruction. Am J Sports Med. 1989;17(6):760-5.

29. Järvelä T, Paakkala T, Kannus P, Järvinen M. The incidence of patellofemoral osteoarthritis and associated findings 7 years after anterior cruciate ligament reconstruction with a bone-patellar tendon-bone autograft. Am J Sports Med. 2001;29(1):18-24.

30. Shino K, Nakagawa S, Inoue M, Horibe S, Yoneda M. Deterioration of patellofemoral articular surfaces after anterior cruciate ligament reconstruction. Am J Sports Med. 1993;21(2):206-11.

31. Neuman P, Kostogiannis I, Friden T, Roos H, Dahlberg LE, Englund M. Patellofemoral osteoarthritis 15 years after anterior cruciate ligament injury--a prospective cohort study. Osteoarthritis Cartilage. 2009;17(3):284-90.

32. Hsieh YF, Draganich LF, Ho SH, Reider B. The Effects of Removal and Reconstruction of the Anterior Cruciate Ligament on Patellofemoral Kinematics. American Journal of Sports Medicine. 1998;26(2):9.

33. Holm I, Oiestad BE, Risberg MA, Aune AK. No difference in knee function or prevalence of osteoarthritis after reconstruction of the anterior cruciate ligament with 4-strand hamstring autograft versus patellar tendon-bone autograft: a randomized study with 10-year follow-up. Am J Sports Med. 2010;38(3):448-54.

34. Spindler KP, Kuhn JE, Freedman KB, Matthews CE, Dittus RS, Harrell FE. Anterior cruciate ligament reconstruction autograft choice: bone-tendon-bone versus hamstring does it really matter? A systematic review. Am J Sports Med. 2004;32(8):1986-95.

35. Barenius B, Nordlander M, Ponzer S, Tidermark J, Eriksson K. Quality of life and clinical outcome after anterior cruciate ligament reconstruction using patellar tendon graft or quadrupled semitendinosus graft: an 8-year follow-up of a randomized controlled trial. Am J Sports Med. 2010;38(8):1533-41.

36. Webster KE, Wittwer JE, O'Brien J, Feller JA. Gait patterns after anterior cruciate ligament reconstruction are related to graft type. Am J Sports Med. 2005;33(2):247-54.

Chapter 5

MRI Assessments of Cartilage Mechanics, Morphology and Composition Following ACL-Reconstructive Surgery

Jarred Kaiser, Michael F. Vignos, Fang Liu, Richard Kijowski, Darryl G. Thelen

(Note that this chapter will be submitted for publication in Clinical Biomechanics as the winner of the 2015 American Society Clinical Biomechanics Award)

Abstract

The pathogenesis of early osteoarthritis following ACL-reconstruction is currently unknown. The purpose of this study was to leverage recent advances in quantitative and dynamic MRI to test the hypothesis that abnormal joint mechanics within four years of ACL-reconstruction is accompanied by evidence of early compositional changes in cartilage. The bilateral knees of eleven subjects with a unilateral ACL-reconstruction and the dominant knees of twelve healthy subjects were statically imaged using MRI to assess tibial cartilage thickness and MRI biomarkers of cartilage degeneration. Subjects also actively flexed and extended their knees against an inertial load while a 3D dynamic MRI sequence continuously collected volumetric data. These dynamic images were used to assess tibial cartilage contact during motion. Cartilage thickness, MRI biomarkers, and contact were averaged within twenty regions of interest on both the medial and lateral tibia plateau for all subjects, and a two-way ANOVA tested for the effect of surgical reconstruction and location. ACL-reconstructed knees had greater contact along the medial spine in the medial plateau and along the posterior aspect of the lateral plateau, when compared with their healthy contralateral knees and healthy controls. No significant differences in cartilage thickness were determined. However, there was a significant reduction in the fraction of water bound by proteoglycan in the ACL-reconstructed knees, most notably along the anterior weight-

bearing portion of the medial plateau and the medial portion of the lateral plateau. This study provides evidence that abnormal mechanics in ACL-reconstructed knees are present coincidently with early biomarkers of cartilage degeneration.

Key Words: biomechanics; cartilage; ACL-reconstruction; dynamic MRI; thickness; biomarkers

Introduction

Early onset osteoarthritis (OA) is common in ACL-reconstructed (ACLR) knees, with >50% of patients displaying some signs of radiographic OA within 20 years post-surgery (Liden et al., 2008). The underlying etiology of early OA in this patient population remains unknown, but identifying potential causes is important for establishing clinical management approaches that can best mitigate OA risk. However, investigating the pathogenesis of post-traumatic OA is challenging given the long time periods typically needed to detect clinical and radiographic manifestations of the disease. (Haughom et al., 2012).

Recent developments in quantitative magnetic resonance imaging (MRI) has enabled noninvasive evaluation of cartilage composition and ultra-structure. For example, T1rho relaxation rates have been correlated with proteoglycan content (Duvvuri et al., 2002), while T2 relaxation rates have been shown to sensitive to changes in the collagen fiber network (Mosher et al., 2000). A more recent bi-component T2 mapping technique, mcDESPOT (Deoni et al., 2008; Liu et al., 2014; Liu et al., 2015), can provide relative measures of the fractions of the short and slow relaxing water components of cartilage which are thought to respectively represent water bound to proteoglycan (F_{PG}) and bulk water loosely associated with the cartilage macromolecular matrix (Reiter et al., 2009). Thus, quantitative MRI can potentially detect compositional changes in cartilage that occur early on in the development in OA (Haughom et al., 2012; Li et al., 2011). Indeed, abnormal T1rho and T2 relaxation rates have been detected in specific regions of the

tibiofemoral cartilage within 1-2 years of ACL reconstructive surgery (Li et al., 2011). However, it remains unclear whether biomechanical factors contribute to the changes in MRI biomarkers of early cartilage degeneration.

There is ample evidence that ACLR knees often exhibit subtle abnormalities in knee motion when compared to the contralateral uninjured knee. For example, a small, but significant, shift toward external tibia rotation and medial tibia translation has been observed during locomotion in ACLR knees (Carpenter et al., 2009; Scanlan et al., 2010; Tashman, 2004), along with a potential progressive increase in anterior tibia translation (Hofbauer et al., 2014). It has been theorized that these abnormal kinematic patterns may alter cartilage loading patterns and thereby initiate a cyclic catabolic response that eventually leads to OA (Andriacchi and Mündermann, 2006; Chaudhari et al., 2008). New dynamic MRI sequences can be coupled with high resolution cartilage imaging to investigate whether abnormal kinematics influence cartilage contact patterns during motion (Borotikar and Sheehan, 2013; Kaiser et al., 2013). Further, quantitative MRI can then be used to investigate the association between changes in cartilage contact patterns and the onset of early cartilage degeneration in ACLR knees.

The goal of this study was to use static, dynamic and quantitative MRI to investigate whether abnormal knee mechanics is linked to the pathogenesis of early post-traumatic cartilage degeneration. To do this, we compared images of tibial cartilage morphology, composition, and contact patterns between healthy and ACLR knees that were re-constructed within the prior 1-4 years. We hypothesized that ACLR knees would display different cartilage contact patterns than their contralateral knees and healthy control knees. Further, we hypothesized ACLR knees would exhibit no change in cartilage morphology but would exhibit region specific reductions in proteoglycan bound water.

Methods

Subjects

The bilateral knees of eleven subjects with a primary unilateral, isolated ACL-reconstruction (6 F, 24.7 ± 4.7 yrs, 83.9 ± 17.8 kg, 2.1 ± 0.7 yrs since surgery, 6 patellar tendon grafts, 5 hamstrings grafts, 1 partial lateral meniscectomy, 1 subject with small, stable medial and lateral meniscal tears) and the dominant knees of twelve healthy controls (5F, 24.5 ± 4.7 yrs, 74.9 ± 10.0 kg) were tested after obtaining informed consent according to an IRB-approved protocol. Control subjects and the contralateral knees of ACLR subjects had no history of knee pain, injury or surgery and no history of septic, inflammatory or crystalline induced arthritis. ACLR subjects had no history of septic, inflammatory or crystalline induced arthritis, and no post-operative complications.

Static and Quantitative MRI

Subjects underwent a bilateral static MR protocol consisting of an axial fat-suppressed three-dimensional spoiled gradient recall-echo (3D SPGR) sequence (TR/TE = 10.48/2.24 ms, in-plane resolution = 0.37x0.37 mm, slice thickness = 0.90 mm resolution, image matrix size = 512x512x304 pixels) and a sagittal three-dimensional fast spin-echo (3D FSE Cube) sequence (TR/TE = 2066.7/19.8 ms, in-plane resolution = 0.39x0.39 mm, slice thickness = 1.0 mm resolution, acquisition matrix size = 384x384 pixels). A mcDESPOT sequence, consisting of twenty five (8 spoiled gradient echo SPGR, 1 inversion recovery SPGR and 16 balanced steady-state free precession bSSFP) steady-state image sequences with varying flip angles, was performed unilaterally on the reconstructed knee of the subjects and a healthy knee of the controls (in-plane resolution = 0.62x0.62 mm, slice thickness = 3.0 mm, image matrix size = 256x256 pixels, (Liu et al., 2014). All static scans were performed in a 3.0T clinical MR scanner (Discovery MR750, GE

Healthcare, Waukesha, WI) using an 8-channel phased array extremity coil (InVivo, Orlando, FL). Foam padding was used to firmly secure the knee within the coil to minimize subject motion during the static MR examination.

Distal femur and proximal tibia bone geometries were manually segmented from the 3D SPGR images. Femoral and tibial articular cartilage surfaces were manually segmented (MIMICS, Materialise Group, Leuven, Belgium) from the 3D FSE Cube images (Fig 1), smoothed and then

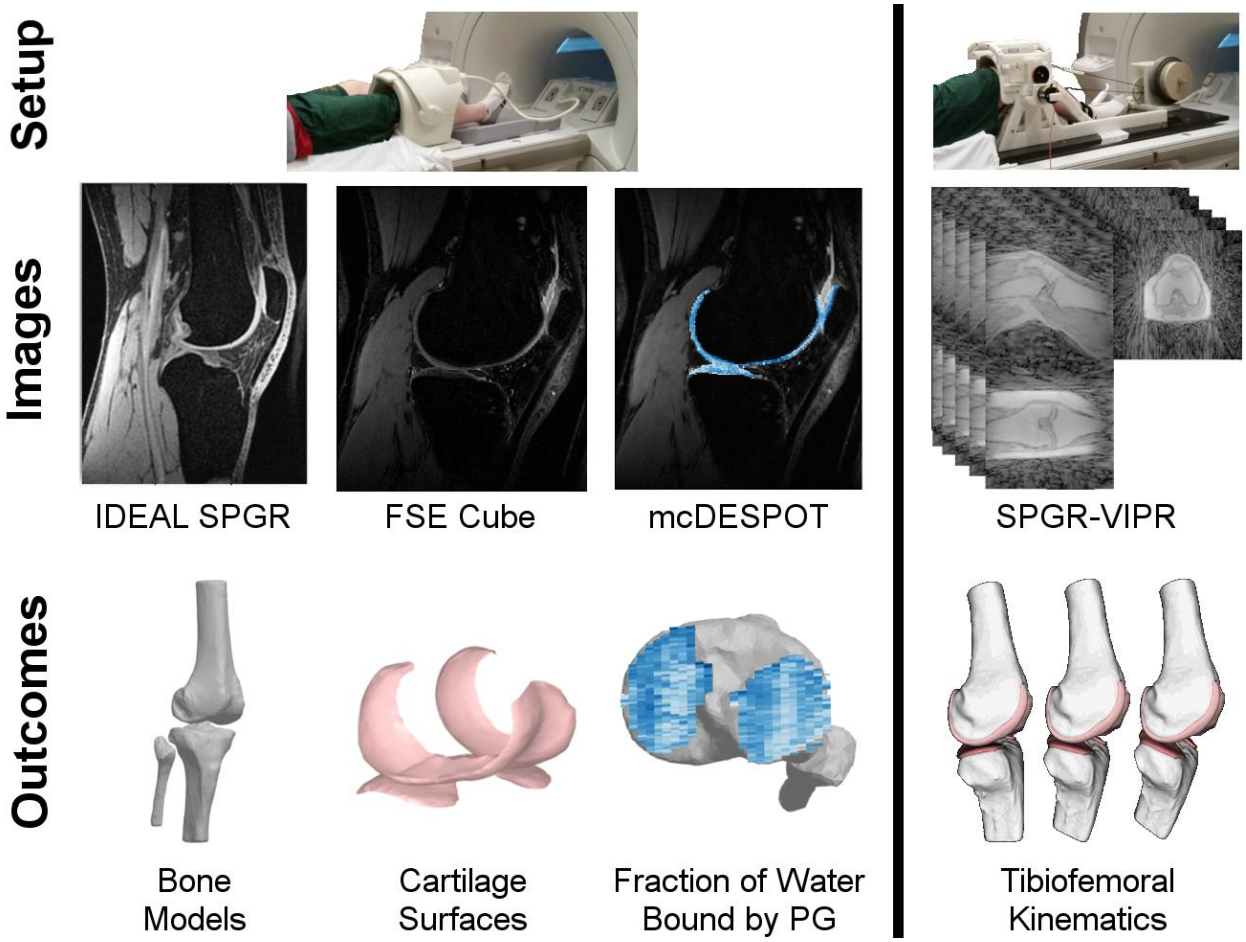

Figure 1. Subjects underwent a MR protocol consisting of two static sequences (IDEAL SPGR, FSE Cube), a quantitative sequence (mcDESPOT) and dynamic imaging (SPGR-VIPR) of a knee flexion-extension task. . The static images were used to create subject-specific models of the bone and cartilage geometries. mcDESPOT was used to compute maps of the fraction of water bound by proteoglycan (PG). Finally, the bone and cartilage models were registered to the dynamic images, providing a quantitative characterization of the tibiofemoral kinematics.

described by polygon meshes (~3 triangles /mm^2) that were registered to the bone models. Anatomical coordinate systems were determined for each bone independently using the bones' inertial and geometric properties (Miranda et al., 2010). Cartilage thickness was defined as the normal distance from each face of the cartilage mesh to the underlying bone.

The mcDESPOT series was used to reconstructed maps of F_{PG} using custom Matlab (MathWorks, Natick, MA) (Liu et al., 2014). Image registration (FLIRT, Functional Magnetic Resonance Imaging of the Brain Analysis Group, Oxford University, UK) was used to align the static and mcDESPOT image sequences. Cartilage masks, segmented from the 3D FSE Cube images, were then interpolated to the mcDESPOT images to separate the articular cartilage from the surrounding tissues. The F_{PG} of three ACLR and one control subjects were omitted from analysis due to substantial motion artifacts.

Dynamic MRI

Immediately following the static MRI protocol, subjects were positioned supine with their lower leg secured on a MRI-compatible loading device. Cyclic knee flexion and extension was performed at 0.5 Hz with the rate maintained via an audible metronome. An inertial loading device induced eccentric quadriceps contraction with knee flexion, similar to the load-acceptance phase of gait (Kaiser et al., 2013). A 3D SPGR sequence with vastly-undersampled isotropic projections (SPGR-VIPR, 1.5 mm isotropic resolution, pulse repetition time/echo time = 4 ms/1.4 ms, flip angle = 8°, receiver bandwidth = 32.5 kHz, unique radial lines = 93,922, field of view = 48 cm, scan time = 5 min) sequence was used to continuously collect image data over five minutes of continuous motion (Fig. 1). A MR-compatible rotary encoder mounted on the device was used to monitor knee flexion angle. The encoder data (collected at 50 Hz) was used retrospectively to bin

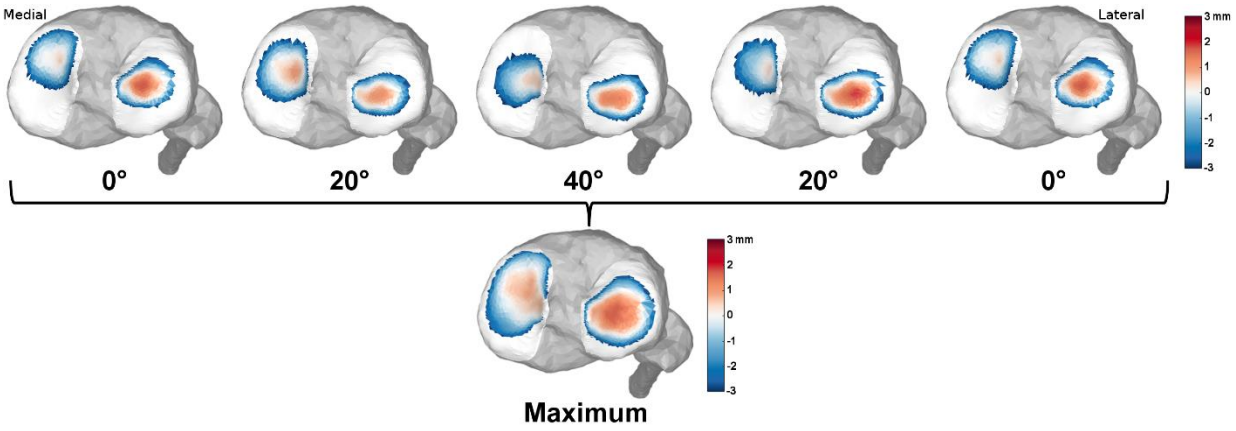

Figure 2. Tibiofemoral kinematics were used to characterize regions of contact (proximity>0) between the tibial and femoral cartilage. Contact maps for each subject were created by then identifying the closest proximity of each face of the cartilage mesh over a flexion-extension motion cycle.

the SPGR-VIPR projections into 60 equal duration intervals over the motion cycle. Sixty SPGR-VIPR images were then reconstructed offline with no view-sharing between frames.

Femoral and tibial bone segments were registered to each frame of the dynamic images. Registration was achieved by using numerical optimization to position the bone segments in a way that minimized the sum squared intensities of the dynamic images at the outer bone model vertices (Powell, 1964). This numerical routine drives the bone models to the dark bone outlines in the dynamic images, and yields the bone 3D translations and rotations in space. Tibiofemoral kinematics were defined as the position and body fixed rotations (flexion-adduction-internal rotation) of the tibia relative to the femur (Grood and Suntay, 1983). Tibiofemoral kinematics were low pass filtered with a third-order bidirectional Butterworth filter with a cut-off frequency of 5 Hz. Cartilage proximity was then calculated at each face of the tibial mesh by projecting along the normal direction to determine the closest femoral mesh face. Positive proximity was indicative of cartilage contact at that location. Tibial cartilage proximity through flexion and extension was re-zeroed such that at least one mesh triangle remained in contact in both the medial and lateral

compartments at each frame (Borotikar and Sheehan, 2013). Tibial plateau proximity maps were presented for those faces in contact or within 3 mm of the femoral cartilage surface. A tibial plateau proximity map was then defined as the closest proximity of each face throughout the motion cycle (Fig 2).

Statistical Analysis

Our primary metrics were cartilage thickness, F_{PG} and contact (proximity) over the tibial plateau surface. Regional analysis was performed by dividing the medial and lateral compartments of the tibial plateau cartilage into 20 rectangular regions of interest (ROIs). Each of the primary metrics were averaged for all cartilage surface pixels within the ROI. F_{PG} measures were averaged through the cartilage thickness. The most lateral and medial ROIs were excluded for the F_{PG} comparisons due to significant partial-volume fractioning at these locations.

A two-way ANOVA tested the effect of surgery and ROI on thickness, F_{PG}, and contact between the ACLR knees and the control subject knees. A repeated measures ANOVA was used to compare the cartilage thickness and contact of the ACLR knees to their healthy contralateral knees. If a significant difference was found ($p<0.05$), a post-hoc Tukey test was performed to identify the location of group differences ($p<0.05$).

Results

The thickest cartilage regions were found in the middle regions of the medial (ACLR: 3.4 ± 0.9 mm, contralateral: 3.4 ± 0.8 mm, control: 3.1 ± 0.7 mm) and lateral (ACLR: 4.5 ± 1.0 mm, contralateral: 4.6 ± 0.8 mm, control: 4.6 ± 0.7 mm) compartments of the tibial plateau (Fig. 4). There were no significant differences in cartilage thickness between any groups (Fig. 5, Fig. 6).

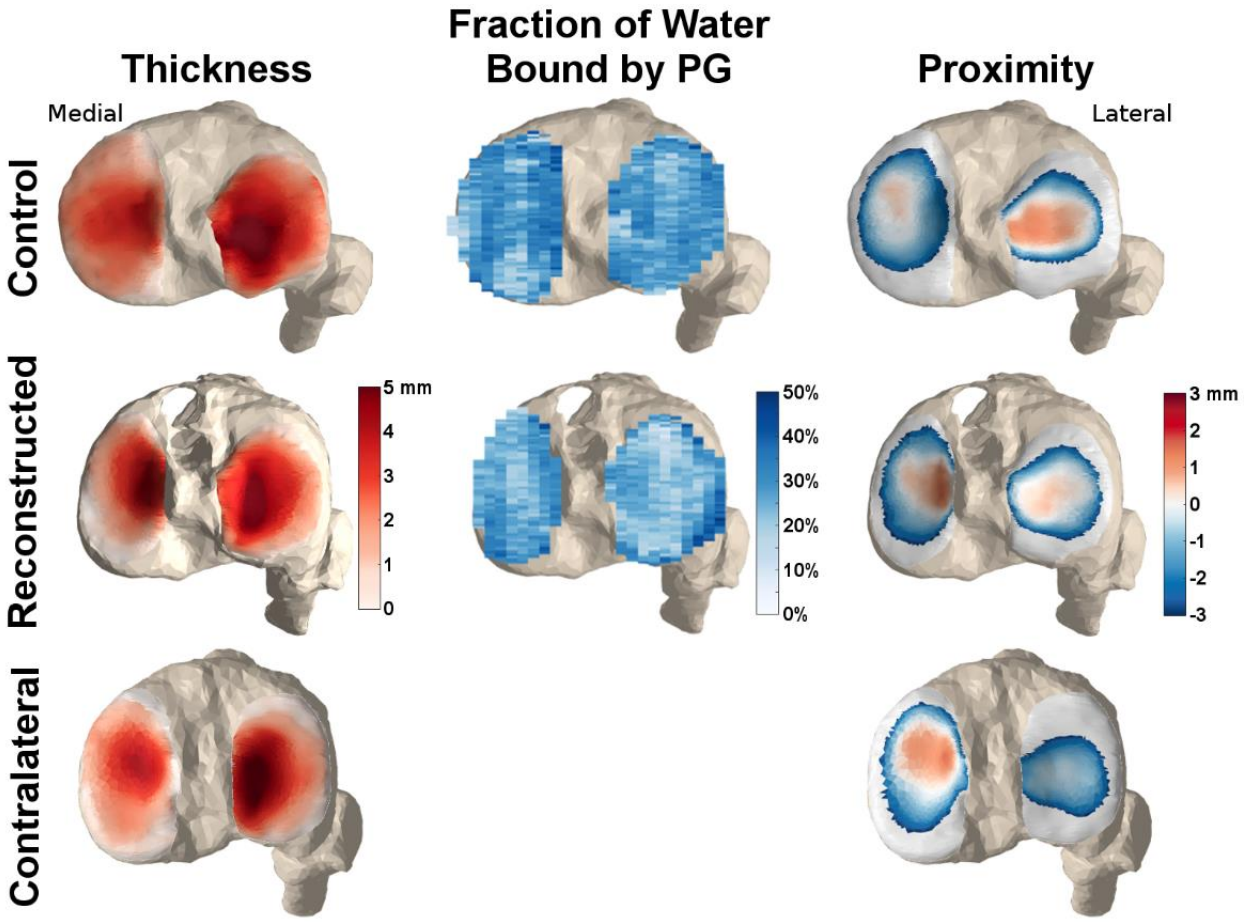

Figure 4. Representative thickness, F_{PG}, and contact (proximity) maps for the tibial plateau of one control subject, an ACL-reconstructed knee and their healthy contralateral knee. Note the greater contact along the medial spine of the medial plateau, and the posteriolateral tibia of the reconstructed knee, when compared to the contralateral and control knees. The subject also exhibits lower F_{PG} relative to the control, particularly in the lateral tibia plateau.

The average F_{PG} in the tibial plateau cartilage ranged from 15.3%-38.5% and 11.3%-37.8% in the control and ACLR knees, respectively. There was a significant decrease in the F_{PG} in the ACLR knees (25.5 +/- 1.5%) when compared with the control knees (27.5 +/- 1.6%). These differences were apparent in the anterior portion of the medial tibia plateau and the medial portion of the lateral tibial plateau (Fig 6).

Cartilage proximity over the tibial plateau cartilage was significantly greater in the ACLR knee when compared to both the control (-0.4 mm average difference) and contralateral (-0.3 mm)

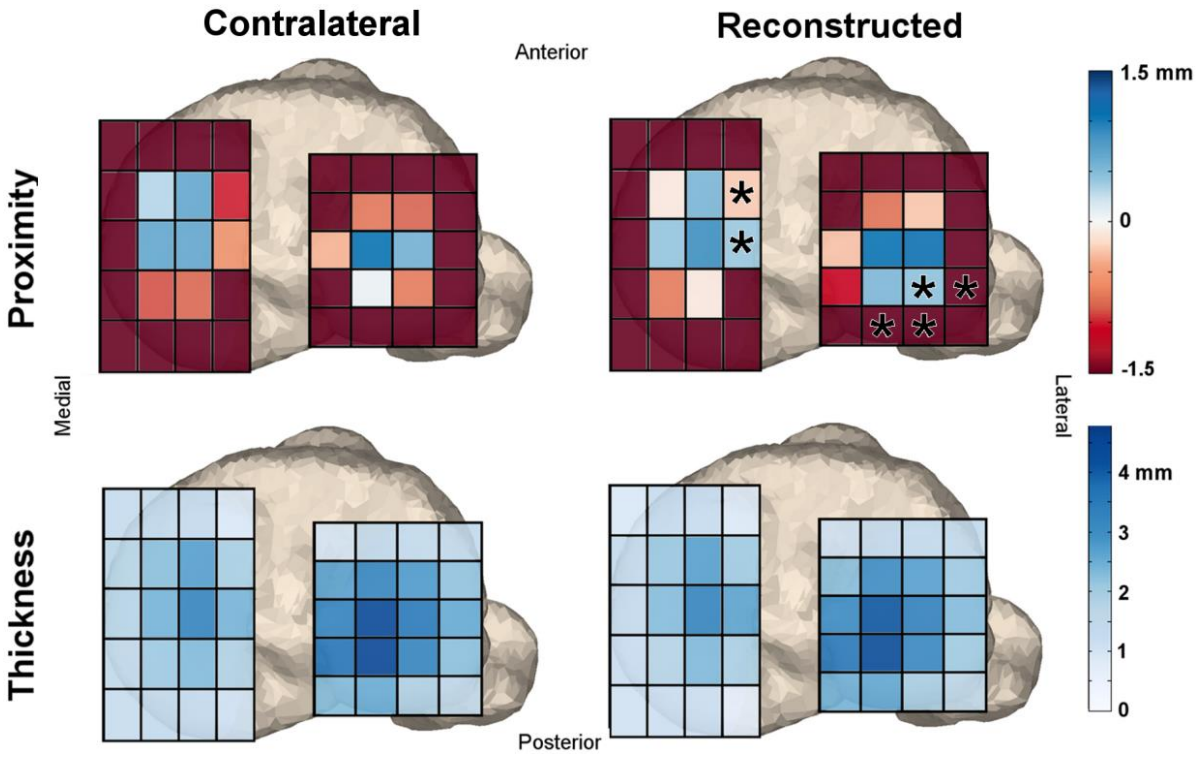

Figure 5. Region of interest comparisons of average cartilage contact (proximity) and thickness between reconstructed and contralateral knees of the subjects who underwent unilateral ACL reconstructive surgery. Asterisks denote areas of significantly larger contact along the medial spine and on the posterior portion of the lateral tibial plateau.

knees. In post-hoc analyses, the significantly greater contact was in the ACLR knees was observed along the medial ridge of the medial tibial plateau and the posterior aspect of the lateral tibial plateau (Fig. 5, Fig. 6).

Discussion

It has been speculated that abnormal knee mechanics can contribute to the development of early OA in ACL-reconstructed knees (Andriacchi et al., 2009). However, direct links between abnormal mechanics and early manifestations of OA are lacking. In this study, we leveraged advances in dynamic and quantitative MRI techniques to test the hypotheses that ACLR knees will exhibit evidence of abnormal cartilage loading and cartilage composition within four years of surgery. Our hypotheses were supported, with ACLR knees exhibiting greater contact in

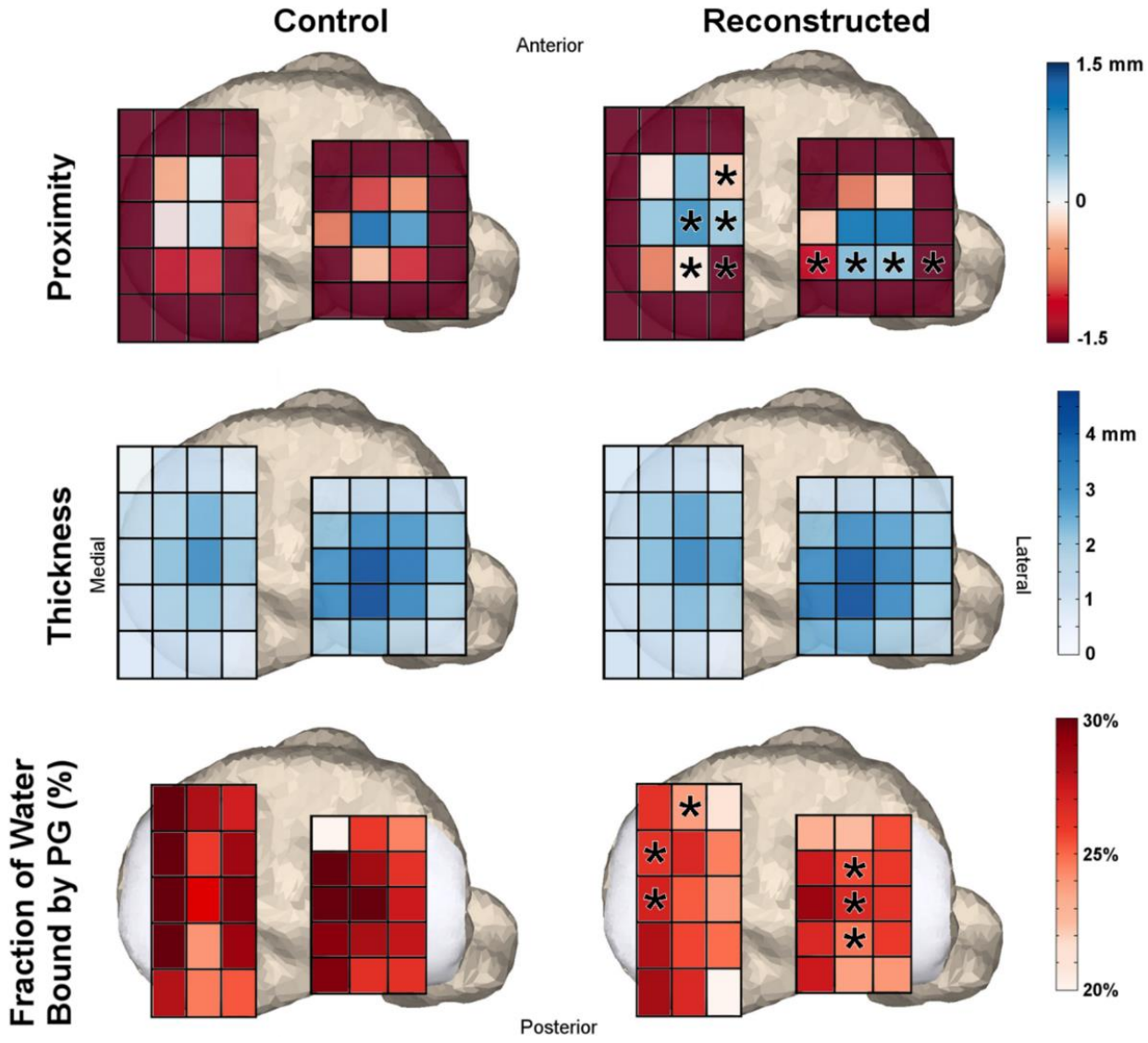

Figure 6. Region of interest comparisons of average cartilage contact (proximity), thickness and F_{pg} between reconstructed knees and healthy control knees. Asterisks denote areas of significant difference between groups. There were no significant differences in cartilage thickness, but there were regions of significantly greater magnitudes of cartilage contact and lower amounts of proteoglycan bound water on both the medial and lateral tibia plateaus.

characteristic regions of both the medial and lateral tibial plateau. Further despite no evidence of cartilage thinning, we noted a decrease in the fraction of water bound by proteoglycan. Thus, this study provides evidence that early MRI biomarkers of cartilage degeneration coincide with the time point at which abnormal knee mechanics can be detected in ACL reconstructed knees.

To our knowledge, this is the first study to show that abnormal tibiofemoral cartilage contact patterns can be detected in reconstructed knees with dynamic MRI. Prior studies using biplanar fluoroscopy have identified greater joint sliding in the medial tibiofemoral compartment during downhill running (Hoshino et al., 2013) A posteriolateral shift in contact in the medial plateau and a posteriomedial shift in the lateral plateau were also found during a single leg quasi-static lunge (Hosseini et al., 2012). Similarly, we observed a significant lateral shift in contact on the medial compartment and a posterior shift on the lateral compartment in the ACLR knees. The similarity of these results suggests that there may be systematic differences in the passive restraint provided by an ACL graft, relative to the native ACL. It is noteworthy that we observed such systematic shifts despite the study population having mixed clinical presentation, graft types and meniscal conditions. This would suggest that other surgical factors, such as graft placement (Abebe et al., 2011; Bedi et al., 2011) and pre-tensioning (Brady et al., 2007; Melby et al., 1991), may contribute to the altered knee mechanics. While greater subject numbers are needed to better test the effects of surgical factors, ultimately computational knee models are important to establish causal relationships between surgical factors and functional knee behavior (Lenhart et al., 2015; Pena et al., 2006; Salehghaffari and Dhaher, 2014; Smith et al., 2015)

The absence of changes in cartilage thickness in the ACLR knees within 4 years is consistent with prior studies suggesting that longer time frames are needed for cartilage thinning to be visible. For example, (Andreisek et al., 2009) found a very small amount of cartilage thinning (on average <0.1 mm) in the lateral aspect of the lateral tibial compartment seven years following ACLR surgery. Additional studies have shown either longitudinal increases in cartilage thickness in ACLR knee over a 2 year follow-up period (Frobell, 2011) or no changes in cartilage thickness in ACLR knees when compared to the contralateral healthy knees at 7 year follow-up (Andreisek

et al., 2009). In contrast, quantitative MRI is able to detect potential evidence of altered cartilage composition within 1-2 years of reconstruction (Li et al., 2011; Tiderius et al., 2005). Quantitative MRI also has the benefit of providing a laminar analysis of cartilage (Li et al., 2011), potentially providing additional information on the depth-dependent changes of early post-traumatic cartilage degeneration. In this study, we found a decrease in the fraction of water bound by proteoglycan. Proteoglycan provides much of the compressive stiffness of cartilage (Buschmann and Grodzinsky, 1995) and the loss of proteoglycan has been identified as a critical event in OA(Rizkalla et al., 1992; Sandy et al., 1992). While quantitative MRI has been directly linked to histological changes evident in OA (Regatte et al., 2006), further study is still needed to see if whether changes in these MRI parameters are associated with in vivo cartilage loss over time and the eventual development of joint pain and radiographic OA

Interestingly, we found no direct correspondence between the regions of abnormal cartilage contact and lower F_{PG}. While reductions in proteogylcan bound water were evident in the reconstructed knees, significant differences were found in cartilage adjoining the higher contact regions. This could be due to several factors. First, all metrics were averaged within ROIs on the order of 60 mm^2. While the ROIs simplify the analysis, it also significantly reduces the quantitative detail available with our methodology. Other studies have shown interesting information exists not only in the magnitude of individual voxels of relaxation rates maps, but also in the spatial distribution of relaxation rates (Blumenkrantz et al., 2008; Li et al., 2009). A voxel-based analysis therefore may further elucidate the relationship between contact, morphology, and composition in the ACLR knees. Furthermore, changes in knee biomechanics may not be the only cause of early cartilage degeneration in ACLR knees. Other factors not investigated in our study including meniscus tears (Li et al., 2011; Neuman et al., 2011) and acute cartilage injury sustained at the

time of joint trauma (Bolbos et al., 2008) and post-traumatic synovial inflammation (Elsaid et al., 2008; Marks and Donaldson, 2005) may have played a role in the onset of early cartilage degeneration in our patient population.

We also recognize that our cartilage contact metric may not fully capture the abnormal mechanical environment of the cartilage tissue. Cellular mechano-transduction is one potential mechanism controlling the catabolic response of cartilage post-ACLR and is influenced by changes in fluid flows and pressures (Mizuno et al., 2002), osmotic levels (Hopewell and Urban, 2002), and changes in pH (Halloran et al., 2012). At a tissue scale, these signals are altered by differing compressive and shear strains (Guilak and Hung, 2005), which are further influenced by cartilage thickness, stiffness, and sliding friction. Our simplified proximity metric likely best reflects compressive pressure and perhaps could be used within a computational model of the cartilage tissue to more fully characteristic factors that can regulate mechano-biological responses.

Our study was limited to an ROI analysis of only the tibial plateau, though early OA has been found in all articular cartilages of the tibiofemoral (Kessler et al., 2008; Meunier et al., 2007; Sward et al., 2010) and patellofemoral (Neuman et al., 2009)joints in ACLR knees. SPGR-VIPR and the mcDESPOT sequences provide a large enough field of view (40x40x40 cm) do enable kinematic and compositional information of all three joints, allowing us to perform a similar analysis of the femoral and patellar cartilages in the future. The flexion-extension task we studied is not upright weight-bearing task. However, the loading paradigm was designed to induce eccentric quadriceps loads of comparable magnitudes to that seen in walking (Kaiser et al., 2013). It is notable that the abnormalities in cartilage contact in the ACLR knees are comparable to that seen during lunges while using biplane fluoroscopy (Hosseini et al., 2012). This result is important since it means that morphology measures, functional behavior and biomarkers of cartilage

degeneration can all potentially be assessed with clinical MRI scanners. Finally, our dynamic MRI methodology acquires image data over many repeat motion cycles, which necessitates the repeatability of the task. Our prior study shows that subjects can closely replicate the desired cycle period when undergoing an inertial loading (Kaiser et al., 2013).

In summary, we found evidence of a shift in the location of contact shift in the medial and lateral tibial plateaus following ACL-reconstruction surgery. We also identified significantly lower fractions of water bound by proteoglycan in the tibial cartilage, which may reflect early cartilage degeneration. Future work will try to explore potential links between surgical factors, cartilage contact and MRI biomarkers following ACLR.

Conflict of Interest

The authors have no conflict of interest to disclose.

Acknowledgements

The authors gratefully acknowledge the funding provided by the NIH (EB015410, AR062733) and the contributions of Oliver Wieben, Kevin Johnson, Kelli Hellenbrand, Jan Yakey, Rachel Lenhart, Colin Smith, James Hermus, and Arezu Monawer.

References

Abebe, E.S., Kim, J.P., Utturkar, G.M., Taylor, D.C., Spritzer, C.E., Moorman, C.T., 3rd, Garrett, W.E., DeFrate, L.E., 2011. The effect of femoral tunnel placement on ACL graft orientation and length during in vivo knee flexion. J Biomech 44, 1914-1920.

Andreisek, G., White, L.M., Sussman, M.S., Kunz, M., Hurtig, M., Weller, I., Essue, J., Marks, P., Eckstein, F., 2009. Quantitative MR imaging evaluation of the cartilage thickness and subchondral bone area in patients with ACL-reconstructions 7 years after surgery. Osteoarthritis Cartilage 17, 871-878.

Andriacchi, T.P., Koo, S., Scanlan, S.F., 2009. Gait mechanics influence healthy cartilage morphology and osteoarthritis of the knee. J Bone Joint Surg Am 91 Suppl 1, 95-101.

Andriacchi, T.P., Mündermann, A., 2006. The role of ambulatory mechanics in the initiation and progression of knee osteoarthritis. Current opinion in rheumatology 18, 514-518.

Bedi, A., Maak, T., Musahl, V., Citak, M., O'Loughlin, P.F., Choi, D., Pearle, A.D., 2011. Effect of tibial tunnel position on stability of the knee after anterior cruciate ligament reconstruction: is the tibial tunnel position most important? Am J Sports Med 39, 366-373.

Blumenkrantz, G., Stahl, R., Carballido-Gamio, J., Zhao, S., Lu, Y., Munoz, T., Le Graverand-Gastineau, M.-P.H., Jain, S., Link, T., Majumdar, S., 2008. The feasibility of characterizing the spatial distribution of cartilage T 2 using texture analysis. Osteoarthritis and Cartilage 16, 584-590.

Bolbos, R.I., Ma, C.B., Link, T.M., Majumdar, S., Li, X., 2008. In vivo T1ρ quantitative assessment of knee cartilage after anterior cruciate ligament injury using 3 Tesla magnetic resonance imaging. Investigative radiology 43, 782.

Borotikar, B.S., Sheehan, F.T., 2013. In vivo patellofemoral contact mechanics during active extension using a novel dynamic MRI-based methodology. Osteoarthritis and Cartilage, 9.

Brady, M.F., Bradley, M.P., Fleming, B.C., Fadale, P.D., Hulstyn, M.J., Banerjee, R., 2007. Effects of initial graft tension on the tibiofemoral compressive forces and joint position after anterior cruciate ligament reconstruction. Am J Sports Med 35, 395.

Buschmann, M., Grodzinsky, A., 1995. A molecular model of proteoglycan-associated electrostatic forces in cartilage mechanics. J Biomech Eng 117, 179-192.

Carpenter, R.D., Majumdar, S., Ma, C.B., 2009. Magnetic resonance imaging of 3-dimensional in vivo tibiofemoral kinematics in anterior cruciate ligament-reconstructed knees. Arthroscopy 25, 760-766.

Chaudhari, A.M.W., Briant, P.L., Bevill, S.L., Koo, S., Andriacchi, T.P., 2008. Knee Kinematics, Cartilage Morphology, and Osteoarthritis after ACL Injury. Med Sci Sports Exerc 40, 8.

Deoni, S.C., Rutt, B.K., Arun, T., Pierpaoli, C., Jones, D.K., 2008. Gleaning multicomponent T1 and T2 information from steady-state imaging data. Magnetic Resonance in Medicine 60, 1372-1387.

Duvvuri, U., Kudchodkar, S., Reddy, R., Leigh, J.S., 2002. T1ρ relaxation can assess longitudinal proteoglycan loss from articular cartilage in vitro. Osteoarthritis and Cartilage 10, 838-844.

Elsaid, K., Fleming, B., Oksendahl, H., Machan, J., Fadale, P., Hulstyn, M., Shalvoy, R., Jay, G., 2008. Decreased lubricin concentrations and markers of joint inflammation in the synovial fluid of patients with anterior cruciate ligament injury. Arthritis & Rheumatism 58, 1707-1715.

Frobell, R.B., 2011. Change in cartilage thickness, posttraumatic bone marrow lesions, and joint fluid volumes after acute ACL disruption. The Journal of Bone & Joint Surgery 93, 1096-1103.

Grood, E., Suntay, W., 1983. A joint coordinate system for the clinical description of three-dimensional motions: application to the knee. J Biomech Eng 105, 9.

Guilak, F., Hung, C., 2005. Physical regulation of cartilage metabolism. Lippincott Williams & Wilkins, Philadephia.

Halloran, J., Sibole, S., van Donkelaar, C., van Turnhout, M., Oomens, C., Weiss, J., Guilak, F., Erdemir, A., 2012. Multiscale mechanics of articular cartilage: potentials and challenges of coupling musculoskeletal, joint, and microscale computational models. Ann Biomed Eng 40, 2456-2474.

Haughom, B., Schairer, W., Souza, R.B., Carpenter, D., Ma, C.B., Li, X., 2012. Abnormal tibiofemoral kinematics following ACL reconstruction are associated with early cartilage matrix degeneration measured by MRI T1rho. Knee 19, 482-487.

Hofbauer, M., Thorhauer, E.D., Abebe, E., Bey, M., Tashman, S., 2014. Altered Tibiofemoral Kinematics in the Affected Knee and Compensatory Changes in the Contralateral Knee After Anterior Cruciate Ligament Reconstruction. Am J Sports Med, 0363546514549444.

Hopewell, B., Urban, J., 2002. Adaptation of articular chondrocytes to changes in osmolality. Biorheology 40, 73-77.

Hoshino, Y., Fu, F., Irrgang, J., Tashman, S., 2013. Can Joint Contact Dynamics Be Restored by Anterior Cruciate Ligament Reconstruction? Clin Orthop Relat Res.

Hosseini, A., Van de Velde, S., Gill, T.J., Li, G., 2012. Tibiofemoral cartilage contact biomechanics in patients after reconstruction of a ruptured anterior cruciate ligament. J Ortho Research 30, 1781-1788.

Kaiser, J., Bradford, R., Johnson, K., Wieben, O., Thelen, D.G., 2013. Measurement of tibiofemoral kinematics using highly accelerated 3D radial sampling. Magnetic Resonance in Medicine 69, 1310-1316.

Kessler, M.A., Behrend, H., Henz, S., Stutz, G., Rukavina, A., Kuster, M.S., 2008. Function, osteoarthritis and activity after ACL-rupture: 11 years follow-up results of conservative versus reconstructive treatment. Knee Surg Sports Traumatol Arthrosc 16, 442-448.

Lenhart, R.L., Kaiser, J., Smith, C.R., Thelen, D.G., 2015. Prediction and Validation of Load-Dependent Behavior of the Tibiofemoral and Patellofemoral Joints During Movement. Ann Biomed Eng, 1-11.

Li, X., Kuo, D., Theologis, A., Carballido-Gamio, J., Stehling, C., Link, T.M., Ma, C.B., Majumdar, S., 2011. Cartilage in anterior cruciate ligament-reconstructed knees: MR T1rho and T2-initial experience with 1-year follow-up. Radiology 258, 10.

Li, X., Pai, A., Blumenkrantz, G., Carballido-Gamio, J., Link, T., Ma, B., Ries, M., Majumdar, S., 2009. Spatial distribution and relationship of T1ρ and T2 relaxation times in knee cartilage with osteoarthritis. Magnetic Resonance in Medicine 61, 1310-1318.

Liden, M., Sernert, N., Rostgard-Christensen, L., Kartus, C., Ejerhed, L., 2008. Osteoarthritic changes after anterior cruciate ligament reconstruction using bone-patellar tendon-bone or hamstring tendon autografts: a retrospective, 7-year radiographic and clinical follow-up study. Arthroscopy 24, 10.

Liu, F., Chaudhary, R., Hurley, S.A., Rio, A., Alexander, A.L., Samsonov, A., Block, W.F., Kijowski, R., 2014. Rapid multicomponent T2 analysis of the articular cartilage of the human knee joint at 3.0 T. Journal of Magnetic Resonance Imaging 39, 1191-1197.

Liu, F., Choi, K.W., Samsonov, A., Spencer, R.G., Wilson, J.J., Block, W.F., Kijowski, R., 2015. Articular Cartilage of the Human Knee Joint: In Vivo Multicomponent T2 Analysis at 3.0 T. Radiology, 142201.

Marks, P.H., Donaldson, M.L.C., 2005. Inflammatory cytokine profiles associated with chondral damage in the anterior cruciate Ligament–Deficient knee. Arthroscopy: The Journal of Arthroscopic & Related Surgery 21, 1342-1347.

Melby, A., Noble, J.S., Askew, M.J., Boom, A.A., Hurst, F.W., 1991. The effects of graft tensioning on the laxity and kinematics of the anterior cruciate ligament reconstructed knee. Arthroscopy: The Journal of Arthroscopic & Related Surgery 7, 257-266.

Meunier, A., Odensten, M., Good, L., 2007. Long-term results after primary repair or non-surgical treatment of anterior cruciate ligament rupture: a randomized study with a 15-year follow-up. Scand J Med Sci Sports 17, 230-237.

Miranda, D.L., Rainbow, M.J., Leventhal, E.L., Crisco, J.J., Fleming, B.C., 2010. Automatic determination of anatomical coordinate systems for three-dimensional bone models of the isolated human knee. J Biomech 43, 4.

Mizuno, S., Tateishi, T., Ushida, T., Glowacki, J., 2002. Hydrostatic fluid pressure enhances matrix synthesis and accumulation by bovine chondrocytes in three-dimensional culture. Journal of Cellular Physiology 193, 319-327.

Mosher, T.J., Dardzinski, B.J., Smith, M.B., 2000. Human Articular Cartilage: Influence of Aging and Early Symptomatic Degeneration on the Spatial Variation of T2—Preliminary Findings at 3 T 1. Radiology 214, 259-266.

Neuman, P., Kostogiannis, I., Fridén, T., Roos, H., Dahlberg, L., Englund, M., 2009. Patellofemoral osteoarthritis 15 years after anterior cruciate ligament injury–a prospective cohort study. Osteoarthritis and Cartilage 17, 284-290.

Neuman, P., Tjörnstrand, J., Svensson, J., Ragnarsson, C., Roos, H., Englund, M., Tiderius, C.J., Dahlberg, L., 2011. Longitudinal assessment of femoral knee cartilage quality using contrast enhanced MRI (dGEMRIC) in patients with anterior cruciate ligament injury–comparison with asymptomatic volunteers. Osteoarthritis and Cartilage 19, 977-983.

Pena, E., Calvo, B., Martinez, M.A., Palanca, D., Doblare, M., 2006. Influence of the tunnel angle in ACL reconstructions on the biomechanics of the knee joint. Clin Biomech (Bristol, Avon) 21, 508-516.

Powell, M.J.D., 1964. An efficient method for finding the minimum of a function of several variables without calculating derivatives. The Computer Journal 7, 155.

Regatte, R.R., Akella, S.V., Lonner, J.H., Kneeland, J.B., Reddy, R., 2006. T1rho relaxation mapping in human osteoarthritis (OA) cartilage: comparison of T1rho with T2. J Magn Reson Imaging 23, 547-553.

Reiter, D.A., Lin, P.C., Fishbein, K.W., Spencer, R.G., 2009. Multicomponent T2 relaxation analysis in cartilage. Magnetic Resonance in Medicine 61, 803-809.

Rizkalla, G., Reiner, A., Bogoch, E., Poole, A., 1992. Studies of the articular cartilage proteoglycan aggrecan in health and osteoarthritis. Evidence for molecular heterogeneity and extensive molecular changes in disease. Journal of Clinical Investigation 90, 2268.

Salehghaffari, S., Dhaher, Y.Y., 2014. A model of articular cruciate ligament reconstructive surgery: A validation construct and computational insights. J Biomech 47, 1609-1617.

Sandy, J.D., Flannery, C.R., Neame, P.J., Lohmander, L.S., 1992. The structure of aggrecan fragments in human synovial fluid. Evidence for the involvement in osteoarthritis of a novel proteinase which cleaves the Glu 373-Ala 374 bond of the interglobular domain. Journal of Clinical Investigation 89, 1512.

Scanlan, S.F., Chaudhari, A.M., Dyrby, C.O., Andriacchi, T.P., 2010. Differences in tibial rotation during walking in ACL reconstructed and healthy contralateral knees. J Biomech 43, 1817-1822.

Smith, C.R., Lenhart, R.L., Kaiser, J., Vignos, M.F., Thelen, D.G., 2015. Influence of Ligament Properties on Tibiofemoral Mechanics in Walking. The journal of knee surgery.

Sward, P., Kostogiannis, I., Neuman, P., Von Porat, A., Boegard, T., Roos, H., 2010. Differences in the radiological characteristics between post-traumatic and non-traumatic knee osteoarthritis. Scand J Med Sci Sports 20, 731-739.

Tashman, S., 2004. Abnormal Rotational Knee Motion During Running After Anterior Cruciate Ligament Reconstruction. American Journal of Sports Medicine 32, 975-983.

Tiderius, C.J., Olsson, L.E., Nyquist, F., Dahlberg, L., 2005. Cartilage glycosaminoglycan loss in the acute phase after an anterior cruciate ligament injury: Delayed gadolinium-enhanced magnetic resonance imaging of cartilage and synovial fluid analysis. Arthritis & Rheumatism 52, 120-127.

Conclusion

This thesis first introduced and validated a novel dynamic MRI technique, termed SPGR-VIPR, which is able to accurately measure 3D knee kinematics with precisions less than 0.8° in joint rotation angles and less than 0.5 mm in joint translations. This technique was then used to determine that bilateral kinematic symmetry exists in healthy subjects during active knee flexion and extension, leading to the exploration of the loading effects in ACL-reconstructed knee when compared to their healthy contralateral limb. While no significant differences were found during passive motion, active flexion-extension against an inertial load elicited external tibial and patellar rotation in the reconstructed knee. These kinematic differences then translated into increased tibial cartilage contact along the medial spine in the medial plateau and in the posterior aspect of the lateral plateau. While no cartilage thickness changes were detected in ACL-reconstructed subjects within 4 years of surgery, a significant decrease in MR biomarkers correlated with proteoglycan content was shown, providing evidence that signs of cartilage degeneration coincide with the time at which abnormal knee mechanics can be detected.

This dissertation stopped short of providing evidence of a direct link between mechanics and early OA. A longitudinal study of pre-surgical, post-surgical and a longer term follow-up is needed for stronger evidence of this connection. Some longitudinal data has already been collected (see Appendix A), but enrollment is still on-going. Another part of the issue, as discussed in Chapter 5, was the averaging of metrics within relatively large regions of interest. The proposed solution was to examine correlations between metrics on a pixel-basis. This has already been shown to work (see Appendix A and B), but has not yet been expanded to include the other quantitative MR metrics (T1rho, single T2) and has not been published. While I have shown the

ability to extend this framework to include patellofemoral kinematics, this work also needs to expand to include contact and biomarker analyses of femoral and patellar cartilage.

Ultimately, it is hoped that this work can point to promising ways in which to reduce the prevalence of early onset osteoarthritis in ACL reconstructed knees. An oft-studied consideration are surgical factors such as graft selection, geometry, placement and pre-loading, which can all be modified. An advantage of MRI is the ability to measure graft geometry and health, which we have started to partially leverage (see Appendix C). If we can correlate changes in knee mechanics with surgical parameters, such as graft selection or placement, then we can potentially give surgeons direct feedback on how to alter their techniques to better long-term outcomes.

To complement this goal, our lab has developed a 12 degree-of-freedom computational knee model, which was created and validated using the dynamic MRI protocol [1]. This model has the exciting potential to predict mechanical outcomes during gait based on stochastic modeling of ligament parameters, spanning thousands of potential combinations of tissue stiffness, reference strain, and placement in very short time frame. Such studies are likely to provide insights and predictions that can be used to more effectively formulate experimental hypotheses and testing paradigms.

The imaging efforts presented in this thesis will continue to support these efforts in two ways. First, new subject-specific models can be created and validated to introduce models spanning different populations (e.g. age, sex, weight, health, etc.). This process is very time-consuming however, so the second use of imaging will be in the development of statistical shape models (SSM), which are analytical models describing the variation of knee morphology over a population. With the large number of subjects already collected (>20 unique healthy knees), we will be able to create a SSM of the whole knee, including cartilage, ligaments and motion, which

can then be used to automatically generate unique knee models based off chosen statistical parameters (e.g. 25th percentile weight male). The SSM can also be directly used to strengthen the imaging project by providing more robust and detailed descriptions of cartilage morphology (e.g. curvature) than thickness. By examining the cartilage in this manner, we may find previously obscured cartilage morphology changes post-ACLR.

This thesis presented evidence of altered mechanics during motion and early cartilage degeneration in a cross-section of subjects within four years of a unilateral ACL-reconstruction. This is the first work to combine these two data sets within the same population. While this data is very exciting, I am even more excited to see the future work coming from the lab in this field.

References

[1] Lenhart, R. L., Kaiser, J., Smith, C. R., and Thelen, D. G., 2015, "Prediction and Validation of Load-Dependent Behavior of the Tibiofemoral and Patellofemoral Joints During Movement," Ann Biomed Eng, pp. 1-11.

Appendix A: MR Imaging of Cartilage Contact and Bound Water in ACL-Deficient and ACL-Reconstructed Knees

Jarred Kaiser, Michael F. Vignos, Fang Liu, Colin R. Smith, Richard Kijowski, Geoffrey Baer, Darryl G. Thelen

(Note that this Appendix was submitted for presentation at the 2016 American Orthopaedic Society for Sports Medicine Conference)

OBJECTIVES: Osteoarthritis (OA) is common following ACL-reconstructive (ACLR) surgery (6). The cause of early OA is not understood, but theories have focused on osteochondral damage at the time of injury (2) and abnormal joint mechanics following surgical repair (7). In this study, we investigate the inter-relationship of cartilage mechanics and biomarkers of OA in both ACL-deficient (ACLD) and ACLR knees. Our approach employs a novel dynamic MR sequence to measure joint mechanics (3) and the recently developed mcDESPOT to assess regional variations in water bound to proteoglycan (PG) (5). We hypothesize that bound water will be diminished in the cartilage of ACLD knees and, after surgery, will continue to adapt in a manner that reflects altered cartilage loading. This abstract presents initial observations on a cross-section of healthy, ACLD and ACLR knees.

METHODS: The dominant knees of 8 healthy controls, ACLD knees of 5 patients and ACLR knees of 8 patients were imaged in a 3T MRI scanner (Table). Controls had no history of pain, injury, or surgery to their knee. Patients had no additional ligament injury and no meniscal damage. ACLD subjects were imaged prior to reconstructive surgery. Femoral and tibial cartilage were segmented from MR images and cartilage thickness was calculated. The mcDESPOT sequence provided a fraction map of water bound to PG (F_{pg}).

Subjects flexed their knee against an inertial load at 0.5 Hz, while a SPGR-VIPR sequence continuously acquired volumetric data. Kinematics were obtained using model tracking of the dynamic images (3). Cartilage was registered to the bone segments for all frames, and contact patterns were characterized by the proximity between surfaces. Spatial representations of tibial cartilage contact, thickness and F_{pg} were co-registered for each subject.

RESULTS: Our initial images suggest lower F_{pg} values in ACLD knees, primarily on the posterior-lateral tibia. This is also observed in ACLR knees, with additional evidence of diminished F_{pg} on the weight-bearing medial tibia. Contact patterns were altered in both groups. ACLD tended to exhibit increased contact on the posterior lateral tibia and anterior contact in the medial tibia. Contact differences in the ACLR knees were subtler, but tended to show a posterior-lateral shift on the medial tibia when compared to control knees (Figure).

DISCUSSION: These initial observations support our hypotheses that cartilage composition may be altered in ACLD knees and continues to adapt following ACLR. While contact in ACLR knees appears to be restored close to the healthy condition, we observed a residual shift in the medial plateau. Interestingly, this shift corresponds with a decrease in PG content not observed in ACLD knees. Loss of PG occurs early in OA, prior to any morphological changes (1,4). Decreased PG content was also observed in ACLD and ACLR knees in the posterio-lateral tibia, consistent with observations of edema and cartilage damage following an ACL injury (2).

CONCLUSION: Initial observations of our novel dynamic and quantitative MR images suggests altered cartilage composition due to both injury and abnormal mechanics following surgical repair.

REFERENCES: **1)** Andreisek G et al. 2009. OA Cartilage 17: 8. **2)** Bolbos RI et al. 2008. Invest Radiol 43: 14. **3)** Kaiser J et al. 2013. MRM 69: 7. **4)** Li X et al. 2011. Radiology 258: 10. **5)** Liu

F. et al 2014. JMRI 39: 8. **6)** Lohmander LS et al. 2007. Am J Sport Med 35: 14. **7)** Tashman S et al. 2007. Clin Orthop Relat Res 454: 8.

Table 1: Subject Information

Subjects	Sex	Age (yrs)	Weight (kg)	Years post-surgery
Healthy	5M/3F	25 ± 4.8	76.8 ± 12.1	-
ACLD	1M/4F	24.4 ± 6.5	73.9 ± 10.2	-
ACLR	4M/4F	25.5 ± 4.5	78.6 ± 15.2	2.0 ± 0.7

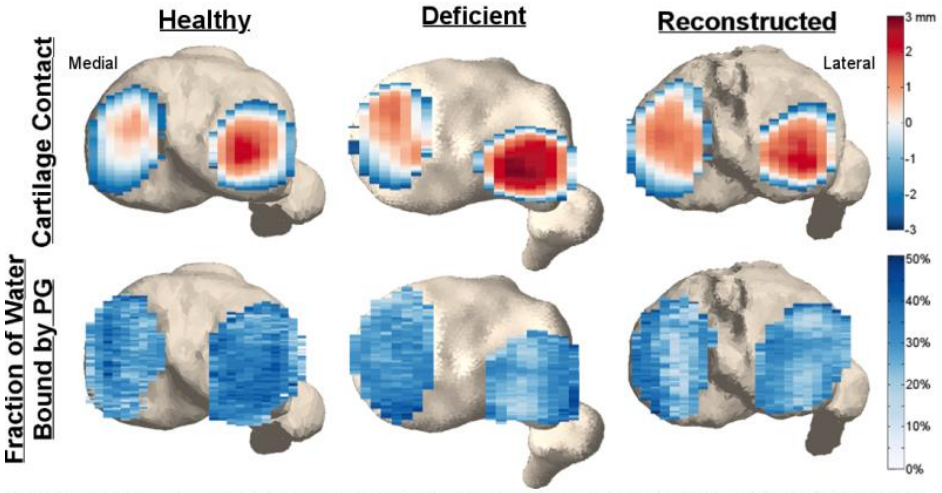

Figure 1. Maps of maximum cartilage contact (top) and fraction of water bound of PG (bottom) for representative subjects of healthy (left), ACLD (center) and ACLR (right) knees. Abnormal contact was observed in the medial compartments of ACLD knees (anterior shift) and ACLR knees (posterior-lateral shift). Decreased PG content was observed in the posterior region of the lateral compartment of the ACLD and ACLR knees, as well as the weight-bearing portion of the ACLR knees in the medial compartment.

Appendix B: Association Between Cartilage Contact, Morphology, and MR Biomarkers in Healthy and ACL-Reconstructed Knees

Jarred Kaiser, Michael F. Vignos, Fang Liu, Richard Kijowski, Geoffrey Baer, Darryl G. Thelen
University of Wisconsin, Madison, WI

(Note that this Appendix was accepted for presentation at the 2016 Orthopaedic Research Society Conference)

INTRODUCTION: Abnormal joint mechanics (8; 10) may explain why early onset osteoarthritis (OA) is common in ACL-reconstructed (ACLR) knees (6). It is theorized that cartilage may be well adapted to accommodate specific loading patterns, and that the tissue may not able to adapt to a shift in contact patterns following ACLR (2). This theory has remained challenging to test due to slow morphological changes during OA. Quantitative MR imaging (T2, T1rho) is enabling earlier detection of OA by tracking biomarkers of water content and collagen structure (5), with abnormalities being detected within one year of ACLR (5). A recently developed MR sequence, termed mcDESPOT, can further distinguish the components of T2, providing estimates of free water and water bound to proteoglycan (PG) (7). However, it remains unclear if these early signs of OA are mediated by mechanical factors. Thus, the goal of this study was to investigate regional variations in cartilage contact, morphology and quantitative MR metrics in both healthy and ACLR knees. We first hypothesized that spatial variations in cartilage thickness and bound water metrics would be positively correlated with cartilage contact in healthy knees. We further hypothesized that areas of contact in the ACLR knees will show no morphological differences, but will show signs of decreased PG content.

METHODS: The dominant knees of eight healthy controls (5 M, 26.25±4.8 yrs, 76.8±12.1 kg, 1.75±0.7 m) and the ACLR knees of eight patients (4 M, 25.5±4.5 yrs, 78.6±15.2 kg, 1.74±0.10

m, 2.0±0.7 yrs post-surgery) were imaged after obtaining informed consent according to an IRB-approved protocol. Control subjects had no history of pain, injury, or surgery to their knee. ACLR subjects had no additional ligament injury, no meniscal repair, and no post-operative complications. All subjects underwent a MRI protocol of a SPGR, a FSE Cube, and a mcDESPOT sequence in a 3T scanner. Femoral and tibial cartilage were segmented from FSE Cube images and cartilage thickness was calculated. Reconstruction of the mcDESPOT sequence provided a fraction map for the fast relaxing T2 signal (Fpg), which is the fraction of water bound to PG within a voxel. Fpg values were averaged through the cartilage thickness.

The lower leg of each subject was then secured to a loading device and a 16-channel flex coil was positioned about the knee. Subjects actively flexed and extended their knee against an inertial load at 0.5 Hz, while a SPGR-VIPR sequence continuously acquired cine 3D volumetric data. Bone segments were then optimally registered to each dynamic frame to reconstruct kinematics (4). Contact was calculated by registering cartilage to the respective bone segments at each time frame, and computing the proximity between cartilage surfaces. The maximum contact of each tibial mesh face through the knee flexion cycle was determined. Spatial representations of cartilage contact, thickness and Fpg were co-registered. 2D maps of each metric were generated by projecting through the maps in the inferior direction. Metrics were linearly interpolated to the center of each pixel of the projected mcDESPOT scans (0.6x3 mm resolution). For every subject, correlations between contact and thickness, as well as between contact and Fpg at every pixel were calculated. For subjects with significant correlations, we used a t-test to determine significant group differences in the slopes of the linear best fits. Significance was set to $p<0.05$.

RESULTS: Thickness had a strong positive correlation with cartilage contact for both the control and ACLR knees, though there were no significant differences between groups in the slopes of the

linear best fit (Fig. 1, controls: 0.38 ± 0.16 mm/mm for medial, 0.36 ± 0.10 mm/mm for lateral; reconstructed: 0.50 ± 0.19 mm/mm for medial, 0.45 ± 0.21 mm/mm for lateral). Fpg had a weak positive correlation with contact in the both plateaus of the control subjects and the lateral plateau of the ACLR subjects, but a weak negative correlation in the medial plateau of the ACLR subjects. There was a significant group difference in the slope of the Fpg correlation best fit in the medial plateau (control: 0.50 ± 0.74 %/mm; reconstructed: -0.95 ± 1.28 %/mm).

DISCUSSION: Our first hypothesis was supported, with the tibial cartilage of healthy knees exhibiting spatial variations in cartilage thickness and PG content that mimicked contact patterns. However, our second hypothesis regarding ACLR knees was only partially supported. The majority of contact remained in regions of thicker cartilage in the ACLR knees despite a difference in contact location and magnitude. The relationship between contact and Fpg differed between the medial and lateral compartments of the knee. Similar to the control subjects, ACLR knees exhibited a positive correlation on the lateral plateau. However on the medial plateau, the correlation was negative, suggesting that contact occurs in regions with lower PG content. A loss of PG is an initiating step of OA, prior to any morphological changes to the cartilage (1; 5), suggesting signs of early OA in the medial plateau of the ACLR knees. While our study does not identify the cause of preferential PG loss on the medial plateau, there is evidence suggesting a link between altered knee mechanics during gait and OA in the medial compartment (3). Further, our results are consistent with clinical studies which report greater prevalence of medial OA in ACLR knees (9). Future studies will explore the extent to which variations in ACL graft geometry and surgical technique may affect the relationship between cartilage contact and tissue health, which could provide insights into the appropriate surgical factors to consider as to diminish risk for OA.

SIGNIFICANCE: We found evidence that tibial cartilage morphology and composition may be dependent on cartilage contact in healthy knees. Further, a negative link between proteoglycan content and cartilage contact in the medial plateau after ACL-reconstruction supports a mechanical initiation of OA.

REFERENCES: **1)** Andreisek G et al. 2009. OA Cartilage 17: 8. **2)** Andriacchi TP et al. 2004. Ann Biomed Eng 32: 11. **3)** Butler RJ et al. 2004. Ann Biomed Eng 32: 11. **4)** Kaiser J et al. 2013. MRM 69: 7. **5)** Li X et al. 2011. Radiology 258: 10. **6)** Liden M et al. 2008. Arthoscopy 24: 10. **7)** Liu F et al. 2014. MRI 39: 7. **8)** Scanlan SF et al. 2010. J Biomech 43: 6. **9)** Seon J et al. 2006. Int Ortho 30: 5. **10)** Tashman S et al. 2007. Clin Orthop Relat Res 454: 8.

ACKNOWLEDGEMENTS: Colin Smith, James Hermus, Oliver Wieben, Kevin Johnson, Kelli Hellenbrand, NIH EB015410, NIH AR06273

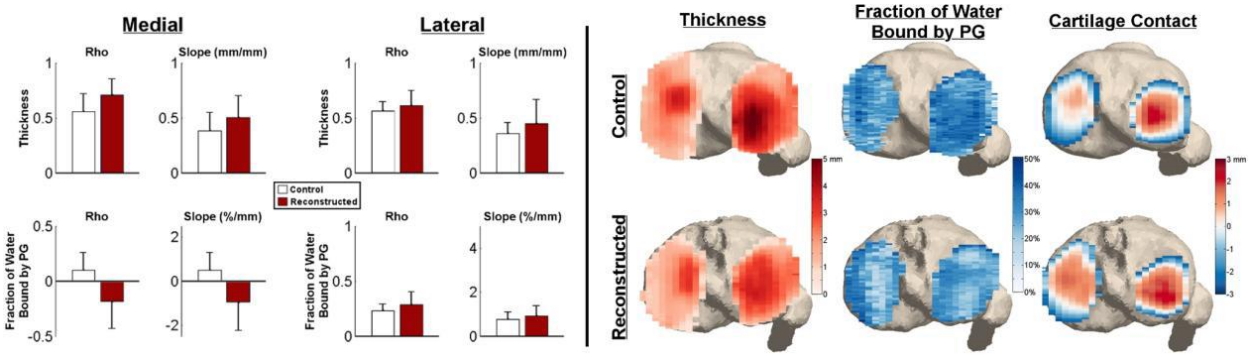

Figure 1. *Left.* Correlation coefficients and slopes of linear best fits for correlations between thickness and contact, and Fpg and contact. *Right.* Spatial maps of tibial cartilage thickness, Fpg, and cartilage contact of a representative control and patient subject.

Appendix C: Asymmetries in Knee Kinematics and Cartilage Contact Patterns are Correlated with ACL Graft Placement Following Reconstructive Surgery

Jarred Kaiser, Michael F. Vignos, Colin R. Smith, Richard Kijowski, Geoffrey Baer, Darryl G. Thelen

(Note that this Appendix was accepted for presentation at the 2016 Orthopaedic Research Society Conference)

INTRODUCTION: Bilateral kinematic differences persist following ACLR (6; 8) and it is theorized that these kinematic differences may shift contact to infrequently loaded regions of cartilage, thereby inducing the development of osteoarthritis (2). ACL graft placement may help explain the bilateral disparities following ACLR (5). In an anatomical ACLR surgery, the surgeon attempts to place the graft within the attachments of the native ACL, though this placement varies up to 7 mm from the native site (7). In this study, we explored the effects of ACL graft placement on *in vivo* tibiofemoral kinematic and contact behavior. We hypothesized that ACL graft orientation can predict bilateral differences in knee kinematics and cartilage contact.

METHODS: The healthy and ACLR knees of ten subjects were tested after obtaining informed consent according to an IRB-approved protocol (5 M, 25.3±4.5 yrs, 80.4±14.3 kg, 1.74±0.09 m, 2.1±0.7 yrs post-surgery, 4 PT grafts). Subjects had no additional ligament injury, no post-operative complications, and no history of pain, injury, or surgery to the contralateral knee. Subjects underwent a MRI protocol of a SPGR and a FSE Cube sequence in a 3T scanner. Subjects then laid supine with their lower leg secured to a loading device and a 16-channel flex coil fixed about the knee. Subjects actively flexed and extended their knee against an inertial load at a rate of 0.5 Hz, while a dynamic imaging sequence (SPGR-VIPR) continuously acquired cine 3D

volumetric data (4). Bone segments, segmented from the SPGR images, were optimally registered to each dynamic image to reconstruct tibiofemoral kinematics.

Native and reconstructed ACLs were segmented from FSE Cube images. We measured the area and location of the ACL attachments, and the orientation of the ACL relative to the tibial plateau in the sagittal and frontal planes. We also segmented the femoral and tibial cartilage, and registered them to the bone models at each dynamic frame in order to characterize cartilage contact. We summarized the dynamic tibiofemoral contact using the following metrics at peak flexion: maximum cartilage overlap, contact area, and center of contact (COC) location. The COC trajectory length was calculated during knee flexion. We computed the bilateral differences in ACL geometry metrics, knee kinematics, and contact metrics for each subject. We then computed the correlations between bilateral differences in ACL geometry with bilateral differences in kinematic and contact metrics. Significance for all tests was set to $p<0.05$.

RESULTS: The ACL grafts were placed 2.7 ± 2.3 mm lateral, and 1.0 ± 1.3 mm anterior in the tibia and 1.8 ± 3.9 mm caudal and 0.4 ± 1.9 mm anterior in the femur. Tibiofemoral kinematics at peak knee flexion were most correlated with the angle of the ACL in the sagittal plane. Specifically, medial (R=0.84) and anterior (R=0.75) tibial translations, as well as interior tibial rotation (R=0.78) were all positively correlated with a more vertical ACL graft. Anterior translation (R=-0.79) and internal rotation (R=-0.78) were also negatively correlated with ACL femoral attachment area.

The angle of the ACL in the sagittal plane accounted for 10 of the 24 significant correlations between bilateral differences in ACL geometry and contact, including COC trajectory length in the lateral tibial (R=0.66), and maximum overlap (R=0.69) and contact area (R=0.64) in the medial femoral compartment (Fig. 1). An increase in sagittal plane angle of the ACL graft relative to the

native ACL was also correlated with a medial shift of the COC at flexion in both compartments of the tibia (R=0.83, R=0.72 for medial/lateral respectively) and femur (R=079, R=0.77 for medial/lateral respectively).

DISCUSSION: We found that bilateral differences in tibiofemoral kinematics and contact were most significantly correlated with differences in the orientation of the ACL in the sagittal plane. These results suggest that a more vertical graft may be associated with greater anterior and rotational laxity, resulting in a medial shift in contact and greater contact in the medial femur. Kinematic correlations are supported by cadaveric (3) and *in vivo* (1) studies which found greater laxity in the knee using a transtibial surgical procedure, which places a more vertical graft than the anteromedial tunnel approach. These studies however were under static (3) or quasi-static (1) loading conditions and do not characterize the complex relationship between ACL graft placement and contact. Surgical parameters other than graft placement, such as graft stiffness and pretension, are also known to have an effect on knee mechanics (5) though the highly significant correlations of contact with graft placement highlights the importance of controlling this parameter during ACLR surgery.

SIGNIFICANCE: Differences in kinematics and cartilage contact in ACL-reconstructed knee were found to be significantly correlated with ACL graft placement, with the angle of the ACL graft in the sagittal plane appearing to be the most important parameter.

REFERENCES: (1) Abebe ES et al. 2011. J Biomech 44: 7. (2) Andriacchi TP et al. 2004. Ann Biomed Eng 32: 11. (3) Bedi A et al. 2011. Arthoscopy 27: 11. (4) Kaiser J et al. 2013. MRM 69: 7. (5) Pena E et al. 2005. Clin Biomech 20: 9. (6) Scanlan SF et al. 2010. J Biomech 43: 6. (7) Scanlan SF et al. 2012 J Ortho Res 30: 9. (8) Tashman S et al. 2007. Clin Orthop Relat Res 454: 8.

ACKNOWLEDGEMENTS: James Hermus, Oliver Wieben, Kevin Johnson, Kelli Hellenbrand, NIH EB015410, NIH AR06273

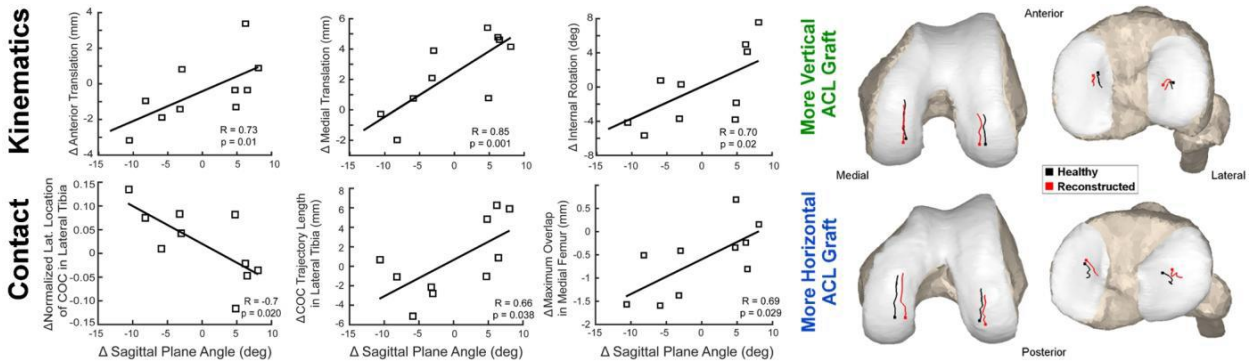

Figure 1. Sagittal plane angle is positively correlated with increased anterior and medial translation and internal rotation, resulting in a medial COC shift and an increased COC trajectory in the lateral tibia as well as an increased overlap in the medial femur (left). Example plots of the bilateral COC trajectory over flexion (right) are shown for a subject with a more vertical ACL graft (top) and a subject with a more horizontal ACL graft (bottom).